3.2 Linac Technology

3.2.1 Cavity Design and Characteristics

3.2.1.1 Introduction

The first multicell niobium cavities were fabricated at Stanford in the early 70's and used in an electron linac. The accelerating gradient was limited to about 2 MV/m due to electron multipacting [1]. A significant step towards higher gradients was the finding that multipacting could be virtually eliminated by changing the cavity geometry from a cylindrical to a spherical or elliptical cross section. The rounded shape permitted a simplified cavity production based on deep-drawing or spinning techniques instead of machining of bulk niobium. Starting in the early 1980's first beam tests with niobium cavities were carried out in the electron-positron storage rings CESR (Cornell), PETRA (DESY-Karlsruhe and DESY-CERN collaboration) and TRISTAN (KEK). In the second half of the 1980's 32 cavities were installed in TRISTAN and successfully used in seven years of high luminosity operation with an operating gradient of 3.5 – 4.5 MV/m. In the HERA electron ring 16 cavities are routinely in operation. Two superconducting linacs with niobium cavities have been built: the S-Dalinac at Darmstadt using 20-cell 3 GHz structures developed at Wuppertal and the CEBAF linac at Newport News using 5-cell 1.5 GHz structures developed at Cornell. The cavities for these machines were produced by industry.

An alternative route has been chosen at CERN for the 352 MHz cavities used in LEP. The resonators are deep drawn from copper and then sputtered with niobium. The major advantage is a considerable savings in the expensive niobium material and an improved heat conductivity in the cavity wall. A total of 272 four-cell cavities will be installed in LEP until 1998.

The largest SRF system presently in operation is the CEBAF linac with 338 cavities. All cavities have been subjected to tests in a vertical cryostat prior to installation in the linac [1]. The typical limitation was either a thermal breakdown or a severe degradation in quality factor due to field emission of electrons. The average accelerating gradient just below quench was about 13 MV/m but with a wide spread from 7 to 20 MV/m. The *usable gradient* in the vertical test, defined by a field emission loading of less than 1 Watt and an X ray level of less than 1 rad/h outside the cryostat, was about 3 MV/m lower. Another loss in gradient has been experienced after installation in the horizontal cryostats and mounting of the couplers: the usable gradient during commissioning ranged from 5 to 14 MV/m with an average of $\approx$ 8 MV/m.

The CEBAF experience is of great relevance for TESLA since the cavities are based on the same design principles and fabrication techniques. Obviously a significant progress is needed to achieve the TESLA design goal of 25 MV/m usable gradient or even the more moderate 15 MV/m in the TESLA Test Facility TTF. Numerous tests with single- and multicell cavities have shown that this is indeed possible. The recently

[1] "Multipacting" is a commonly used abbreviation of "multiple impacting" and disgnates the resonant multiplication of free electrons which gain energy in the RF electromagnetic field and impact on the resonator surface where they induce secondary electron emission.

introduced technique of cleaning the surface by high-pressure water rinsing [2, 3] has led to a considerable supression of field emission loading. Moreover, extreme care in cavity handling is essential to avoid dust particles that might act as field emitters and to preserve a low surface resistance. An elaborate infrastructure has been set up at DESY for cavity treatment and handling: industrial clean rooms according to semiconductor standards, an automated chemistry system, a high-pressure water rinsing system and an ultrahigh-vacuum furnace for heat treatment. These facilities are in use for the preparation of the TTF cavities.

The cavity test area comprises a bath cryostat for vertical tests at 1.5 to 4.2 K and a horizontal cryostat for the test of cavities that are welded into their liquid helium container and equipped with the input and higher-order-mode couplers used in the linac. A special feature is the possibility to apply short RF pulses with an instantaneous power of up to 1 MW to destroy field emitters in a cavity (the so-called high power processing technique HPP). Two temperature mapping systems to find "hot spots" are also available.

At present it appears that only cavities made from solid pure niobium have the potential of achieving accelerating fields of 25 MV/m or more while the gradients in niobium-sputtered copper cavities are typically in the 10 MV/m range. For this reason the decision was taken to consider only pure niobium as cavity material.

3.2.1.2 Basic principles of RF superconductivity

Surface resistance

In contrast to the d.c. case superconductors are not free of energy dissipation in microwave applications. The reason is that the RF magnetic field penetrates a thin surface layer and induces oscillations of the electrons which are not bound in Cooper pairs. The number of these "free electrons" drops exponentially with temperature. According to the Bardeen-Cooper-Schrieffer (BCS) theory of superconductivity the surface resistance is given by the expression

$$R_{BCS} \propto \frac{\omega^2}{T} \exp(-1.76\, T_c/T) \; . \tag{3.2.1}$$

where $f = \omega/2\pi$ is the frequency of the RF. In the two-fluid model of superconductors one can derive a refined expression for the surface resistance ([4, 5])

$$R_{BCS} = \frac{C}{T}\, \omega^2\, \sigma_n\, \Lambda^3 \exp(-1.76\, T_c/T) \; . \tag{3.2.2}$$

Here C is a constant, σ_n the normal-state conductivity of the material and Λ an effective penetration depth, given by

$$\Lambda = \lambda_L \sqrt{1 + \xi_0/l} \; .$$

λ_L is the London penetration depth, ξ_0 the coherence length and l the mean free path of the unpaired electrons. The fact that σ_n is proportional to the mean free path l leads

to the surprising conclusion that the surface resistance does not assume its minimum value when the superconductor is as pure as possible ($l \ll \xi_0$) but rather in the range $l \approx \xi_0$. For niobium the BCS surface resistance at 1.3 GHz amounts to about 800 nΩ at 4.2 K and drops to 1 nΩ at 1.5 K, see Fig. 3.2.1. This exponential dependence is the reason why cooling with superfluid helium is essential for achieving high accelerating gradients and at the same time very high quality factors. In addition to the BCS term there is a residual resistance R_{res} caused by impurities or lattice distortions. This term is temperature independent and amounts to a few nΩ for very pure niobium but may readily increase by large factors if the surface is contaminated.

Heat conduction in niobium

The heat produced at the inner cavity surface has to be guided through the cavity wall to the superfluid helium bath. Two quantities characterize the heat flow: the heat conductivity λ of the bulk niobium and the temperature drop at the niobium-helium interface caused by the Kapitza resistance. The heat conductivity of niobium at cryogenic temperatures scales approximately with the residual resistivity ratio[2] RRR, a rule of thumb being

$$\lambda(4.2\mathrm{K}) \approx 0.25 \cdot RRR \quad [\mathrm{W}/(\mathrm{m} \cdot \mathrm{K})]$$

but one has to keep in mind that λ is strongly temperature dependent and drops by about an order of magnitude when lowering the temperature to 2 K (Fig. 3.2.2). A good heat conductivity is the main motivation for using high purity niobium with $RRR \approx 300$ as a starting material. The RRR may be further improved by heat treatment of the finished cavity (see below).

Critical magnetic field

Superconductivity breaks down when the RF magnetic field exceeds the critical field of the superconductor. In the radio frequency case the so-called "superheating field" is relevant which for niobium is about 20% higher than the thermodynamical critical field of 200 mT. Niobium is in principle a soft type II superconductor without flux pinning. Hence weak magnetic fields like the Earth's field should be expelled upon cooldown but in practice a severe degradation in performance is observed in cavities without magnetic shielding.

3.2.1.3 Layout of the TESLA cavities

Choice of frequency

The losses in a radio-frequency cavity are proportional to the product of conductor area and surface resistance. For a given length of a multicell resonator, the area scales with $1/f$ while the surface resistance of a superconducting cavity goes like f^2 for

[2] RRR is defined as the ratio of the resistivities at room temperature and at 10 K (just above T_c).

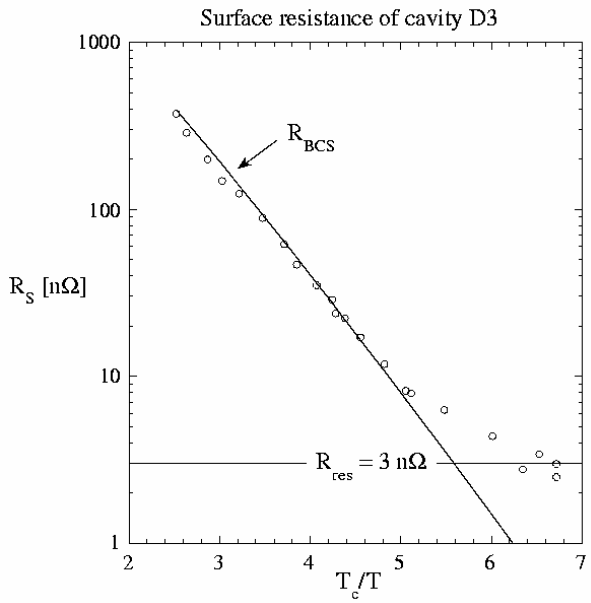

Figure 3.2.1: *The surface resistance of a 9-cell TESLA cavity plotted as a function of T_c/T. The residual resistance of 3 nΩ corresponds to an "unloaded" quality factor $Q_0 = 3 \cdot 10^{10}$.*

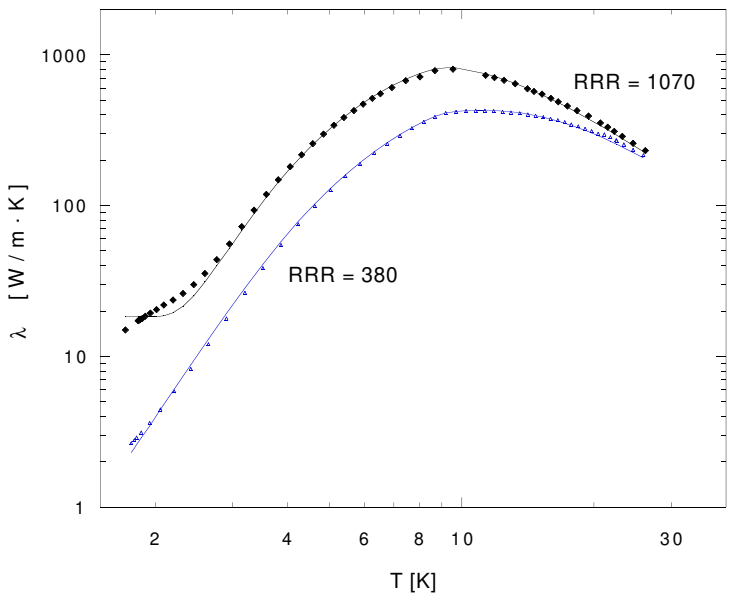

Figure 3.2.2: *Measured heat conductivity in niobium as a function of temperature [6]. Continuous curves: parametrisation by B. Bonin, using only RRR and the average grain size as input parameters [7].*

$R_{BCS} \gg R_{res}$ and is independent of f for $R_{BCS} \ll R_{res}$. Above 3 GHz the BCS term dominates and hence the losses grow linearly with frequency whereas below 300 MHz one obtains a growth with $1/f$. To minimize the Ohmic losses in the cavity wall one should therefore select f in the range 300 MHz to 3 GHz.

Cavities in the 350 to 500 MHz regime are in use in electron-positron storage rings. Their large size is advantageous to suppress wake field effects and higher order mode (HOM) losses. However, for a linac of 10 km length the niobium and cryostat costs for these bulky cavities are prohibitive, hence a higher frequency has to be chosen. Considering material costs $f = 3$ GHz might appear the optimum but there are compelling arguments for choosing about half this frequency.

a) At 1.5 GHz the iris diameter is a factor of two larger than at 3 GHz. The wake fields scale inversely with the second to third power of this diameter and are hence much weaker at the lower frequency. Beam emittance growth and cryogenic losses are correspondingly lower.

b) For very pure niobium the surface resistance grows with f^2, so a lower frequency is favourable to prevent thermal breakdown. In fact, a quality factor above 10^{10} can only be reached at 3 GHz if the helium temperature is lowered to 1.5 K which implies a significant increase in cooling costs in comparison with the 2 K cooling scheme of 1.3 GHz cavities. Moreover, the BCS resistance sets an absolute limit of about 30 MV/m at 3 GHz, hence choosing this frequency would definitely preclude a possible upgrade of TESLA to 35 – 40 MV/m [8].

c) The maximum number of cells per cavity is limited by the requirements that higher order modes must be extractable and no trapped modes be present. With this boundary condition the number of input and HOM couplers increases with frequency.

In summary, the arguments for a frequency around 1.5 GHz are far more compelling than for 3 GHz. The value of 1.3 GHz was chosen since high power klystrons are commercially available for this frequency.

Choice of geometry

A multicell structure is advantageous for maximizing the beam energy in a linac of a given length. With increasing number of cells per cavity, however, difficulties arise from trapped modes, uneven field distribution in the cells and too high power requirements on the input coupler. Based on experience with 4- and 5-cell cavities a choice of 9 cells was made for the TESLA cavities. A side view of the TTF cavity with the input and HOM coupler flanges is given in Fig. 3.2.3.

The shape of a cell is governed by the following considerations:

- the contour should strongly suppress multipacting,
- the electric and magnetic fields at the cavity wall should be minimized to reduce field emission and Ohmic heating,
- a sufficiently large iris diameter is desirable to reduce wake field effects.

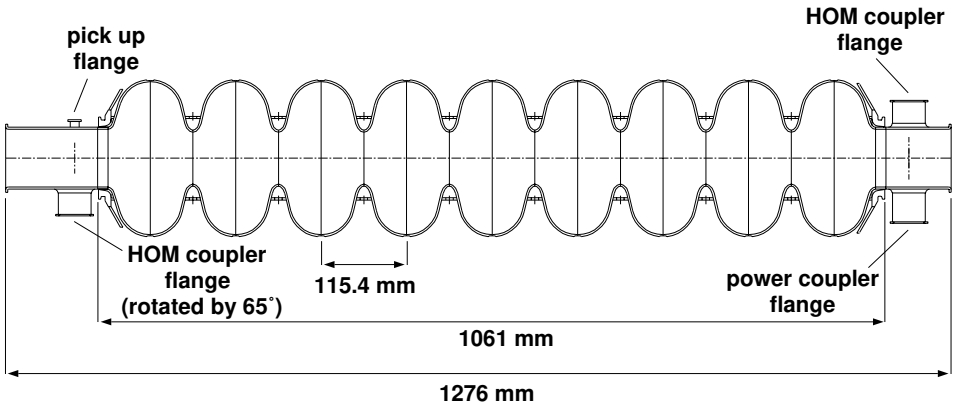

Figure 3.2.3: *Side view of the 9-cell TTF cavity with power coupler and HOM coupler ports.*

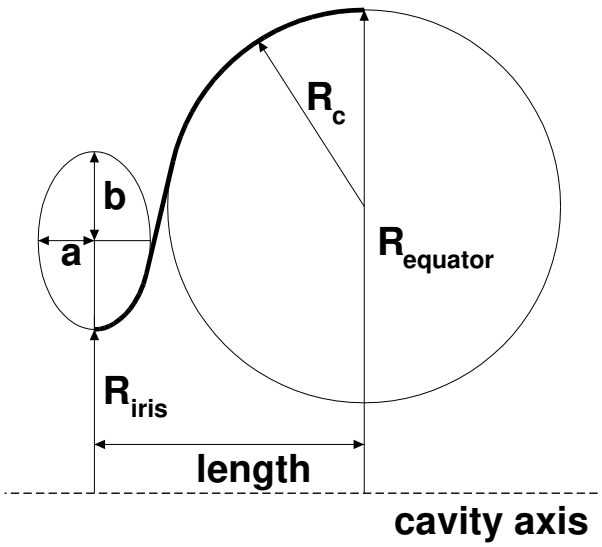

Figure 3.2.4: *Contour of a half cell.*

The shape of the TESLA cell was optimized using URMEL. The resonator is operated in the π mode (180° phase difference between adjacent cells). The longitudinal dimensions are determined by the condition that the electric field has to be inverted in the time a relativistic particle needs to travel from one cell to the next; the separation between two irises is therefore $c/(2f)$. The iris diameter influences the cell-to-cell coupling κ, the excitation of higher order modes and other important cavity parameters, such as the ratio of the peak electric (magnetic) field at the cavity wall to the accelerating field and the ratio (R/Q) of shunt impedance to quality factor. For the TTF cavities an iris diameter of 70 mm was chosen, leading to $\kappa = 1.8\,\%$ and $E_{peak}/E_{acc} = 2$. The most important parameters are listed in Table 3.2.1.

The contour of the half-cells, called "cups", is shown in Fig. 3.2.4. It is composed

Table 3.2.1: *TESLA cavity design parameters*

type of accelerating structure:	standing wave
accelerating mode	TM0 π mode
fundamental frequency	1300 MHz
design gradient E_{acc}	25 MV/m
quality factor Q_0	$> 5 \cdot 10^9$
active length L	1.038 m
number of cells	9
cell-to-cell coupling	1.87 %
iris diameter	70 mm
geometry factor	270 Ω
R/Q	1036 Ω
E_{peak}/E_{acc}	2.0
B_{peak}/E_{acc}	4.26 mT/(MV/m)
tuning range	$\pm$ 300 kHz
$\Delta f/\Delta L$	315 kHz/mm
Lorentz force detuning at 25 MV/m	$\approx$ 600 Hz
Q_{ext} of input coupler	$3 \cdot 10^6$
cavity bandwidth at $Q_{ext} = 3 \cdot 10^6$	430 Hz
RF pulse duration	1330 μs
repetition rate	5 Hz
fill time	530 μs
beam acceleration time	800 μs
RF power peak/average	208 kW/1.4 kW
number of HOM couplers	2
cavity longitudinal loss factor $k_{\parallel}$ for $\sigma_z = 0.7$ mm	10.2 V/pC
cavity transversal loss factor $k_{\perp}$ for $\sigma_z = 0.7$ mm	15.1 V/pC/m
parasitic modes with the highest impedance : type	TM_{011}
$\pi/9$ $(R/Q)/$ frequency	160 Ω/2454 MHz
$2\pi/9$ $(R/Q)/$ frequency	135 Ω/2443 MHz
bellows longitudinal loss factor $k_{\parallel}$ for $\sigma_z = 0.7$ mm	1.54 V/pC
bellows transversal loss factor $k_{\perp}$ for $\sigma_z = 0.7$ mm	1.97 V/pC/m

of a circular arc around the equator region and an elliptical section near the iris. The dimensions are listed in Table 3.2.2. The half cells at the end of the 9-cell resonator need a slightly different shape to ensure equal field amplitudes in all 9 cells.

3.2.1.4 Cavity treatment and test results

Summary of cavity production

The cavities for TTF have been or are being produced by four European companies. The present design is based on welding the 9-cell resonator from half cells that are

Table 3.2.2: *Half-cell shape parameters (all dimensions in mm).*

cavity shape parameter	midcup	endcup 1	endcup 2
equator radius $R_{equ.}$	103.3	103.3	103.3
iris radius R_{iris}	35	39	39
radius R_c of circular arc	42.0	40.3	42
horizontal half axis a	12	10	9
vertical half axis b	19	13.5	12.8
length l	57.7	56.0	57.0

deep-drawn from niobium sheet metal. The starting material is a niobium ingot which is highly purified by five- to six-fold electron beam melting by which the O_2, N_2 and C contamination is reduced to a few ppm. After rolling, the Nb sheets are degreased, a surface layer is removed by etching and then the Nb sheets are heat-treated at 800 °C in a vacuum furnace to achieve full recrystallization and a uniform grain size. Half cells are produced by deep-drawing, are then machined at the iris and equator weld zones, and cleaned by a suitable combination of degreasing, etching and clean water rinsing. They are welded together in a multistep process by electron-beam welding in a vacuum of $< 5 \cdot 10^{-5}$ mbar. A demanding requirement is to produce a smooth weld seam at the inner surface of the cavity which is particularly difficult for the equator welds because they are usually made from the outside. Also the requirements on mechanical precision are very demanding for a structure with about 20 weld connections.

Cavity treatment

A thin surface layer is damaged by the rolling of the Nb sheets and contaminated with oxygen by the subsequent 800 °C heat treatment. The damage layer, which may be 100-200 μm thick, has to be removed to obtain a good superconducting surface. Different approaches exist for this procedure, here we describe the method presently used at DESY. After degreasing the cavity receives chemical etching (also called Buffered Chemical Polishing BCP) using HF (48 %), HNO_3 (65 %) and H_3PO_4 (85 %) in the ratio 1:1:2. A layer of 80 μm is removed from the inner surface and about 30 μm from the outer surface. After careful rinsing and drying the cavity is tuned to obtain the correct fundamental frequency and equal field amplitudes in all cells. Since the tuning procedure may have introduced some dirt into the cavity, it is followed by a chemical etching of about 20 μm, a clean water rinsing and three steps of high pressure (100 bar) rinsing. The resistivity of the water leaving the cavity must be more than 18 MΩ cm to ensure that no drying stains are left on the surface. Several cavities have been tested after this step. The best result is shown in Fig. 3.2.5 where the quality factor of a nine-cell cavity is plotted as a function of accelerating field (this type of plot will be called "excitation curve" in the following).

While the cavity shown in Fig. 3.2.5 exceeds the 15 MV/m requirement for TTF

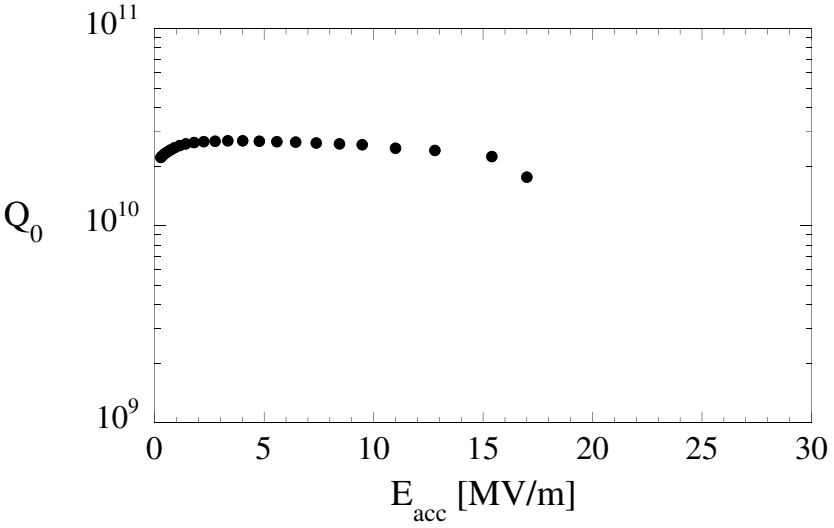

Figure 3.2.5: *Quality factor as a function of accelerating field for a cavity without heat treatment.*

already without heat treatment, this is not the case for the majority of cavities. Empirically it has been found [9] that a several-hour heat treatment at 1350-1400° C in an ultra high vacuum furnace leads to a significant improvement of the high-field capabilities of Nb cavities. Two effects play a role: the material is homogenized, and dissolved gases like hydrogen, oxygen and nitrogen diffuse out of the niobium thereby increasing the heat conductivity by about a factor of two. This high-temperature heat treatment, though quite successful in many cases, has a number of disadvantages:

The residual gas pressure in the ultra high vacuum furnace is too high to achieve the desired reduction of oxygen in the bulk niobium unless a getter material like titanium is applied. A titanium layer is deposited on the cavity surface which must be removed later by chemical etching. Titanium may diffuse deep into the niobium at grain boundaries. Moreover, the niobium material becomes extremely soft, the yield strength is reduced by almost an order of magnitude. Heat treated cavities must be handled with extreme care to avoid plastic deformation and detuning. Finally, the procedure is very time consuming and costly.

For these reasons alternative schemes are being explored like reducing the oven temperature to 800°C which is sufficient to drive hydrogen out of the niobium but not oxygen. This way the *RRR* will not be improved above the starting value of 300 but tests with single-cell cavities at KEK [10] have demonstrated that gradients of more than 30 MV/m can be realized with this moderate heat treatment.

In the following we present several "typical" test results to demonstrate the effect of the various cavity treatment steps. Fig. 3.2.6a shows the excitation curve of a cavity with heavy field emission. Starting from an excellent value at low field, the quality factor exhibits a steep decrease for fields above 8 MV/m. The reason is probably a single strong field emitter. In this and similar cases the HPP (high power processing)

technique [11] has been very successful: the high instantaneous power destroys the emitter (which can be seen on temperature maps) and afterwards the cavity can be excited to much larger fields. A drawback of this technique is also visible from the figure: the quality factor has dropped by a factor of 2-3 probably because of surface contamination from the evaporating emitter. Some of the loss can be recovered by warming up the cavity and cooling down again.

Fortunately, the long-standing problem of field emission can be largely eliminated by rinsing the cavity with ultraclean water at a pressure of about 100 bar. In several rinsing steps most of the particles sticking to the surface are removed. If the subsequent handling is done with sufficient care in a class-100 clean room, then field emission is no longer the limiting factor. An impressive example of the benefits of high pressure rinsing is shown in Fig. 3.2.6b. In spite of the progress achieved by this cleaning method, the possibility of processing with high RF power should still be foreseen for the cavities mounted in the linac to remove field emitters that might occur after some vacuum accident. This is important to provide a high operating gradient since demounting of the cavities from the cryomodule, high pressure water rinsing and reinstallation would certainly imply too much effort.

Fig. 3.2.6c demonstrates that a substantial gain in accelerating field can be achieved by heat treatment at 1400 °C. However, care must be taken that the titanium getter layer is completely removed. This is evident from the two curves in Fig. 3.2.6d. After the furnace treatment at 1400° a total of 80 μm was removed but the $Q(E)$ curve exhibited a steep drop at 10 MV/m. Removing an additional 75 μm led to the best test result obtained so far.

Also in non-heat-treated cavities an additional etching may lead to an enhanced performance. In a sample of 15 CEBAF 5–cell cavities the average gradient was 8 MV/m after the standard removal of 60 –80 μm, well below the average of 13 MV/m in the majority of the CEBAF cavities. Applying an additional chemical polishing of 70 μm raised the average gradient of these "substandard" cavities to the much improved value of 16 MV/m. Four of the 15 cavities received a 4-hour heat treatment at 1400°C with titanium getter, followed by 120 μm chemical etching to remove the Ti layer. All of these exceeded 20 MV/m.

Summary of TTF cavity tests

The design goal for the cavities of the TESLA Test Facility is a gradient of 15 MV/m at $Q = 3 \cdot 10^9$. The majority of cavities built and tested up to now have reached or exceeded this specification when operated in pulsed mode, as required in the linac (1.3 ms long pulses at a 10 Hz repetition rate).

Seven cavities from 2 manufacturers exceed 20 MV/m even in cw (continuous wave) mode and are actually close to the TESLA goal of 25 MV/m at $Q = 5 \cdot 10^9$. Their excitation curves are shown in Fig. 3.2.7. R & D work for TESLA has also been carried out at Cornell. One 4-cell and three 5-cell cavities reached 25 MV/m after a 1400 °C heat treatment.

A number of cavities reveal limitations and problems which, however, are now well

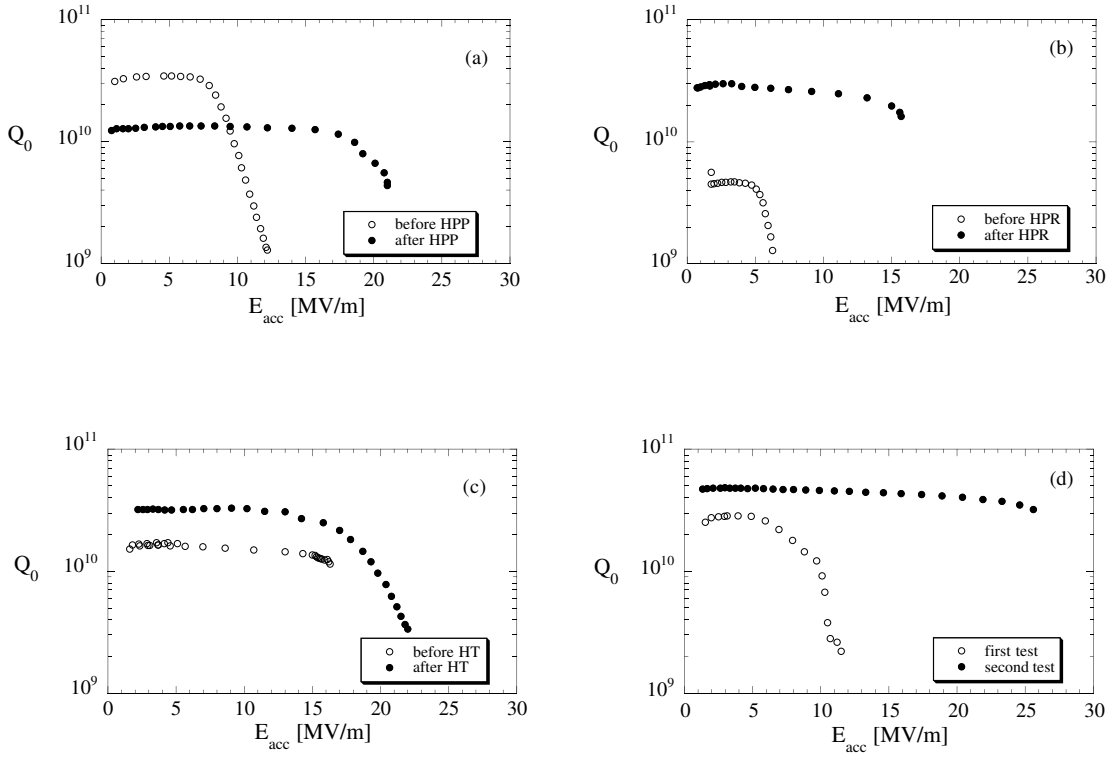

Figure 3.2.6: *Improvement in cavity performance due to various treatments: (a) High power processing, (b) high pressure water rinsing, (c) heat treatment for 4 hours at 1400 °C, (d) removal of surface defects or titanium in grain boundaries. In all four cases shown the cavities were limited by thermal breakdown.*

understood. A material defect has been found in the center cell of a resonator by means of the temperature mapping system. It has been identified as a ≈ 0.5 mm thick tantalum grain in the bulk niobium whose rim is touching the RF surface. As a conseqence the cavity was limited to 13 MV/m in the center cell. This cell has been cut out and the resonator will be repaired by welding in a new cell.

Measurements of all nine coupled modes of the 9-cell resonator are useful to determine the high-field performance of individual cells[3]. The single-cell statistics is shown in Fig. 3.2.8. It is seen that the majority of cells is well above 20 MV/m while only four cells are below the TTF specification of 15 MV/m. The observation that only a few percent of the niobium sheets are impaired by material defects is very important for future cavity production. With the eddy-current scanning method described below it will be possible to eliminate the defective sheets and thereby improve the overall performance.

The cavities from a third manufacturer exhibit a different type of limitation: the

[3]There is an ambiguity owing to the symmetry of the modes with respect to the center cell: it is not possible to distinguish between cell 1 and 9, cell 2 and 8 etc.

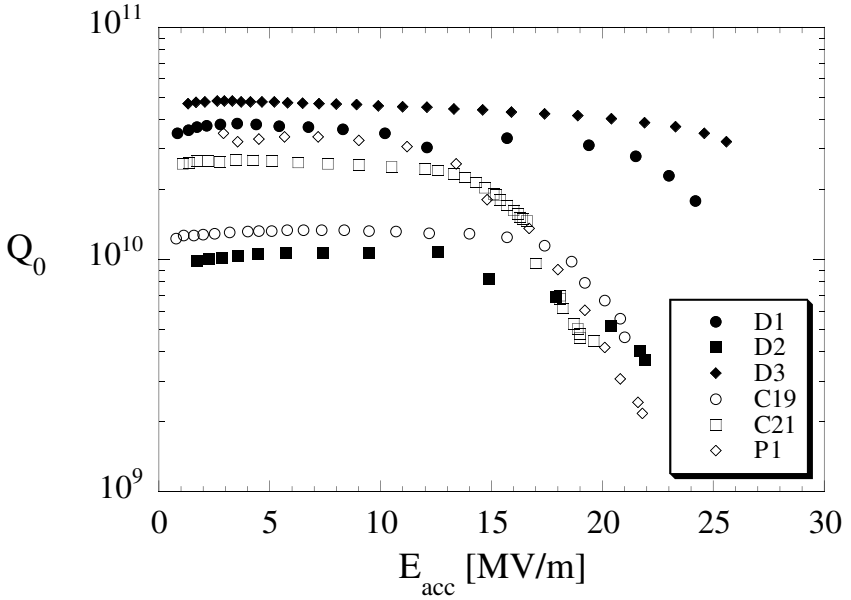

Figure 3.2.7: *The excitation curves $Q(E_{acc})$ of good TTF cavities*

quality factor starts at a high value but drops by a factor of 2 – 3 with increasing field until a quench occurs at about 13 – 14 MV/m in cw operation. Such "Q slopes" are routinely observed in niobium-sputtered copper cavities and are attributed to grain boundary effects. In pulsed mode most of these cavities can be excited beyond 15 MV/m and are hence useable for TTF, but fail the TESLA specification.

Using temperature mapping the origin of the reduced performance has been clearly identified. Spots with unusually strong heating were detected in various equator welds, leading to premature thermal breakdown and to a reduction of quality factor with increasing gradient. With an improved preparation of the weld regions and an optimized electron-beam welding procedure this type of degradation can be avoided in future cavities.

Nine cavities, fully equipped with main power and higher-order-mode couplers, have been tested in a horizontal cryostat prior to their installation in the capture cavity tank and the first cryomodule of the TTF linac, respectively. The average gradient in pulsed mode was 17 MV/m at $Q_0 = 3 \cdot 10^9$, almost as high as the average gradient of 17.5 MV/m achieved in the vertical test in continuous-wave mode.

Material research

Various diagnostic tools are in use to search for inclusions and to study surface defects. DESY collaborates with a number of universities and research centers which have expertise in materials science.

Scanning electron microscopes with energy-dispersive X ray analysis (EDX) have been and are being used to identify foreign elements on the surface. Only a depth of about 1 μm can be penetrated, so one has to remove layer by layer to determine the

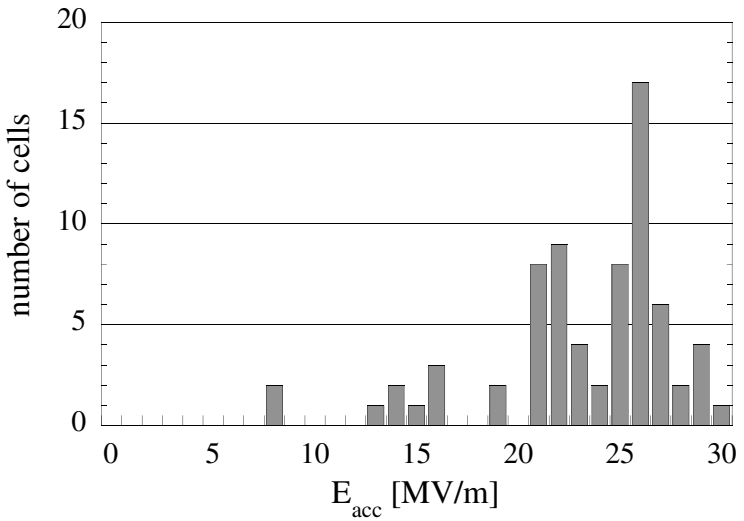

Figure 3.2.8: *Distribution of accelerating field achieved in the individual cells of eight 9–cell TTF resonators.*

diffusion depth of titanium or other elements. Alternatively one can cut the material and scan the cut region. The titanium layer applied in the high temperature treatment extends to a depth of about 10 μm in the bulk niobium. The sensitivity of the EDX method is rather limited, a Ti fraction below 0.5 % is undetectable. Auger electron spectroscopy offers higher sensitivity and using this method titanium migration at grain boundaries has been found to a depth of 60 μm. The microscopic methods are restricted to small samples and cannot be used to study entire cavities.

The narrow-band X ray beams at Hasylab permit element identification via fluorescence analysis. The cut-out cell was investigated this way and tantalum was identified at the spot detected by the temperature mapping system. In principle the apparatus allows the scanning of a whole niobium sheet such as used for producing a half cell, however this procedure is far too time-consuming.

A high-resolution eddy current system has been developed at the Bundesanstalt für Materialforschung (BAM) in Berlin. Using this system the tantalum inclusion mentioned above was easily detectable. For the future production it is foreseen to scan the niobium sheets before they go into cavity production.

Superconductor magnetization measurements offer the possibility to search for magnetic flux pinning. Pinning should be absent in pure niobium but will occur in a NbTi surface layer after the heat treatment with titanium getter. A working apparatus exists and will be routinely used to examine Nb samples which accompany all steps of cavity treatment. A new addition to this apparatus is a device to measure the upper critical field B_{c2} of the sample. This technique was developed at Wuppertal [12]. For pure niobium B_{c2} amounts to 0.27 T while with increasing titanium admixture B_{c2} will rapidly rise to values of many Tesla. The magnetic measurements are foreseen to provide on-line information on the required removal rate in the etching process.

Research and development for cavity improvement

The TTF cavity program and recent results from CEBAF and Cornell demonstrate that accelerating fields of 25 MV/m in multicell cavities are within reach. Two new limiting effects have been found that did not impair previous cavities with design gradients of 5 – 10 MV/m: tantalum or other foreign material inclusions in the niobium sheets and small irregularities in the electron-beam welds. Diagnostic instruments are at hand to avoid these defects. With some additional R&D effort the TESLA design goal of 25 MV/m can be safely achieved. Two routes are followed in parallel.

The first route is based on the present welded design. Here the emphasis is on improved cleanliness and quality control at all stages: niobium ingot production and sheet rolling in a clean environment; eddy current scan of Nb sheets to detect inclusions or defects at an early stage; tight quality control at the companies which are carrying out the deep-drawing and welding of the resonators; optimization of cavity treatment. An important improvement would be to raise the RRR of the niobium ingot material to values of more than 500. In that case a 1400 °C heat treatment of the cavity could probably be avoided.

In the second route a new method of cavity fabrication is investigated, namely hydroforming of the entire multicell resonator from a seamless niobium tube. First attempts with copper have been very promising. If this method should prove practical it would offer considerable advantages, concerning the simplicity of production, the quality of the inner surface and the costs. Increasing the iris radius from 35 to about 50 mm would greatly ease the hydroforming process. Cavities with this larger aperture feature smaller HOM losses and a lower sensitity to detuning [13]. On the other hand the peak electric and magnetic fields would be about 15 % higher than in the TTF cavities so a careful balance of the relative benefits and drawbacks must be found.

3.2.1.5 Cavity Tuning

Lorentz-force detuning and cavity stiffening

The electromagnetic field exerts a pressure on the cavity wall

$$P = \frac{1}{4}(\mu_0 H^2 - \epsilon_0 E^2) \tag{3.2.3}$$

which results in a deformation of the cells and a change ΔV of their volume. The consequence is a frequency shift

$$\frac{\Delta f}{f_0} = \frac{1}{4W}\int_{\Delta V}(\epsilon_0 E^2 - \mu_0 H^2)dV \ . \tag{3.2.4}$$

Here

$$W = \frac{1}{4}\int_V (\epsilon_0 E^2 + \mu_0 H^2)dV \tag{3.2.5}$$

is the stored energy and f_0 the resonant frequency of the unperturbed cavity. The computed frequency shift at 25 MV/m amounts to 900 Hz for an unstiffened cavity

of 2.5 mm wall thickness. The bandwidth of the cavity equipped with input coupler ($Q_{ext} = 3 \cdot 10^6$) is about 430 Hz, hence a reinforcement of the cavity is needed. Niobium stiffening rings are welded in between adjacent cells as shown in Fig 3.2.9. They reduce the frequency shift to about 400 Hz for a 1.3 ms long RF pulse[4]. The deformation of the stiffened cell is negligible near the iris where the electric field is large, but remains nearly the same as in the unstiffened cell near the equator where the magnetic field dominates. No simple scheme exists to reduce the deformation in this region except by increasing the wall thickness.

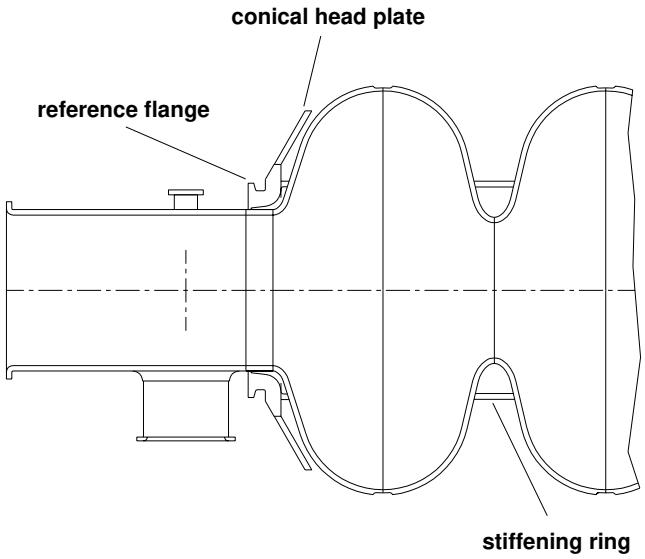

Figure 3.2.9: *End section of a cavity with stiffening ring, conical head plate for welding into the helium tank and reference flange for alignment.*

Tuning system

The goal of the tuning system is to adjust the cavity frequency to the desired value within a few % of the resonance width. Tuning is achieved via variation of the overall length of the cavity.

The tuning system consists of a stepping motor with a gear box and a double lever arm. The thrust is transmitted to the conical head plate at the diameter of the stiffening rings. The moving parts operate at 2 K in vacuum. The tuning range is about ± 1 mm, corresponding to a frequency range of ± 300 kHz. The resolution is 1 Hz. The

[4]Half of this shift is due to cell deformation, the other half to a shortening of the liquid-helium tank surrounding the cavity.

tuning system is adjusted in such a way that after cooldown the cavity is always under compressive force to avoid a backlash if the motion changes from pushing to pulling.

Microphonics

The cavity welded into its helium tank can be considered as a mechanical oscillator with many eigenmodes. The computed mechanical resonances are all above 10 Hz. Mechanical vibrations can be excited by external sources (ground motion, 50 Hz noise, vacuum pumps) but also by the pulsed electromagnetic field. Most of these vibrations will influence the resonance frequency and hence periodically detune the cavity. Details are presented in section 3.2.4.8.

3.2.1.6 Main Power Coupler

Design requirements

A critical component of a superconducting cavity is the power input coupler. For TTF two versions have been developed. The couplers consist of a "cold part" which is mounted on the cavity in the clean room and closed by a ceramic window, and a "warm part" which is mounted after installation of the cavity in the cryomodule. The warm section contains the transition from waveguide to coaxial line. This part is evacuated and sealed against the air-filled wave guide by a second ceramic window. The elaborate two-window solution was chosen to protect the cavity as well as possible against contamination during mounting in the cryomodule and against window failures during linac operation. An important mechanical requirement is that the couplers must allow for up to 15 mm of longitudinal motion inside the 10 m long cryomodule when the cavities are cooled down from room temperature to 2 K. For this reason bellows on the inner and outer conductors of the coaxial line are needed. Since the coupler connects the room-temperature waveguide with the 2 K cavity, a compromise must be found between a low thermal conductivity and a high electrical conductivity. This is achieved by several thermal intercepts and by using stainless steel pipes with a thin copper plating at the RF surface. The design heat loads are 6 W at 70 K, 0.5 W at 4 K and 0.06 W at 2 K. To reduce the danger of multipacting, future couplers will be equipped with a capacitive transition in the inner conductor to permit the application of a dc bias voltage.

Electrical properties

An instantaneous power of 210 kW has to be transmitted to provide a gradient of 25 MV/m for an 800 μs long beam pulse of 8.25 mA. At a repetition rate of 5 Hz this corresponds to an average power of 1.4 kW. The filling time of the cavity amounts to 530 μs and the decay time, after the beam pulse is over, to an additional 500 μs. At the beginning of the filling, most of the RF power is reflected. In the resulting standing-wave pattern the voltage is doubled at the points of constructive interference between incident and reflected wave. To verify that the coupler can safely stand these voltage

enhancements the tests in travelling wave mode have to be performed at four times the nominal power, namely 840 kW.

An adjustment of the external Q of the coupler is achieved by moving the inner conductor of the coaxial coupler section[5]. The range $Q_{ext} = 1 \cdot 10^6 - 9 \cdot 10^6$ is needed to compensate for variations in cavity geometry, couplers and beam current. The input coupler should be impedance-matched (power reflection less than 1%). It must also be capable of transmitting up to 1 MW at a reduced pulse length for *in situ* high power processing of the cavity if the performance should have degraded due to a vacuum failure.

Input coupler A

The coupler version A is shown in Fig. 3.2.10. It has a conical ceramic window at 70 K and a commercial planar waveguide window at room temperature. Variable coupling is achieved by the use of bellows on the inner and outer conductors of the coaxial line. The adjustment mechanism is located outside the cryomodule and permits 25 mm range of motion, which is more than adequate for the required range of Q_{ext}.

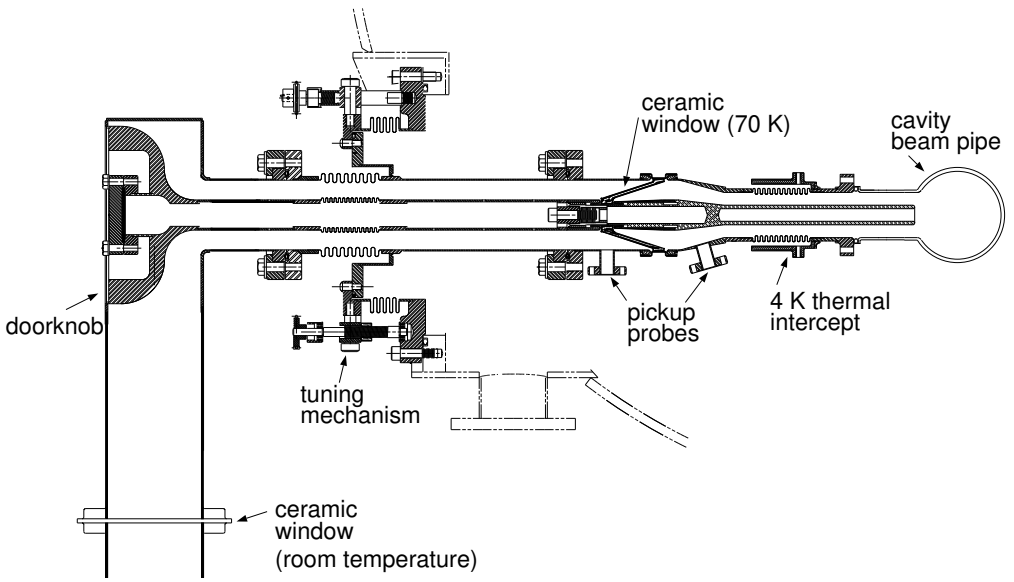

Figure 3.2.10: *Simplified view of the power input coupler version A.*

Flexibility for axial motion during cooldown is achieved via the inner and outer conductor bellows. The pivot point is outside the vacuum vessel. When the coupler

[5]Power coupler plus waveguide can be considered as an external load which extracts energy from the cavity once the pulsed RF has been switched off. The damping provided by the coupler is much bigger than that caused by the surface resistance, hence $Q_{ext} \ll Q_0$, where Q_0 is the quality factor of the "unloaded" cavity.

is mounted at room temperature, the center conductor will be off-center with respect to the input port of the cavity but center itself upon cooldown. The "cold" part of the coupler, together with the conical window, is permanently mounted on the cavity after it has been chemically processed, rinsed, and assembled in the clean room. The "warm" part of the coupler extends beyond the vacuum vessel of the cryomodule and can therefore be installed only after the cavity has been inserted into the vessel. The two coupler parts are joined by a metal-sealed flange at the outer tube and a screw at the inner conductor.

Conical ceramic window A conical shape was chosen for the cold ceramic window to obtain broad-band impedance matching. The Hewlett-Packard High Frequency Structure Simulator program HFSS was used to model the window and to optimize the shape of the tapered inner conductor. The reflected power is below 1 %. The ceramic penetrates into the inner and outer conductor to reduce the field strengths at the braze joints to approximately 50 % of their values at the surfaces of both conductors.

The ceramic window is made from 99.5% Al_2O_3. OFHC copper rings are brazed to the ceramic using Au/Cu (35%/65%) braze alloy. The inner conductors on each side of the ceramic are electron-beam welded, the outer conductors are TIG welded. The ceramic is coated on both sides with a 10 nm thick titanium nitride layer to reduce multipacting.

Doorknob transition and warm window The waveguide-to-coaxial transition is realized using a cylindrical knob as the impedance-transforming device. A planar waveguide window, such as used in commercial klystrons, is mounted upstream. A pair of matching posts is required on the air side of the window for impedance matching at 1.3 GHz. The shape of the doorknob was designed using HFSS. It is impedance-matched over a fairly broad frequency band.

Input coupler B

Coupler version B features two cylindrical ceramic windows, the first at the 70 K level near the cavity, the second at 300 K inside the transition from waveguide to coaxial line. The 70 K window has no direct view of the beam and is insensitive to electron multipacting.

A wave guide of reduced height and two stubs provide broad-band matching between the WR650 waveguide and the 50 Ω coaxial line. The warm ceramic window serves as a vacuum barrier towards the waveguide. Flexibility during cooldown is achieved by two bellow sections in the inner and the outer conductor. The tip of the inner conductor is movable to adjust the external Q. Low cryogenic losses and low RF losses are achieved by using stainless tubes of 0.5 mm wall thickness with a 10-20 μm plating with high-conductivity copper. The bellows of the inner conductor are made of hydroformed thin-walled stainless steel and have sufficient thermal resistance to permit the rest of the inner conductor to be made from copper.

Coupler tests and further development

Prototype couplers have been equipped with ports for diagnostics: a window to observe light effects with a photomultiplier and pick–up probes to measure charged particles. The presence of electrons is an indication of multipacting or plasma discharge and must be avoided since the resulting pressure rise may lead to material evaporation and permanent damage. Five resp. four couplers of each version have been successfully operated and reached a power level of 250 kW after some conditioning time. A simplified and improved version has been designed and is presently under construction. It features two ceramic windows, a 60 mm diameter coaxial line with reduced sensitivity to multipacting and the possibility to apply a dc potential to the center conductor of the coaxial line. In case of the LEP couplers a dc bias has proved very beneficial in suppressing multipacting.

3.2.1.7 Higher Order Modes

The intense electron bunches passing the cavity excite eigenmodes of higher frequency in the resonator which must be damped to avoid multibunch instabilities and beam breakup. This is accomplished by extracting the stored energy via HOM couplers and dissipate it in a load resistor outside the liquid helium container. The HOM couplers are mounted on the beam pipe sections of the nine-cell resonator. Therefore only those higher modes can be extracted which have a sizeable amplitude in the end cells. A problem is related to the so-called "trapped modes" which are concentrated in the center cells and have a low field amplitude in the end cells.

"Trapped" modes

The TE_{121} mode is an example of a trapped mode with a small amplitude in the end cells. In a multicell resonator the end cells are distorted by the presence of the beam pipe. Their shape is adjusted to ensure equal field amplitudes in all nine cells for the fundamental TM_{010} mode (the accelerating mode). This correction does not automatically improve the end-cell field of trapped higher modes. There is, however, an interesting way out. By an asymmetric tuning of the end cells one can enhance the field amplitude of the TE_{121} mode in one end cell while preserving the "field flatness" of the fundamental mode and also the good coupling to the "traveling" modes TE_{111}, TM_{110} and TM_{011}. For this purpose the curvature from equator to iris, the iris ellipse and the iris distance are modified. The effects of asymmetric end cell tuning are summarized in Fig. 3.2.11.

Polarization of dipole modes

Dipole modes can be excited in two orthogonal field patterns. Therefore a single-cell cavity should be equipped with a HOM coupler at each side with a relative angle of 90° between the couplers. In a multicell cavity the situation is more complicated, in principle two couplers on each side are needed to provide damping of trapped modes.

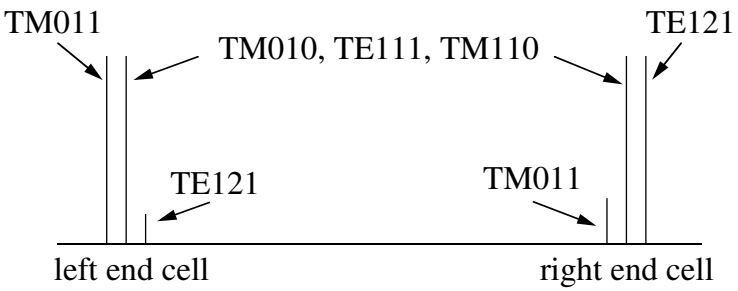

Figure 3.2.11: *Effect of asymmetric end cell tuning on various modes. The accelerating mode TM_{010} and the modes TE_{111} and TM_{110} are not affected while TM_{011} is enhanced in the left end cell, TE_{121} in the right end cell.*

This complexity can be avoided by breaking the azimuthal symmetry of the cavity, e.g. by giving it an elliptical cross section. Thereby the planes of polarization are fixed. For such a "polarized" multicell resonator, only one HOM coupler at each end is needed whose azimuthal orientation with respect to the main axes of the ellipse is 45° resp. 135°. Producing cavities with an elliptical instead of a circular cross section is technically feasible but increases the production costs. Fortunately, in a string of cavities dipole modes of arbitrary polarization can be damped even if the cavities possess cylindrical symmetry. To illustrate the principle we consider again the dipole mode TE_{121}. By asymmetric tuning it acquires a sizeable amplitude in the right end cell, for example. Sufficient damping for both planes of polarization is then provided by the right HOM coupler of the cavity in question and the left HOM coupler of the next cavity in the string, which has the orthogonal orientation. The viability of this idea was verified in measurements.

HOM couplers

The HOM couplers are mounted at both ends of the cavity with a nearly perpendicular orientation[6] to ensure damping of dipole modes of either polarization. A notch filter is incorporated to prevent that energy is extracted from the accelerating fundamental mode. Two types of HOM couplers have been developed and tested, one is mounted on a flange, the other one welded to the cavity.

The demountable HOM coupler is shown in Fig. 3.2.12a. Coupling to the RF field is provided by an open loop whose plane is orthogonal to the beam axis. The loop couples mainly to the magnetic field for TE modes and to the electric field for TM modes. It is capacitively coupled to an external load at 70 K. The rejection filter for the fundamental mode is formed by the inductance of the loop and the capacity at the 1.9 mm wide gap between the lower part of the loop and the wall of the coupling port. Tuning of the filter can be performed without opening the cavity vacuum with help of a niobium bellow. The loop is thermally connected to the 2 K helium bath.

[6]The angle between the two HOM couplers is not 90° but 115° to provide also damping of quadrupole modes.

The coupler has been tested in cw (continuous wave) operation up to an accelerating field of 21 MV/m (this was the field limit of the cavity). The temperature measured at the end of the coupling loop reached a maximum of 4 K which is totally uncritical. In the linac the coupler will be operated in pulsed mode with a duty cycle of 0.6 % hence heating should present no problem.

The welded version of the HOM coupler is shown in Fig. 3.2.12b. It resembles the coupler used in the 500 MHz HERA cavities which have been operating for several years without quenches. The good cooling of the inner conductor by two stubs makes the design insensitive to γ radiation and electron bombardment.

Many copper models of both versions have been built to optimize the coupler dimensions, the position of the ports, and the orientation and penetration of the coupling elements. Pairs of demountable and welded couplers have been tested on the asymmetrically tuned cavity models. The measured values of Q_{ext} are well below the tolerable limits. Both couplers provide sufficient damping for those higher order modes that might lead to emittance growth or beam breakup.

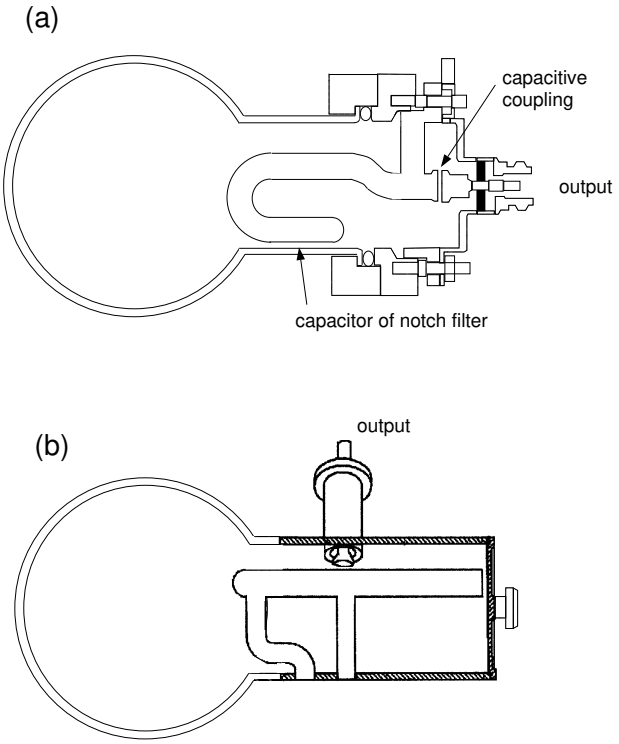

Figure 3.2.12: *The higher-order-mode couplers: (a) demountable HOM coupler, (b) welded HOM coupler.*

Fundamental mode rejection filter Both coupler versions permit tuning of the fundamental mode rejection filter when the HOM coupler is mounted on the cavity. It is possible to achieve a Q_{ext} of more than $1 \cdot 10^{11}$, limiting the extracted power to less than 50 mW at 25 MV/m. During the TESLA operation the rejection filter will remain stable since the couplers are placed in the insulating vacuum. In the welded HOM coupler the rejection filter is quite insensitive to detuning: a detuning by as much as $\pm$20 MHz raises the average extracted fundamental–mode power to just 1 W at $E_{acc} = 25$ MV/m.

3.2.1.8 Helium vessel

The helium tank contains the superfluid helium needed for cooling, supports the cavity and is part of the tuning mechanism. The tank is made from titanium since the thermal contraction relative to niobium is 20 times smaller than for stainless steel. Cooldown produces therefore negligible stress at the joints between cavity and tank and a stress of only $3\,\mathrm{N/mm^2}$ in a cavity that was stress-free at room temperature. With a stainless steel tank this number would rise to an untolerable $60\,\mathrm{N/mm^2}$ unless the tuning mechanism would be operated during cool-down. Titanium has the additional advantage that it can be directly electron-beam welded to niobium while stainless steel-niobium joints would require an intermediate metal.

The assembly of cavity and helium tank proceeds in the following sequence: the bellow unit is electron-beam (EB) welded to the conical head plate at one side of the cavity, a titanium ring is EB welded to the head plate at other side. The cavity is then introduced into the tank and the bellow as well as the titanium ring are TIG welded to the vacuum vessel. The two-phase He tube is rigidly connected to one end of the He tank and equipped with a bellow at the other end to permit longitudinal expansion relative to the He tank.

3.2.1.9 Magnetic Shielding

In principle, a perfect type II superconductor should expel the magnetic flux from its volume when cooled down in a static magnetic field smaller than B_{C1}. In niobium cavities, however, the magnetic flux is found to be trapped in the walls if the cavity is cooled down in a small external field of a few Gauss. The pinning of the flux lines is attributed to lattice imperfections in the niobium or to surface contamination. Trapped magnetic flux gives rise to an RF dissipation, which can be represented by a local surface resistance:

$$R_{surf} \simeq R_n \frac{B_\perp}{B_{c2}}$$

where R_n is the normal-state surface resistance of niobium and $B_\perp$ is the component of the ambient magnetic field that is perpendicular to the cavity surface. For a TESLA cavity this corresponds to an average surface resistance of 0.35 nΩ/mGauss, in good agreement with experimental results. In order to achieve $Q_0 = 3 \cdot 10^{10}$, the residual

surface resistance due to trapped flux must be smaller than 3 nΩ, corresponding to a remanent field of < 10 mGauss.

At the latitude of Hamburg, the earth magnetic field has a magnitude of 400 mGauss with roughly equal horizontal and vertical components. The necessary magnetic field attenuation is achieved by combining passive shielding and active compensation with Helmholtz coils. A two-step passive shielding is provided by the vacuum vessel of the cryomodule and by high-permeability cylinders around the individual cavities. The vacuum vessel is made from conventional steel with a remanent field in the order of several Gauss. To remove the remanence a "premagnetization" technique [14] has been applied. For this purpose a 40-turn toroidal coil is mounted on the cylindrical vessel and subjected to a current cycling between $\pm I_0$ at a rate of 6 A/s where I_0 starts at 400 A and is gradually reduced to zero. The resulting attenuation of the ambient field is found to be better than expected from a cylinder without any remanence. The explanation is that the procedure does not demagnetize the steel but rather *premagnetizes* it in such a way that the dangerous axial component of the ambient field is counteracted. This interpretation becomes obvious if the cylinder is turned by 180°: in that case the axial field measured inside the steel cylinder is almost twice as large as the ambient longitudinal field component. In Fig. 3.2.13a we have plotted the ambient field in the experimental hall and the field along the axis of the steel vessel after premagnetization. The striking observation is that the steel vacuum vessel by itself is almost capable of achieving the desired reduction to 10 mGauss, except near the ends. However, it is important to apply the premagnetization procedure at the exact location and orientation of the cryomodule.

The shielding cylinders of the TTF cavities are made from Cryoperm which retains a high permeability of more than 10000 when cooled to liquid helium temperature. Figure 3.2.13b shows the measured horizontal, vertical and axial components inside a cryoperm shield at room temperature, which was exposed to the Earth field of a few hundred mGauss. The combined action of premagnetized vacuum vessel and cryoperm shield is obviously more than adequate to reduce the ambient field to the level of a few mGauss. An exception are the end cells of the first and last cavity near the end of the cryomodule where the vessel is not effective in attenuating longitudinal fields. Here an active compensation is possible. With an arrangement of three Helmholtz coils, mounted on the end section of the steel vessel and the interconnection to the next cryomodule, the fringe field at the last cavity can be reduced to a harmless level.

3.2.2 The Module

The module described here is essentially identical to the one presently built for the TESLA Test Facility [15]. Based on the experiences that will be gained at the TTF a redesign will be made in due time.

The present TTF layout of the cryostat was largely driven by the goal to reduce the cost compared to existing superconducting cavity systems.

The concept is to build large modules incorporating many 9–cell cavities (eight at present), quadrupoles, steering coils and a beam position monitor and to combine

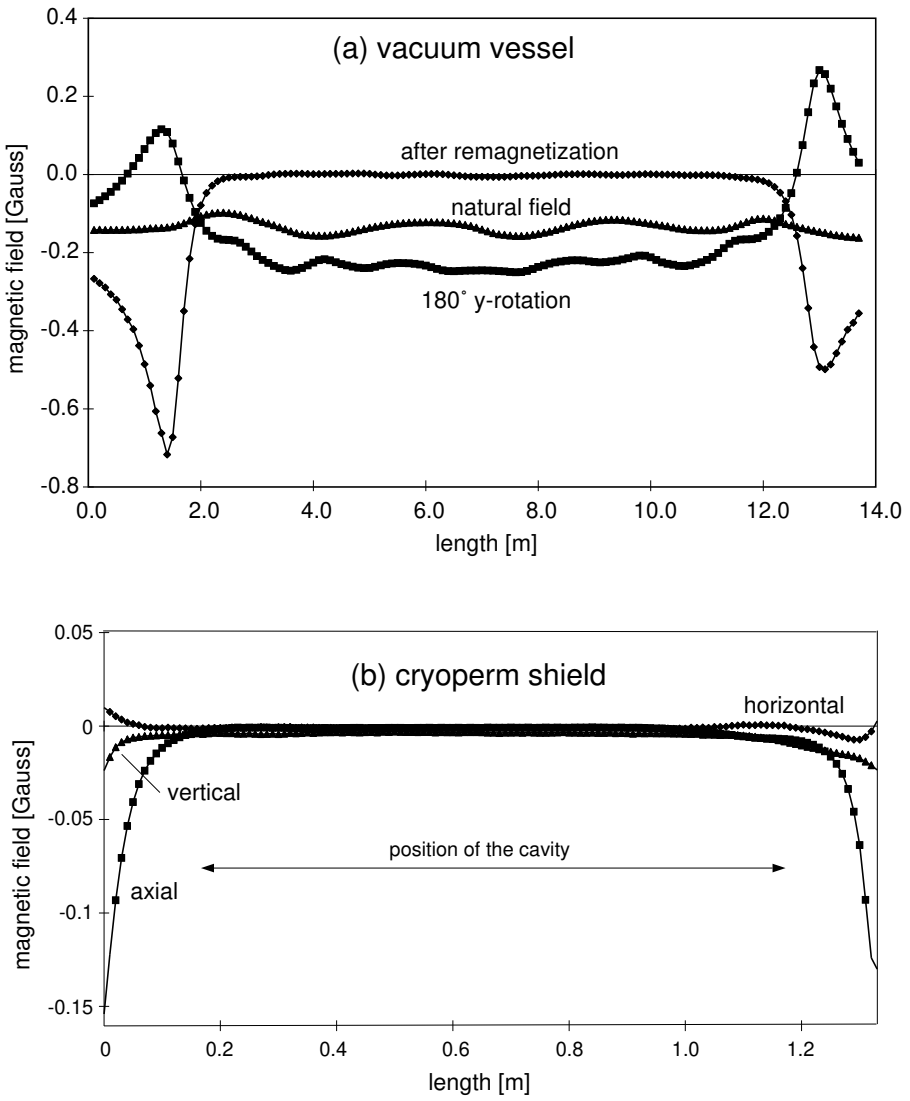

Figure 3.2.13: *Shielding of Earth magnetic field. (a) Shielding of axial component by the steel vacuum vessel of the cryomodule. (b) Shielding of axial, horizontal and vertical components by the cryoperm shield surrounding the cavity (without vacuum vessel).*

these modules to a continuous cryogenic string of about 2.5 km length. The helium distribution system needed to operate the superconducting cavities at 2 K and the magnets at 4.5 K at low thermal losses is also integrated into the cryostats. There will be only one cryogenic supply box at the end of the string. This basic concept avoids the large number of warm to cold transitions and the separate cryogenic supply boxes which constitute a major fraction of the cost of present superconducting cavity systems.

3.2.2.1 The Cryostat

Figure 3.2.14 shows a longitudinal view of the cryostat. The 300 mm diameter helium two-phase pipe is the main support beam for the accelerator module. The two-phase pipe is supported from above by three support posts that provide the necessary thermal insulation from room temperature. These posts are fastened to large flanges on the upper part of the vacuum vessel by adjustable suspension brackets. The purpose of the adjusting mechanism is to allow for the accelerator module axis to be brought into its proper position, independent of the absolute position of the vacuum vessel flanges on which it rests.

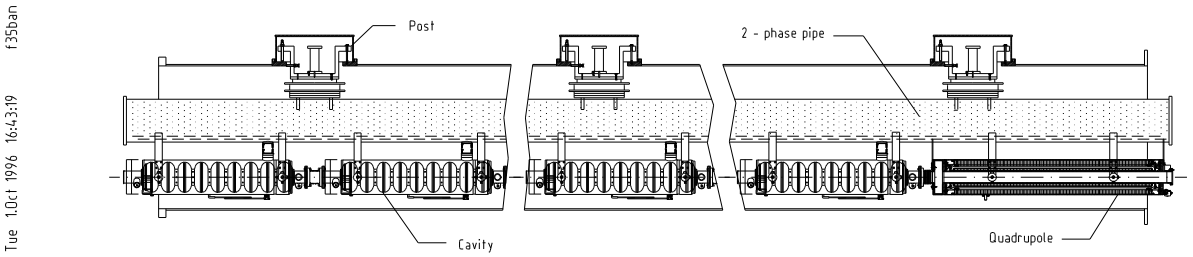

Figure 3.2.14: *Longitudinal view of the cryostat*

In the longitudinal direction the center post is fixed to the vacuum vessel while the two end brackets are allowed to move in the axial (z) direction to accommodate differential shrinkage during temperature cycling. The posts consist of a fiberglass pipe terminated by two shrink - fit stainless steel flanges. At appropriate intermediate positions, optimized to minimize the heat leak, two additional shrink - fit flanges are provided to allow intermediate heat sink connections to 4.5 K and 70 K. The post diameter has been chosen to push up the assembly main mechanical resonance frequency, corresponding to a pendulum-like motion in the x - y plane to 19 Hz and in the x - z plane to 20 Hz. These resonances are significantly above the dangerous 5 Hz (rep. rate) frequency. A further shift of the latter resonance away from the integer multiple of the rep. frequency seems necessary, though.

The 8 cavities (and the quadrupole package in the case of some of the modules) are attached to the two-phase pipe by means of stainless steel brackets equipped with adjusting screws for alignment.

The support system is designed to allow the accelerator module to move with respect to the vacuum vessel during thermal cycling. As the center point of the assembly is fixed to the vacuum vessel, the outer ends will be displaced longitudinally by up to 15 mm. The cavity main couplers must have sufficient flexibility to accommodate a displacement of the same magnitude. For a redesign of the cryostat rigid input couplers will also be investigated.

The cryostat includes two aluminum radiation shields at nominal temperatures of 4.5 K and 70 K. Each shield is divided in half longitudinally and each half consists of one upper section and six lower sections. The upper sections are supported by the post intermediate flanges. They are fixed to the center post but can slide on the end posts in the axial direction to avoid buildup of stress during thermal cycling. Experience with the earlier TTF cryostat design has shown that to reduce costs it is best to use cooling pipes that are directly welded to the aluminum shields and to weld the shields together where required. This design is similar to that successfully used on the SSC, LHC and HERA magnet cryostats.

Blankets of Multilayer Insulation (MLI) are placed on the outside of the 4 K and 70 K shields. The 4 K shield blanket is made of 10 layers while the 70 K blanket contains 30 layers. In addition, the cavity helium vessels, gas return pipe and 4 K pipes are wrapped with 5 layers of Multilayer Insulation to reduce heat transfer in the event of a vacuum failure.

The cryostat outer vacuum vessel is constructed of carbon steel and is evacuated to a pressure of less than 10^{-6} mbar during operation. Its design critical internal over pressure is 1.25 bar. Adjacent vacuum vessels are connected to each other by means of a cylindrical sliding sleeve. The vacuum vessel of the cryostat for the TTF are connected by sliding sleeves with O-Ring seals similar to the connection of the HERA s.c. magnets. For the linear collider a cheaper welding solution will be used (see also section 3.2.3). Radiation shield bridges are also provided. A relief valve on the sleeve and appropriate venting holes on the shields prevent excessive pressure build-up in the vacuum vessel in the event of accidental spills of liquid He from the cavity helium vessels. Wires and cables of each module are brought out at the module itself using flanges equipped with vacuum tight connectors. Figure 3.2.15 shows a cross section of the cryostat.

The following piping necessary for the cryogenic operation of the linac is incorporated in the cryostat:

1. The 2 K forward line: This line transfers single phase helium through the cryostat to the end of the string of modules furthest away from the refrigerator.

2. 2 K two-phase line: This line supplies the cavities with liquid helium and returns the cold gas pumped off the saturated He II baths to the refrigeration plant. This line is connected to the cavity helium vessels via a tube containing bellows for adjustment purposes. This line is also a key structural component of the cryostat (see the alignment and assembly section).

3. The 4.5 K forward and return lines: The 4.5 K forward line cools the quadrupole/-correction magnet package. The 4.5 K return line cools the 4.5 K radiation shield and the 4.5 K intercept on the main coupler.

4. The 40 K forward and 70 K return lines: The 40 K forward line cools the High Temperature Superconducting (HTS) current leads of the quadrupole and correction magnets. The 70 K return line cools the 70 K radiation shield, the 70 K

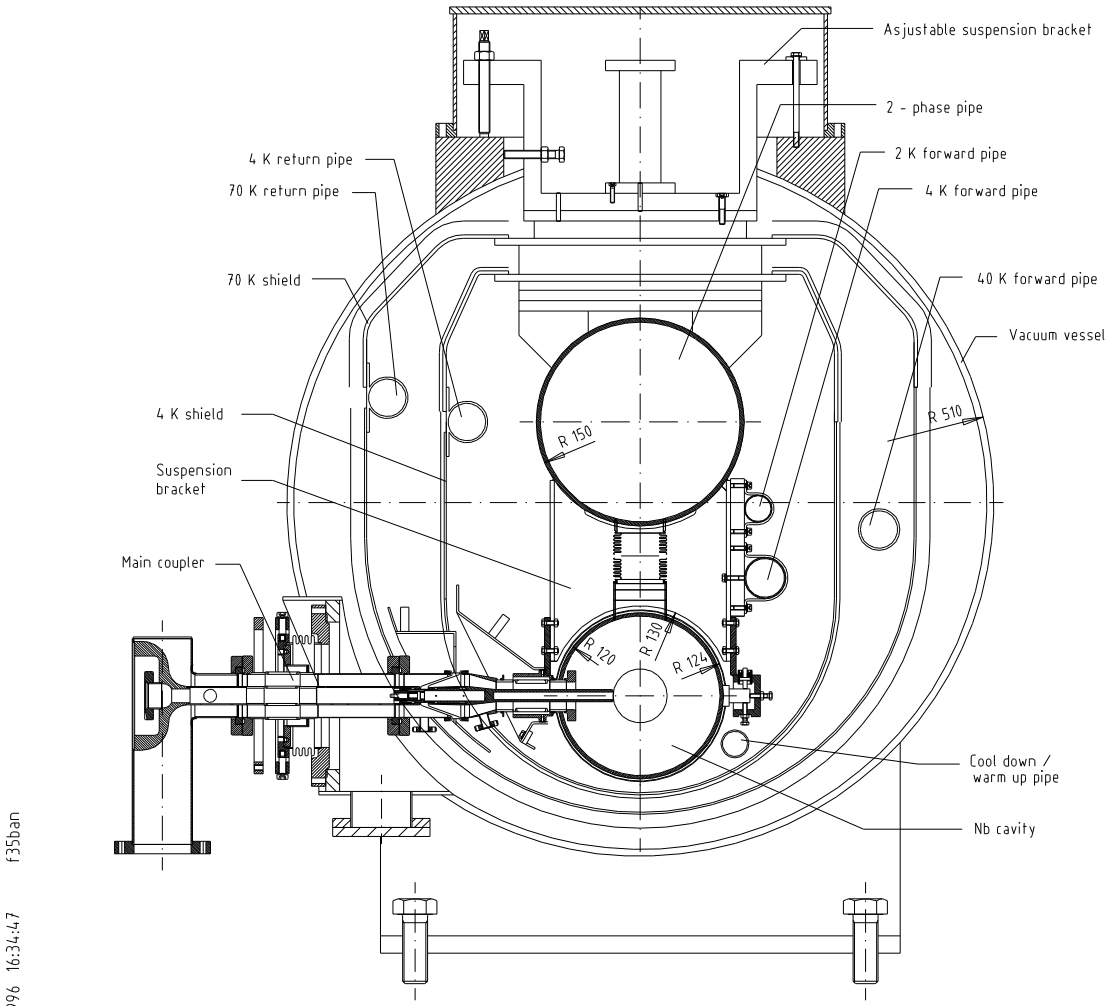

Figure 3.2.15: *Cross section of cryostat*

intercept on the main coupler and the HOM absorber in the cryomodule interconnection region.

5. Warm up/cool down line: This line parallels the two-phase supply line and connects to the bottom of each of the cavity helium vessels. It is used during cool down and warm up of the cryostat.

All cryogenic lines with the exception of those connected to the cavity He vessel must be able to withstand a test pressure of 20 bar absolute. The lines connected to the cavity He vessel must be able to withstand 4 bar absolute.

The helium lines of adjacent modules will be connected by welding similar to the

connection of HERA s.c. magnets making use of welding machines. The beampipes of adjacent mudules will be joined by flange connection (see section 3.2.3).

The cryostat must maintain the cavities and quadrupoles at their operating temperatures. For the cavities this temperature is 2 K and for the quadrupoles the operating temperature is 4.5 K. The static heat load is determined by the cryostat design while the total heat load is dominated by the RF losses and thus principally determined by the cavity performance. Table 3.2.3 shows the predicted heat load for a cryomodule.

The alignment requirements are driven by the beam dynamics. The result is that the axes of the 8 cavities must be aligned to the ideal beam axis to within 0.5 mm and those of the quadrupoles to within ± 0.1 mm within one betatron wavelength (the latter tolerance is less critical if beam-based methods to align the quadrupoles are applied). Additionally, the vertical mid plane of the quadrupole package must be aligned to the vertical direction to ≤ 0.1 mrad.

The alignment of the components is done while the cryostat is warm. In the TTF cryostats it will be investigated how well these alignments are maintained during installation, cool down and operation.

In order for the cavity performance not to be degraded by trapped magnetic fields, the cryostat must reduce the ambient magnetic field at the outer wall of the cavities to $\leq 0.5\,\mu$T.

In order to meet the $\leq 0.5\,\mu$T residual field requirement, a combination of active and passive magnetic shields is used. The active shield consists of a series of Helmholtz coils wrapped around the outside of the vessel. When powered, these coils will do a good job of canceling out the average longitudinal field. Passive shields made by cylinders of Cryoperm placed around the cavity helium vessels serve to reduce the remaining magnetic field. The vacuum vessel is made of soft steel and is demagnetised before assembly of the cryomodule.

The TESLA beam optics design requires different quadrupole strengths along the length of the linac. As a result, there are 7 different types of cryostats. The standard one without a quadrupole and 6 others with quadrupoles of different lengths (see Table 3.2.4)

The standard cryostat is 11.37 m long and has an outer diameter of roughly 1.2 m. Each cryostat contains 8 superconducting RF cavities (each enclosed within its own helium vessel).

3.2.2.2 Quadrupole and Correction Magnets

The quadrupole package is shown in Fig. 3.2.16. It consists of

- a superferric quadrupole enclosed in a stainless steel vessel cooled by supercritical helium at 4.5 K (at least less than 5.2 K),
- a pair of dipole correction coils wound on the beam pipe inside the quadrupole to provide horizontal and vertical correction dipole field,
- an RF beam position monitor (BPM) consisting of a pill box RF cavity, rigidly connected to the quadrupole,

	static (W)	dynamic (5 Hz)+static (W)
2 K		
RF load		7.32
radiation		
supports	0.60	0.60
input coupler	0.24	0.36
HOM load		1.54
HOM coupler	0.10	0.32
HOM coupler cable		0.35
beam tube bellows (9)		0.20
cables	0.12	0.12
Total	**1.06**	**10.81**
4 K		
RF load		
radiation	3.98	3.98
supports	2.40	2.40
input coupler	2.52	3.24
HOM load		
HOM coupler	1.00	1.69
HOM coupler cable		1.13
cables	0.37	0.37
Total	**10.27**	**12.81**
70 K		
RF load		
radiation	22.74	22.74
supports	6.00	6.00
input coupler	18.00	30.60
HOM absorber		16.11
cables	3.72	3.72
Total	50.46	79.17

Table 3.2.3: *Heat load for module of 11.37 m length (without quadrupole)*

- three pairs of conduction cooled current leads where the cold part is made from High Temperature Superconductor (HTS). The current leads run from the liquid He vessel to a flange on the cryomodule vacuum vessel.

Quadrupoles Each linac contains quadrupoles for beam focusing, incorporated at the beam exit end of each second cryomodule up to an energy of 50 GeV, at each third cryomodule between 50 GeV and 150 GeV and at each fourth cryomodule between 150 GeV and 250 GeV. The required integral field gradient generally varies linearly

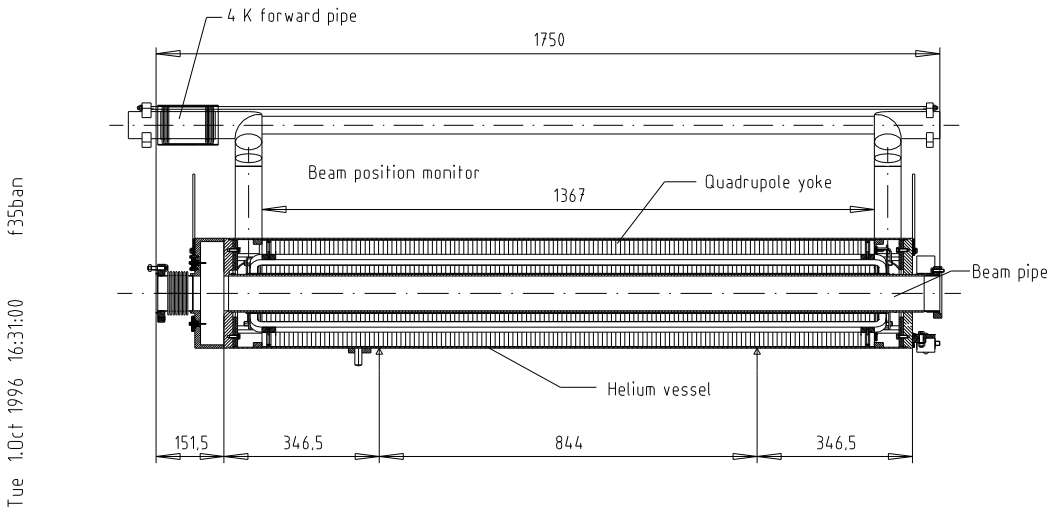

Figure 3.2.16: *Quadrupole package (longitudinal cut)*

with beam energy reaching a maximum of 31.03 T. This value already includes an upgrade of the accelerating voltage gradient in the cavities from the nominal 25 MV/m to 40 MV/m which would result in a 400 GeV beam energy for each linac. Because of the change in quadrupole per number of modules there is a step in the required integral field gradient at 50 (80) GeV and at 150 (240) GeV.

Due to easy manufacturing, easy alignment and low amount of superconductor required the quadrupoles are chosen of the superferric type with a maximum gradient of 22.7 T/m. As the integral field gradient scales with the beam energy and in order to provide maximum flexibility for beam-based alignment and beam optics, all quadrupoles need individual currents. Therefore, in order to limit the required cooling power, the maximum current is limited to less than 100 A.

With the above mentioned maximum field gradient of 31.03 T the maximum length of the quadrupole field is 1.367 m. The total length of the quadrupole package including coil ends, mirror plates, helium vessel end plates, beam position monitor, bellow and connection flanges amounts to 1.750 m. This length generally is needed only in the cryogenic unit of the high energy end. At lower energies the length of the quadrupole package is reduced in steps generally from unit to unit. This leads to 6 different lengths of quadrupole packages as shown in Table 3.2.4.

A later doubling of the linear collider energy could be achieved by doubling the whole length of the collider and shifting the collision point from between the first two linacs to the end of the second linac (the end of the whole collider in the first version). In this case, the electrons are accelerated in the second linac from 250 (400) to 500 (800) GeV running through it in a direction opposite to the previous one. For beam focusing in this extended version, quadrupoles of full strength (31.03 T) are needed in every fourth cryomodule up to 560 GeV, and in every sixth cryomodule up to the end (800 GeV). The same structure is foreseen for the first linac which would also permit

type	int. grad. (T)	max. grad. (T/m)	field length (m)	add. length (m)	quad. pack. length (m)
B	6.14	22.7	0.270	0.383	0.653
C	10.94	22.7	0.482	0.383	0.865
D	14.06	22.7	0.619	0.383	1.002
E	20.84	22.7	0.918	0.383	1.301
F	25.92	22.7	1.142	0.383	1.525
G	31.03	22.7	1.367	0.383	1.750

Table 3.2.4: *List of different quadrupole packages*

quadrupole type	number (standard version)	number (extended version)
B	108	72
C	96	64
D	146	78
E	136	68
F	224	40
G	102	490
Total	812	812

Table 3.2.5: *Required numbers of quadrupoles of different types (total collider)*

the beam to run in the opposite direction for collisions with protons from HERA. The required numbers of quadrupoles for the standard and extended versions of TESLA are listed in Table 3.2.5.

The superconducting coils are of the racetrack type, wound from a wire of rectangular cross section (about 200 turns per pole) and impregnated with epoxy. The yoke is made from 5 mm thick punched laminations assembled on a tool and locked through keys which give the required positional accuracy (0.02 mm). The keys are connected through pins and bolts to the outer stainless steel helium vessel tube surrounding the quadrupole and to the stainless steel end plates of the vessel.

Both end plates are covered with soft steel magnetic mirror plates for reducing the fringe field at the position of the superconducting cavities. The helium vessel endplate on the beam entrance side of the quadrupole is also a part of the beam position monitor (pill box type).

The main parameters of the quadrupoles are listed in Table 3.2.6.

Correction Dipoles The purpose of the correction dipoles is beam steering. They are layed out for a maximum orbit steering range of ± 3 mm per correction coil. The maximum integral field required for this purpose is 31 mT·m at the high energy end. However the integral field scales with energy in the same manner as the quadrupoles leading to 12.4 mT·m at 50 (80) GeV (with a dipole in every second cryomodule) and

quadrupole type	superferric
beam tube inner diameter	78 mm
pole tip (yoke inner) radius	45 mm
yoke outer radius	116 mm
yoke length	
B	0.270 m
C	0.482 m
D	0.619 m
E	0.918 m
F	1.142 m
G	1.367 m
coil cross section	16 mm × 13 mm
max. current	100 A
max. field gradient	22.7 T/m
max. field at conductor	2.1 T
b6 at r = 10 mm	$3.5 \cdot 10^{-4}$
b10 at r = 10 mm	$8.2 \cdot 10^{-7}$
conductor	rectangular cross section

Table 3.2.6: *Main parameters of quadrupoles*

24.7 mT·m at 150 (240) GeV (with a dipole in every third cryomodule). There are two dipole coils in each quadrupole, one for horizontal and one for vertical correction. The coils are one layer windings of 15 turns of round multifilamentary superconducting wire on the beam pipe which closes the helium vessel from the inside. They have the same length as the quadrupole. The maximum current is ~ 33 A. The main parameters of the correction dipoles are listed in Table 3.2.7.

Beam Position Monitor The beam position monitor (BPM) is of the pill box type attached to the beam entrance end plate of the helium vessel. It is equipped with two antennas for each direction (x and y). The beam position measurement resolution is aimed at 10 μm and the installation tolerance w.r.t. the quadrupole axis at 0.1 mm. The beam pipe part between the beam position monitor and the cavity contains a stainless steel bellow to compensate for misalignments and cooldown motions. With the exception of the beam position monitor cavity, the whole beam pipe of the quadrupole package as well as the bellows are copper coated inside.

Heat Loads The heat loads calculated for the quadrupole package of maximum length are listed in Table 3.2.8. As can be seen, due to the use of HTS current leads the heat load on the 4 K level is rather low. The load on the 2 K level takes the connection to the cavities into account. Dynamic losses occur at the beam tube bellows and at the beam position monitor.

dipole type	one layer cosΘ in superferric quadrupole
beam tube inner diameter	78 mm
pole tip (yoke inner) radius	45 mm
yoke outer radius	116 mm
yoke length	
B	0.270
C	0.482
D	0.619
E	0.918
F	1.142
G	1.367
average coil radius	42.5 mm
max. current	33.2 A
max. Ampere turns	1494 A
max. field	44 mT
number of turns	45
max. field at conductor	0.98 T
b3 at r = 10 mm	$7.8 \cdot 10^{-3}$
b10 at r = 10 mm	$9.5 \cdot 10^{-4}$
superconducting wire	round, 0.98 mm Ø

Table 3.2.7: *Main parameters of correction dipoles*

Quadrupole Supports and Alignment The quadrupole package is supported at the 300 mm diameter two-phase pipe in the same manner as the cavities. The system consists of two brackets (one at each end of the helium vessel). Bolts in the brackets allow the adjustment of the quadrupole unit with respect to the ideal beam axis inside the cryomodule with the aid of reference targets on temporary extension arms attached to each helium vessel end.

Alignment and survey play an important role because of the given tolerances (Table 3.2.9, rms values).

The alignment of the quadrupole is the most critical one. In order to achieve the required tolerances we have chosen:

- a superferric quadrupole where the accuracy of the field is mainly given by the accuracy of the yoke;
- a laminated yoke where the contours are most accurate by punching and due to punching keys locating the yoke laminations precisely;
- a helium vessel with pins to locate the keys and yoke inside the vessel;
- grooves in the endplates accurately machined to take over the position of the keys;

	static (W)	dynamic (5Hz) + static (W)
2 K		
bellows		0.02
BPM		0.07
radiation		
conduction	0.10	0.10
cable	0.01	0.01
Total	**0.11**	**0.20**
4 K		
BPM		0.10
radiation	0.61	0.61
current leads	0.02	0.03
cable	0.03	0.03
Total	**0.66**	**0.77**
70 K		
radiation	3.50	3.50
current leads	14.03	32.04
cable	0.26	0.26
Total	**17.79**	**35.80**

Table 3.2.8: *Loads of a full length (1.75 m long) quadrupole package*

component	tolerance (rms)
cavity position	0.50 mm
quadrupole position	0.10 mm
quadrupole field angle	0.10 mrad
quadrupole jitter	1 μm
BPM position	0.1 mm

Table 3.2.9: *Tolerances of alignment*

- reference targets at the helium vessel end plates machined in one set-up with the endplates;
- mechanical integration of the beam position monitor with the helium vessel end plate.

At the TTF accelerometers will be attached to the cold mass of the quadrupoles in order to measure vibrations in x and y direction. The measuring sensitivity at 2 Hz is about 20 nm and is mainly determined by the noise of the amplifier. The actual vibration tolerance in the TESLA linac is as large as 1 μm, because orbit jitter is

removed within one beam pulse by means of the fast orbit feedback.

3.2.2.3 Assembly and Alignment

The assembly and alignment of the cryostat are closely linked together.

First, the two-phase pipe (TPP), which is the basis for the support system, is straightened to better than ± 3 mm and heat treated to relieve any residual stress that might cause deformation later in the assembly process. Then this pipe is transferred to a work bench on which an ideal beam axis is defined. The pipe is placed on three supports that reproduce the effect of the three posts in the final cryostat. While on these supports the pipe is adjusted so that the centers of its end sections define the pipe reference axis to within ± 2 mm. The brackets and the support post flanges are then welded on to within ± 1 mm of their ideal position. The adjustable suspension brackets (ASBs) and the cryostat fiberglass support posts are also attached with this precision.

Next, the upper parts of the thermal radiation shields, cryogenic pipes and cabling are attached. This portion of the cryostat i.e. the structure excluding the cavity string and vacuum vessel is referred to as the cold support system. Three optical targets (Taylor - Hobsen spheres) are attached to the top of the three cryostat support posts. Using the ASBs these targets, and thus the posts and the TPP, are aligned within 0.1 mm to the previously defined ideal beam axis. They are also aligned to a horizontal reference plane to within 0.2 mm/m. The cold support system is flexible to a degree and may go out of this alignment during transport and further assembly. However, as long as the optical targets can be realigned using the ASBs, the alignment of the cold support system relative to the ideal beam axis can be recovered.

In the meantime, an ideal axis is defined for each cavity before it is welded into its helium vessel. An ideal axis is also defined for the quadrupole package which is also equipped with reference arms.

The objective of the final assembly of the cryostat is to attach the cavities and magnets to the cold support system and align the ideal axes of the cavities and magnets with the ideal beam axis defined on the cold mass. Of course, this also has the effect of aligning the cavity and magnet ideal axes with each other.

This work starts in the clean room where the cavities and quadrupole package are connected to each other by flanges. The cavities are aligned in the proper axial position (based on the position of the main coupler) and aligned so that the main coupler port axis is parallel to the floor. This cavity string is now moved out of the clean room to the first assembly station. At this station, the cold support system is lowered onto the cavity string attached to it via the support brackets and the connections between the helium vessels and the TPP are welded. The Cryoperm magnetic shielding is then installed. Next the cavities and quadrupole package are aligned to the ideal beam axis of the cold mass using adjustment screws at the support brackets. Bellows between the cavities on the beam tube and at the connections between the helium vessels and the TTP allow adjustment of the cavities relative to each other and to the quadrupole package. Once the alignment is finished the adjustment screws are locked in place via

set screws. The system is designed to keep the components in their aligned position during thermal cycling. The assembly is moved to the second station where the lower part of the thermal radiation screens, the MLI blankets, and remaining cabling are added.

This completed assembly is then moved to the third station where it is suspended between two cantilevers. The completed assembly is then inserted into the vacuum vessel. During this process, the ASBs are removed. Appropriate pins ensure that the ASBs can be replaced to $< \pm 0.1\,\mathrm{mm}$ of their original position.

Once the assembly is installed in the vacuum vessel, the Taylor - Hobsen spheres on top of the ASBs are brought back into alignment thus returning all components back to their appropriate position relative to the ideal beam axis of the cold mass.

As a final step, the axis defined by the Taylor - Hobsen spheres is transferred to another set of reference marks on the side of the vacuum vessel. It is these reference marks that are used to align the vacuum vessel (and thus the cold mass) to the beam axis of the linac.

3.2.3 Vacuum System

There are three vacuum systems on the collider linacs with different requirements: The beam vacuum system, the insulating vacuum system and the vacuum system for the room temperature part of the RF input couplers. The layout concepts of the systems are based on the experiences gained at HERA and in the TESLA Test Facility. With more experience from the TTF linac the concept may have to be modified.

3.2.3.1 The beam vacuum system

One of the major objectives for the beam vacuum system is to preserve the cleanliness of the superconducting cavities' surfaces and thus the operation at high gradients and high Q. So contamination by any sort of dust or condensation of gases during assembly and operation has to be absolutely avoided.

Therefore the string of 8 cavities for a module is at present assembled and the connections between adjacent parts are done inside the clean room. All parts which are connected to the cavity, input couplers for example, have to fulfill the same requirements concerning cleanliness and have to undergo similar treatments before the assembly. The string of 8 cavities and the beam pipe inside the quadrupole is evacuated and closed off by manual all metal valves in the clean room after assembly. There is some concern on the production of metallic dust by these valves. However, as they are only operated a few times this seems not very probable. This will be investigated in the Test Facility.

The present solution to connect adjacent cavities by flanges and a rather long compensator, which is necessary for independent tuning and mechanical decoupling during thermal cycles, fulfills the requirements on cleanliness. The compensator is a copper coated stainless steel bellow. For the linear collider a high filling factor saves on tunnel length. It will be designed for to keep the cavities as close together as possible

and to keep the bellows between cavities as short as possible. RF-shielding of the connecting bellows has been avoided in the present test setup as to prevent rubbed off dust particles which eventually could enter the cavity and cause field emission. The wake fields generated by the bellows are tolerable as they constitute only 12 % of the unavoidable longitudinal wake fields from the cavity itself. However, shortening of the bellows for the linear collider will be beneficial.

Investigations are planned to eliminate the flanges at the interconnection between cavities and to the input coupler by an adequate welding technique.

The way the beam vacuum of adjacent modules is connected in the linac tunnel is again dictated by the necessity to prevent dust from entering the cavity vacuum. The beam pipe section between the modules is installed in a local clean room, similar to the one which is used in the TTF–linac to assemble the vacuum system. The connecting beam pipe contains stainless steel bellows to allow for the thermal shrinkage of the cavity string during cool down. It is planned to also incorporate a HOM absorber into this section, which is at present in the beampipe inside the quadrupole. Its purpose is to absorb power from travelling HOM fields at a temperature level of 70 K, thus reducing the thermal load of the 2 K level.

The connecting beam pipe is pumped via a pumping port and a manual all-metal valve by an oil free pump station to avoid any pollution of the cavity system by hydrocarbons, which increase the probability of field emission. The gate valves to the neighboring cavity sections will only be opened when the connecting beam pipe is clean and evacuated.

The present layout of the beam vacuum does not foresee any sector valve within the cryogenic section of about 2.5 km length. Only at the sector ends short room temperature sections between adjacent cryogenic sections are foreseen which contain sector gate valves.

Ten permanent pumping ports are foreseen for a sector. The connection to the pumping port of a connecting beam pipe between modules is done via a double knee shaped pipe which penetrates the heat shields and the vacuum vessel. These ports will be used to pump the vacuum sections when the cavities are at room temperature and to make sure that there are no helium leaks in the system. The pumps will not be connected to the beam vacuum when the cavities are cold as the base pressure of the pump station is higher than the pressure in the beam vacuum.

In case a module would have to be removed from the tunnel, the manual gate valves to the neighboring modules are closed. If venting of the module is necessary it will be done with filtered, dust free and pure argon at laminar flow to avoid any contamination or transport of dust by turbulences.

In a vacuum system which is in great part surrounded by superfluid helium, one has to worry about leaks. In the design of the cavities the input coupler and the HOM coupler are located outside the helium vessel, thus avoiding the situation of flange connections or feed-throughs being exposed to liquid helium. Thus only through leaks in the wall of the cavity itself can helium get into the beam vacuum. The cavities which have been tested in the test facility have welds made by electron beam welding on the equator and the iris of each cell. Up to now no leak has been detected at a sensitivity

of 10^{-14} mbar/sec. The risk of leaks will certainly get even less when hydro-formed cavities become feasible.

3.2.3.2 Insulating vacuum system

The layout of the insulating vacuum system is strongly influenced by the experiences gained with the insulating vacuum system of the superconducting magnets at HERA.

As the O-Ring seals in the sliding sleeves which connect adjacent vacuum vessels caused a lot of problems at HERA due to leaks and large permeation it is foreseen to connect adjacent vacuum vessels by welding. The connections will be done with welding lips which allow for several openings by cutting and consequent welding by special tools. The penetrations of the vacuum vessel for the input couplers are sealed by O-Rings in the present cryostat. For the final layout of the cryostat a welding connection is also aimed for at these penetrations. The vacuum vessel is made from cheap carbon steel protected with an appropriate paint.

The various helium pipes will be connected between modules by welding in a similar way as it was done at HERA. There the experience with welding of the helium pipes between neighboring superconducting magnets has been very positive. Only a fraction of less than 0.1 % had a leaky weld. Very similar procedures to the ones established at HERA will be used to assure leak tightness or to localise leaks.

At HERA there is a vacuum barrier in each quadrupole cryostat that means about every 25 m. This barrier essentially is for free as it was used as mechanical support of the cold mass. These barriers were very helpful during installation and commissioning of the vacuum system and speeded up the leak check of the outer vacuum vessel and localisation of helium leaks. During operation, however, these barriers are permanently bridged by bypass tubes. Due to the larger number of helium tubes and the large diameter of the 2 K gas return tube a vacuum barrier is complicated in the case of the linear collider modules. At present it is assumed that there will be no vacuum barrier at all within a 2.5 km long sector. However, this topic needs further discussions and more detailed layout of the whole cryogenic system.

Again from the experience gained at HERA permanent pump stations will be necessary only every 250 m during normal operation due to the large conduction of the cryostat. However, there will be additional pumping ports at about 50 m distance which allow to connect movable pump stations for initial pump down and in case of a larger helium leak.

During pump down and leak test, about 50 pump stations will be concentrated in one sector. Once the sector is commissioned they will be moved to the next sector with only 10 pump stations remaining per sector. There will be no gauges on the system except at the pump stations.

At present it is assumed that the probability of helium leaks to the insulating vacuum is not much different from HERA, where there are presently three larger leaks which were there right from the beginning. It was only needed to place two additional pump stations nearby. The size of the leaks stayed stable and no further leak developed. The layout of the helium vessel has avoided the potential of leaks at the penetrations

of the feed throughs and contains only circular welds.

3.2.3.3 Input coupler vacuum system

The present layout of the input coupler has two ceramic windows, one which is at a temperature of 70 K during operation and one at room temperature. There are several reasons for having a second ceramic window in the input coupler: It enables one to close off the cavity completely by mounting the coupler up to this window in the clean room, thus preventing any contamination during the further assembly of the module. If a crack of the ceramic window occurs during operation there will be no danger of gas and dust entering the cavities as there is vacuum on both sides of the window. In case the outer window develops a crack the inner window will protect the cavities.

The disadvantage of this concept is that one needs an additional vacuum system for the room temperature side of the input coupler. The tempting possibility of connecting the outer part of the coupler to the insulating vacuum is not possible as the pressure may not be low enough due to leaks in the insulating system. Also conditioning of the couplers would become necessary after venting of the insulating vacuum system.

In the present concept pumping of the outer coupler part is achieved through slots or holes in the wave guide directly connected to the input coupler. All eight couplers are connected to a common vacuum header which is pumped by one ion getter pump.

The vacuum system of the input coupler needs further study to simplify it as much as possible. Special care will be taken to select proper materials and treatments to achieve a low thermal out-gassing rate as well as low gas desorption during RF-operation. It is planned to bake and precondition the input coupler on the modules prior to the installation in the tunnel.

3.2.4 RF Generation and Control

3.2.4.1 Introduction

In each TESLA cryomodule there are eight cavities. The peak RF power needed for one nine cell cavity at full gradient and maximum beam current, i.e. 25 MV/m and 8.22 mA during the pulse, is 213.5 kW.

Based on the experience gained from the TTF we plan to supply a set of 4 cryomodules with a 10 MW RF source.The nominal peak power needed for 4 cryomodules is only 6.83 MW, but as we will show in section 3.2.4.8, a power margin of 10-30 % is needed for phase and amplitude control. The maximum available pulse power of 10 MW provides, therefore, an additional power reserve of more than one MW.

The RF source foreseen for TESLA is a 10 MW Multibeam-klystron (MBK) which has 2 output windows, each delivering 5 MW.

Since, especially at the beginning of the RF pulse, there is almost fully reflected power, circulators will be used to limit the reflected power seen by the klystrons to 1.2:1 VSWR or better.

The beam pulse consists of 1130 micropulses with a spacing of 0.708 μs, and 530 μs are needed to fill the cavity with RF. Hence the RF pulse length is 1.33 ms. The

repetition rate is 5 Hz for the major part of the linac. At the low energy end of the linac there are some sections running at the repetition rates of 10 and 20 Hz.

In the following we will describe the Multibeam-klystron which is specially being developed for TESLA. Subsequently we describe the modulator which is presently in use in the TTF and which would also be appropriate for TESLA. Then, an alternative modulator concept, the SMES, is presented, followed by a possible scenario for the primary power handling and the distribution of pulsed electrical power in the tunnel. The last sections are devoted to the wave guide RF distribution system and to the low level RF system for phase and amplitude control.

3.2.4.2 The 10 MW Multibeam-klystron

In the spectrum of the commercially available L-band klystrons there are several tubes, which can deliver about 5 MW peak power for pulse lengths up to 2 ms. For 10 MW peak power typical pulse lengths lie rather in the 100 μs range. For the TTF we had decided to power the four cryomodules by two 5 MW klystrons TH 2104 C from Thomson. These are conventionally pulsed cathode klystrons without modulating anode.

Our motivation to look for another RF source for TESLA was threefold:

In view of the total AC power consumption for the RF system of TESLA, which is of the order of 50 MW, we felt that any possibility to increase the 45 % efficiency of the 5 MW tubes should be exploited to reduce operation cost.

Furthermore, doubling the RF power to 10 MW will reduce the total number of klystrons to 604. From this a reduction of capital investment cost is expected, since the experience of existing klystrons shows that the solution of many smaller tubes is more expensive than fewer high power tubes.

Finally, we are heading for an increase in tube lifetime from today's 15-20000 hrs to at least twice as much. It is believed that this goal can be achieved by the use of specially coated cathodes with reduced operation temperature.

The electronic efficiency of a klystron is highest for minimum beam current I and maximum beam voltage U because the space charge forces of the beam counteract the beam bunching. A characteristic quantity, which allows to estimate the maximum achieveable efficiency of a klystron, is the perveance defined as $P = I/U^{\frac{3}{2}}$. For $P = 2 \cdot 10^{-6}$ an efficiency larger than 45 % is possible whereas at $P = 0.5 \cdot 10^{-6}$ one may hope for more than 70 % efficiency. For a single beam 10 MW klystron this implies a gun voltage of 240 kV. The design of a gun at this voltage level and pulse length would be very critical. The main limitation for high peak power and pulse duration in klystrons is electrical breakdown which can occur along the insulators or between the electrodes of the gun and in the RF circuits of the tube. For very high peak power arcing can occur across the gap of the output cavity since the gap voltage has to be comparable to the gun voltage for high efficiency. From existing tube performances the empirical relation $E \cdot V = 100/\tau^{0.34}$ between achieved pulse length τ[s], max. field strength E [kV/mm] in the gun region and gun voltage V [kV] has been established [16].

Therefore the favoured solution is a Multibeam–klystron with 7 beams, each having the microperveance of 0.5, proposed by Thomson. The gun voltage will be only 110 kV

and the total beam current 130 A. There will be two RF output windows. From the experience with the existing 5 MW klystrons we know that this window is uncritical.The solenoid focusing power will be only 4 kW. The layout of this klystron is sketched in Fig. 3.2.17.

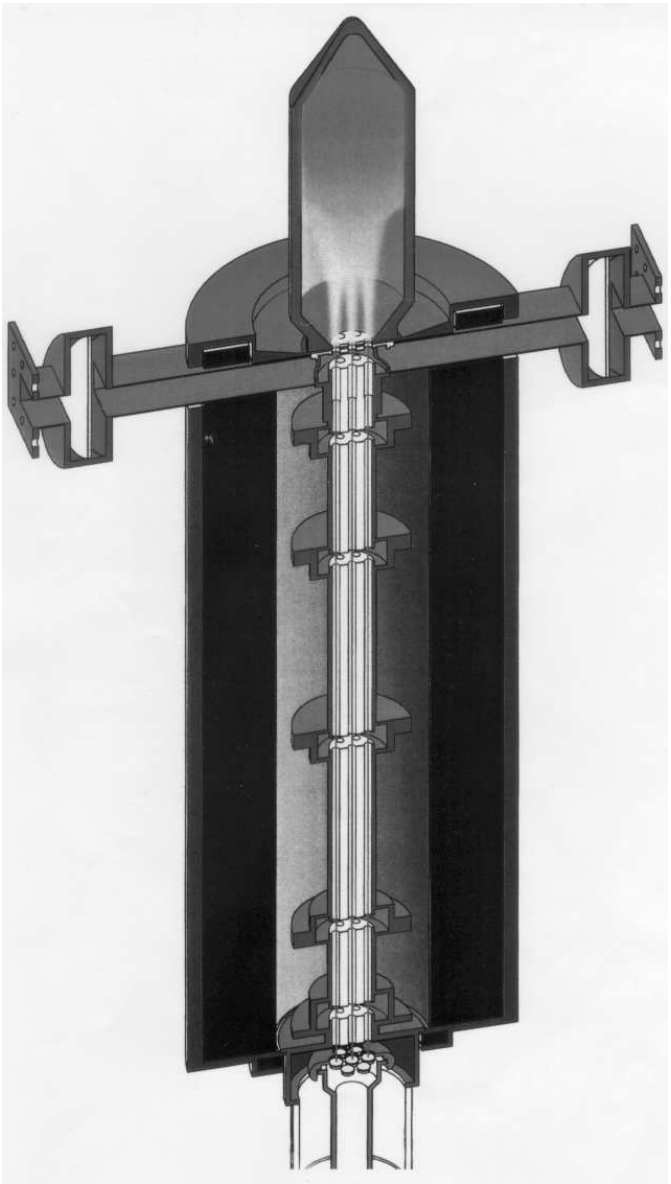

Figure 3.2.17: *Schematic layout of the 7 - beam klystron.*

A contract has been signed for the development of a 1.3 GHz 10 MW Multibeam-klystron with 1.7 ms pulse length and 10 Hz repetition rate. The specified efficiency is between 70 % and 75 %. Commissioning is forseen for fall 1997.

A prototype of a 64 kW 4-beam klystron operating at 425 MHz has demonstrated

an efficiency of 44 %. The cathode voltage was only 18 kV [17]. A proof of existence and feasibility of 5 MW L-band MBKs operating at ms pulse lengths comes from the Moscow Meson Factory, where 33 MBKs are running. These tubes have 6 beams and the operating voltage is only 75 kV. The microperveance of 1.4 per beam should allow for a higher efficiency than the 40 % of the actual tubes.

A fact which is often ignored is that reducing the RF output power by decreasing the drive power alone will also decrease the efficiency since reducing or switching off the RF drive power has no influence on the average dc electron beam current, and in the latter case the full energy of the beam is wasted in the collector. The efficiency of the device becomes zero.

Large power variations are performed more efficiently either by variation of the operating voltage or by means of a modulating anode or a gridded gun. For high power tubes which operate at cathode voltages well above 100 kV there are practically no tubes with a modulating anode because of isolation problems, and the technology of gridded guns for high power tubes is not yet very mature. Therefore our Multibeam-klystron will be a diode without modulating anode.

The design allows to decrease the saturation power limit by some 26 % by reduction of the gun voltage without loosing more than 5 % in efficiency. This is very important for the case where the maximum power needed, i.e. nominal power + regulation reserve, is below the maximum possible output power of the klystron.

The klystron 1 dB bandwidth is 3 MHz. This is more than adequate for fast response of phase and amplitude regulation loops.

Frequency:	1300 MHz	
RF Pulse length:	1500 μs	
Repetition rate:	10 Hz	
Beam Voltage:	110 kV	
Beam Current (total):	130 A	
Perveance per beam:	$0.5 \cdot 10^{-6}$	
Drive Power:	200 W max.	
Output Power:	10 MW peak	150 kW average
Body Dissipation:	15 kW max.	
Efficiency:	> 70 %	
Gain:	48 dB	
Bandwidth (1 dB):	3 MHz min.	
No. of beams:	7	

Table 3.2.10: *Design parameters of the Thomson multibeam-klystron*

The gain of 48 dB means that the drive power is below 160 W. This power can be generated at low cost with solid state amplifiers.

3.2.4.3 Other Possible RF Sources for TESLA

An interesting possible alternative to the MBK could be the Magnicon, a source developed at Budker Institute (Novosibirsk). It consists of a continuous electron beam which is deflected by the RF magnetic field of a circular deflection cavity [18].

In the subsequent drift space electrons deviate from the device axis and get into a stationary magnetic field of a solenoid. While entering the magnetic field the longitudinal velocity of the electrons is transformed into a rotational transverse one.

Further on, traveling along a helical trajectory in the output cavity, the electrons excite a TM_{110} oscillation mode. If the cyclotron frequency is equal to the one of operation, then the interaction can remain effective during many periods of RF oscillation resulting in a very high efficiency. Feasibility of the magnicon has been demonstrated by two prototypes. One has delivered 2.6 MW RF pulses of 30 μs length at 915 MHz. Here the electronic design efficiency was 85 %. The efficiency actually reached was 73 % due to the quality of the aluminum alloy used for cavity fabrication. The other magnicon was a frequency doubler which has demonstrated 25 MW output power at 7 GHz for 2 μs pulses. In this case the design efficiency of 60 % was reached.

It has been claimed that a 10 MW Magnicon with an efficiency close to 78 % could be built [19]. The disadvantage of the Magnicon is its high operating voltage. For the TESLA Magnicon it would be 250 kV.

There are also attractive features for TESLA from Klystrodes which are also called **I**nductive **O**utput **T**ubes (IOT). Here the beam is modulated with the RF frequency by a thin grid close to the cathode such that no drift space and bunching cavities as in a klystron are necessary. Without RF drive power the beam current is zero. The extra amount of RF power needed for phase and amplitude control in the superconducting cavities does not reduce the effective efficiency as in the case of a normal klystron. A disadvantage of this tube is its low gain which is well below 30 dB. The feasibility studies of such a tube for TESLA are, however, only in a very early stage.

3.2.4.4 Klystron Modulator Schemes

Already for the TTF we were confronted with the task of designing a cathode modulator for the 5 MW diode klystron which produces 130 kV pulses at a current of almost 100 A.

The solution of a switch tube in series with the klystron is not attractive. To our knowledge, at most one tube exists, which could switch currents of about 100 A for intervals like 2 ms. We were concerned whether this solution, if feasible at all, would be very expensive and unreliable.

The more exotic solution of a **S**uperconducting **M**agnetic **E**nergy **S**torage (SMES) seemed promising, but was too far from maturity to be used for the TTF in the first place. It will be described in the next section.

A proven solution consists of a **P**ulse **F**orming **N**etwork (PFN) in conjunction with a pulse transformer. This technique has been successfully used at SLAC, FNAL and at other places, but only with pulse lengths up to some hundred μs.

Evaluation of the costs of a 1.3 ms PFN stimulated search for other solutions. A very elegant solution, which has finally been adopted was proposed by Quentin Kerns

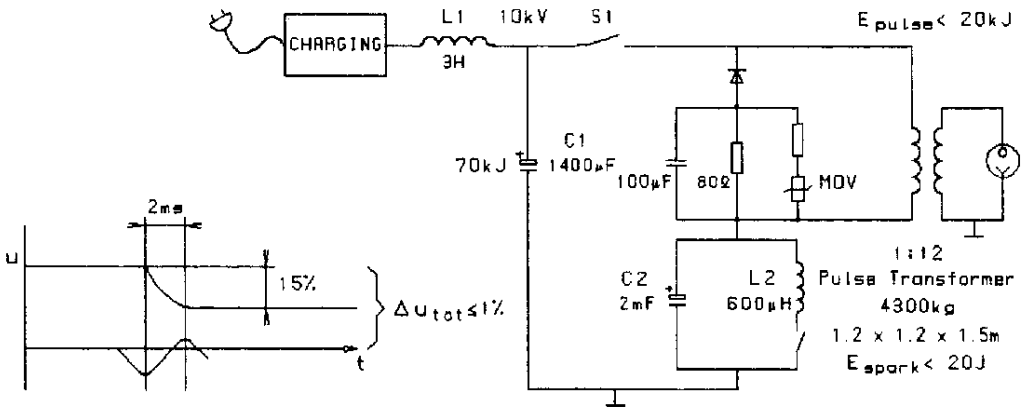

Figure 3.2.18: *Diagram of the TTF modulator with bouncer circuit. The bouncer circuit reduces the fluctuations of the pulse flat top to the* $\pm 1\,\%$ *level.*

from FNAL and is sketched in Fig. 3.2.18.

In operation, the DC power supply keeps capacitor C1 charged to the 9 kV level. The output pulse is started by turning on the **I**solated **G**ate **B**ipolar **T**ransistor (IGBT) switch S1, which connects C1 to the pulse transformer primary. The pulse is terminated after 1.5 ms (1.3 ms flat top + 0.2 ms rise time) by turning the IGBT off. The nominal current switched by the IGBT's is 1.56 kA. The primary pulse is stepped up to the klystron operating level by the 12 : 1 pulse transformer.

During the pulse, capacitor C1 discharges by 13 % of its initial voltage, putting an intolerable slope on the output pulse. To decrease the slope to the 1 % level without resorting to an 18 mF capacitor in the C1 location, the slope is corrected with a bouncer circuit. This is a resonant LC circuit which creates a single sine wave with a period of 7 ms. The bouncer is triggered slightly before the main pulse so that the linear, bipolar portion of the cycle is playing during the main pulse. The bouncer wave form cancels out the 13 % slope from C1, and reduces it to less than $\pm$ 1 %.

The need for a 1.3 ms pulse transformer, which is a fairly unique device, might be considered a disadvantage of this solution. For the TTF three such modulators were, however, built by FNAL and several suppliers for appropriate pulse transformers have been found. Here the pulse length was even 2.2 ms. The modulators have been running very reliably for several years for the TTF operation. A very detailed description of this modulator is given in [20] and [26].

The pulse rise time of these modulators is of the order of 150 μs, and the voltage droop during the pulse is $\pm$ 1 %. The measured overall wall plug power to useful HV conversion efficiency was 86 % for a pulse length of 2.2 ms. "Useful" here means that only the flat top of the HV pulse, which is good for RF generation, has been taken into

Electronic klystron efficiency	70 %
Electronic modulator efficiency	92 %
Rise time efficiency $\frac{T_p}{T_p+T_R}$	86.6 %
HV cable losses	2 %
Wave guide losses	4 %
Overall efficiency	52.5 %
Duty cycle	0.65 %
Total peak RF power	$4.125 \cdot 10^9$ W
Average RF power	26.8 MW
Wall plug power	51 MW
10 % power reserve for regulation	5.1 MW
Solenoid power	2.4 MW
Total wall plug power	58.5 MW
Nominal RF power to total wall plug power	
Conversion efficiency	45.8 %

Table 3.2.11: *Efficiencies*

account.

The average rise time of the HV pulse will, however, be closer to 200 μs because of the long cables between the pulse forming units in the service buildings and the pulse transformer-klystron units in the tunnel (see below). With the 1.3 ms length of the RF pulse an overall modulator efficiency close to 78 % is expected. The specified electronic efficiency of the klystron is above 70 %.

Assuming 10 % power reserve for amplitude and phase regulation and 4 % power loss in the circulators and wave guides, and taking the klystron focusing solenoid, which needs a continuous power of 4 kW into account, the wall-plug power to RF power conversion efficiency of the TESLA Linac will be about 46 % for a duty cycle of 0.65 %. All this is summarized in Table 3.2.11.

One may hope to reduce the modulator costs by replacing the energy storage capacitor by a SMES. In order to demonstrate the feasibility of such a system and to get a reliable cost estimation we have decided to build a prototype SMES modulator for the TTF which will be briefly described in the following.

3.2.4.5 Design of a 25 MW SMES Modulator for the Generation of Long Power Pulses

A SMES based power modulator for providing 25 MW pulsed power at TESLA conditions is described in this chapter. The maximum electrical output pulse power is 25 MW. It can be used to supply either two 5 MW klystrons or one 10 MW klystron. The modulator is thought to be used for the free electron laser at TTF and serves as a demonstrator of a larger modulator which should then supply about 10 klystrons in the collider. The requirements for the 25 MW modulator are listed in Table 3.2.12.

Output Voltage	130 kV
Output Current	190 A
Pulse width	1.7 ms
Flat Top	± 1 %
Repetition Rate	10 Hz

Table 3.2.12: *Output characteristic of a 25 MW SMES modulator for TESLA*

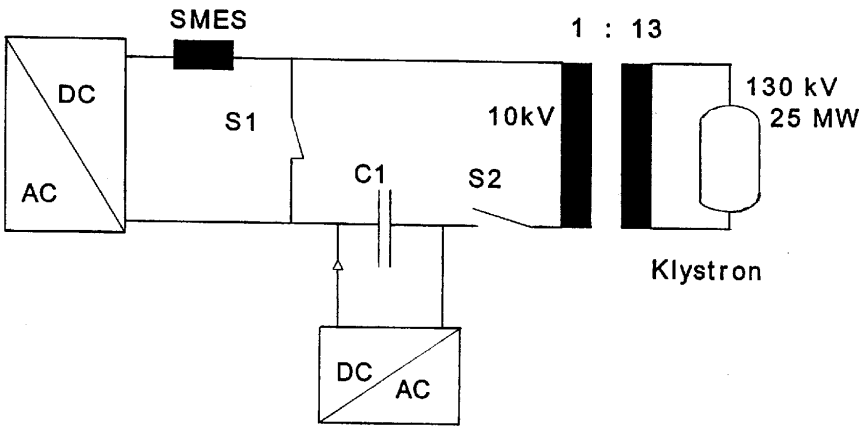

Figure 3.2.19: *Basic SMES modulator circuit.*

Principles of Operation

The basic modulator is shown in Figure 3.2.19. First it was described in [21]. The operation of this system can be devided into a charging mode and the pulse generation mode.

During the conduction time of the switch S1, which can be realised as a thyristor-switch proposed in [22] and the opening time of S2, which is made up of IGBT's, the SMES and the capacitor bank C1 are being charged. The SMES current and the capacitor voltage increase to their nominal values of 2500 A and 12 kV, respectively. For generation of an output pulse the switch S2 is closed. The thyristor S1 will be opened by the current of C1. In this pulse generation mode the SMES, the capacitor bank, and the klystron impedance (transformed to the primary side of the step up transformer) are forming a serial ringing circuit with the initial conditions I_{SMES} and $U_{capacitor}$.

The current in the circuit and in the klystron during the pulse generation time, referred to the primary winding of the step up transformer are described by the following equations, if we neglect the power supplies:

$$i_{klystron}(t) = I_{SMES}(0)(e^{-at}cos(bt) - \frac{a}{b}e^{-at}sin(bt)) - \frac{U_{Capacitor}(0)}{L_{SMES}}\frac{1}{b}e^{-at}sin(bt)$$

where

$$a = \frac{R_{klystron}}{2L_{SMES}}$$

$$b^2 = \frac{1}{CL_{SMES}} - a^2$$

After the 1.7 ms pulse generation time the thyristor will be closed and S2 will be opened so the charging mode begins again. During the generation time the SMES is first charged by the capacitor bank because the initial voltage of the capacitor is higher than the voltage across the primary side of the pulse transformer. Due to the TESLA requirement on the pulse shape and the series connection between the klystron (transformed to the primary side of the transformer) and the SMES, the current variation in the SMES is lower than 2 %. The versatile design of this modulator allows for a variable use such as the generation of pulses at a lower power (for supplying just one klystron, e.g.) and a varying repetition rate as well.

Simulation and Calculation of the Circuit

The calculated parameters of a 25 MW SMES modulator for TESLA conditions are listed in Table 3.2.13. The corresponding electrical circuit diagram is shown in Fig. 3.2.19.

SMES	L_{SMES}	= 70 mH	$I_{SMES}(0)$	= 2500 A	E_{SMES}	= 220 kJ
Capacitor	C	= .6 mF	$U_C(0)$	= 12 kV	E_C	= 43 kJ

Table 3.2.13: *Calculated modulator components*

The circuit has been investigated by simulations. In Figure 3.2.20 the output voltage across the klystron is shown. The amplitude of a single pulse varies within a tolerance band from +0.2 % to -1.4 % during a 1.7 ms pulse.

The change of 1.6 % of the magnitude of the pulse voltage also applies to the current in the SMES. The SMES current increases during the charging mode of the circuit from 2470 A to the initial value of 2500 A.

The maximum change of the SMES current during the pulse is 1.6 % corresponding to a decrease of the SMES energy of about 10 kJ. This energy drop of 10 kJ has to be reloaded during the 100 ms of the charging mode. Therefore a SMES power supply with an average power of 100 kW is necessary. The SMES power supply used in the simulations was a 30 V/2500 A voltage source.

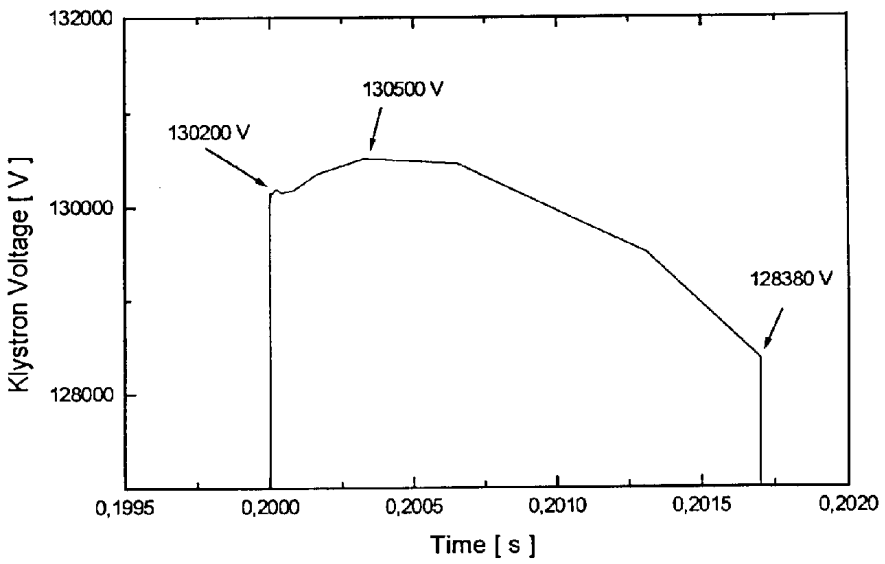

Figure 3.2.20: *SMES modulator output voltage. Single pulse across the klystron.*

There is a huge variation of the capacitor voltage during a cycle. The initial capacitor voltage of 12 kV drops during a pulse to about 5 kV. The voltage blocking capability of switch S2 has to be at least the maximum voltage across the capacitor bank. The capacitor energy decreases to 25 % of its value at the beginning of the pulse generation. The discharge is about 40 kJ. It is four times higher than the discharge of the SMES. This energy has to be recharged during the 100 ms cycle. Therefore the supply for the capacitor bank requires an average power of 400 kW. The average current of this supply was calculated to be 44 A. The properties of the required power supplies for the modulator are listed in Table 3.2.14.

SMES Supply	I_{av} = 2500 A	V_{load} = 30 V	P = 75 kW
Capacitor Supply	I_{av} = 44 A	V_{max} = 12 kV	P = 530 kW

Table 3.2.14: *Power supplies*

Summary and Conclusions

The calculations and simulations show that a SMES-based 25 MW modulator can be built with components that have been made available recently. A fast 250 kJ SMES was built in [23]. A bigger capacitor bank than required here was realised and described in [20].

There are several enterprises that can build the required power supplies. Dominant properties of the semiconductor switches needed for this modulator were proven in [23] and [20]. Problems concerning a reliable klystron protection have been solved in [20]

and will be adapted to this system.

This modulator concept may be applied also for higher output power and simultaneous supply of a larger number of klystrons.

3.2.4.6 Modulator Primary Power Handling and Pulsed Power Distribution

It is impressive to note that the peak RF power needed during each pulse is 4.125 GW for the whole linac. For a duty cycle of 0.65 % and with the efficiencies mentioned in 3.2.4.4, including 10 % regulation reserve, this results in an average wall plug power close to 59 MW.

Clearly the primary power handling system must be such that the mains see only the average power consumption. A possible scenario is shown in Fig. 3.2.21.

Each klystron together with its own pulse transformer forms a unit which is installed in the tunnel and which is exchanged as a whole in case of failure. The pulse forming circuits, i.e. capacitor banks with a bouncer or SMES units and their charging power supplies are located in the cryo-buildings. The distance between the cryo-buildings is 5 km, hence modulators for 2×50 klystrons requiring 2×12 MW total average mains power (at 10 Hz rep. rate) must be installed in each building.

Resonant charging of each of the 50 capacitor banks and their bouncer circuits will be accomplished by multiplexing a common power supply. This can be done by firing thyristors at the anticipated begin of the (re)charging process. The zero crossing of the charging current blocks the thyristors and terminates the charging process.

Each pulsing unit has an additional fast power supply with some 3 % charging capacity for individual matching. There is also a simple supply for initial charging of units which had tripped.

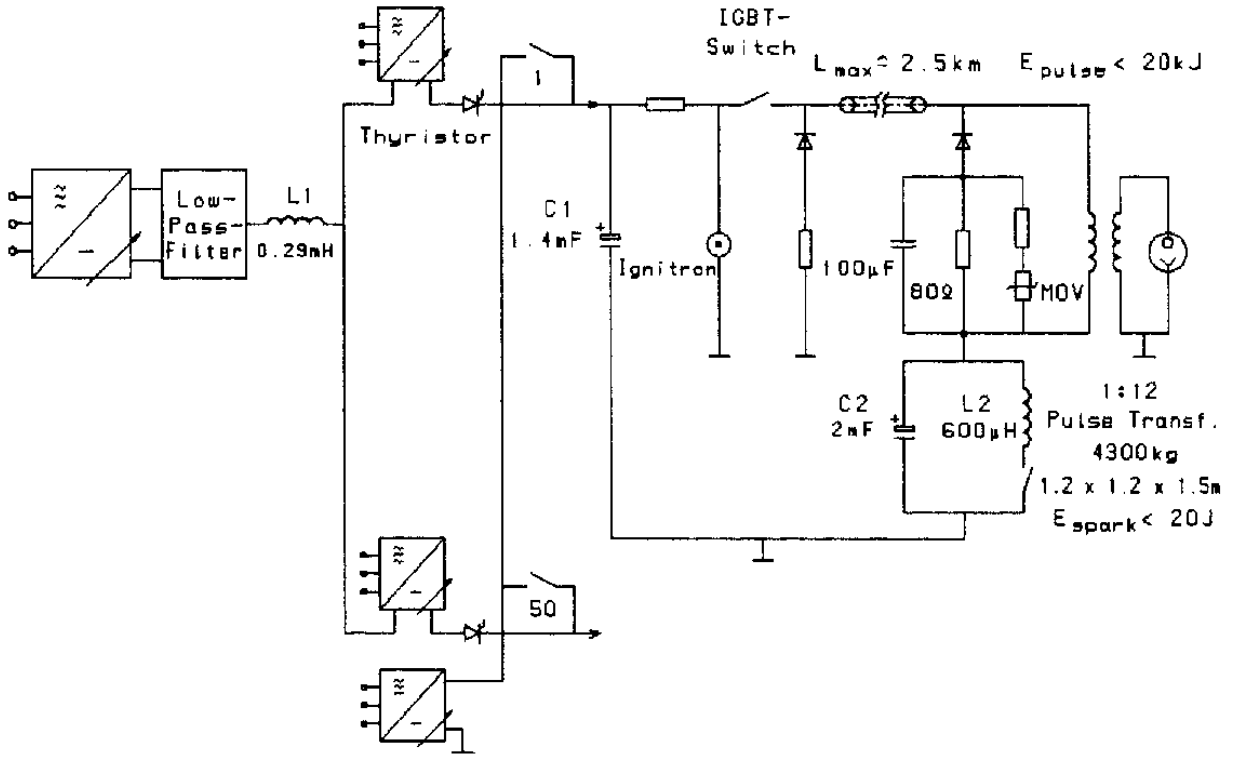

Figure 3.2.21: *Possible scenario for resonant sequential charging of 50 pulser units and power distribution over the average length of 1.25 km into the tunnel. In the tunnel only the klystrons and pulse transformers are located.*

For the stations running at 10 Hz repetition rate 50 current half waves are needed within 100 ms to subsequently charge each of the the 50 units in the time interval between two pulses. Therefore the charging frequency 250 Hz has been chosen. It is realized by the common 0.29 mH choke in conjunction with the 1.4 mF capacitor of each unit.

For the majority of the stations running at 5 Hz repetition rate the charging frequency can be halved by using a 1.16 mH choke.

The alternative solution of charging all the 50 units simultaneously by dimensioning the choke such that the variation of the charging current, which is shaped like the top of a cosine curve, does not exceed $\pm 1\,\%$ seems less attractive. In this case a 0.89 H choke is required at 10 Hz operation and 3.56 H at 5 Hz repetition rate. There would be no multiplexing, but thyristors would still be needed to disconnect units which have failed. These thyristors, however, never see a zero crossing of the charging current in this scenario, and would, therefore, require additional networks for controlled interruption. In addition, the cables connecting the pulser units with the pulse transformers in the tunnel can be disconnected rather than having extra manual switches.

The fluctuations seen by the mains are reduced to the 2 % level by a low pass filter. The capacitance of this filter is 0.2 mF and its inductance is 0.1 H. It also limits the current rise time in the case of a short circuit in one of the 1.4 mF capacitor banks to 100 A/ms. This gives sufficient safety margin for the primary thyristors to open and disconnect the mains.

The thyristor of the damaged capacitor bank will stay open, and a reserve RF system must be started. Then operation can restart immediately. If the short circuit occurs behind the IGBT switches, for example in a klystron gun, it can be handled by opening the corresponding IGBT switch within a few μs.

The power transmission lines between the pulser units and the pulse transformers deserve special attention. Their average length in the tunnel is 1.25 km and the maximum length is 2.5 km. Due to the inductance of these cables, which is of the order of 300 μH/km and hence comparable to the leakage inductance of the pulse transformer, the rise time of the pulse is significantly increased. Simulations [24] have shown that the optimum rise time and pulse shape is obtained for the cable impedance close to 10 Ω. This is close to the transformed klystron impedance of 8.3 Ω. Then the pulse rise time is increased from 150 μs for the case of a pulse transformer directly connected to the bouncer unit to 250 μs when a cable of 2.5 km length is present. These results refer to the case of a bouncer pulse forming unit. In the SMES case the optimum cable impedance is closer to 40 Ω [25].

The cable cross section must be at least 400 mm^2 to keep the average power loss on the cables below 2 %. Frequency components up to 6 kHz should be transmitted without significant loss, otherwise there will be furher increase of the pulse rise time. Since the penetration depth at 6 kHz is only 0.82 mm it seems appropriate to use 3 coaxial cables of 30 Ω impedance and about 55 mm diameter in parallel. The inner conductor must be stranded wire.

Klystron Interlocks

In the event of a klystron gun spark, which is detected in three different ways for redundancy, the energy deposited in the spark must be kept below 20 J to avoid damage of the gun.

The response to a spark will be an immediate opening of the concerned IGBT switch (see Fig. 3.2.21) to disconnect the capacitor bank from the sparking klystron. The energy stored in the transformer leakage inductance and in the power transmission cable is dissipated in two networks, one at the cable end near the IGBT consisting essentially of a reverse diode and a resistor. The second one is made up by an 80 Ω resistor across the transformer primary and by a 100 μF capacitor which limits the peak inverse voltage at the primary to 800 V when the IGBT is opened.

Should it fail to open the ignitron crowbar is fired and, in addition, a second independent switch installed in series with the IGBT is opened. Important interlocks are control of cooling water flow and temperature, the focusing solenoid current, and a vacuum interlock. Other interlock conditions result from sparks in the RF distribution system, reflected power, RF leaks, power couplers and from cryogenics.

3.2.4.7 The RF Distribution System

The 10 MW Multibeam-klystron has two RF output windows. Therefore the RF distribution system is based on two cryounits per 5 MW output window. Each unit contains eight 9-cell cavities. In principle, a tree-like RF distribution can be used, but a linear system branching off identical amounts of power for each cavity from a single line by means of directional couplers matches the linear tunnel geometry better. Such a system is already in use for the HERA superconducting RF system and has also been successfully tested in the TTF. All required components are readily available. This geometry permits to install additional power splitters to reduce the RF power sent into an individual arm if this particular cavity or its coupler can not handle the full nominal power.

One might object that unlike the case of the tree-like system, where all paths have the same electrical length, thermal expansion could be a problem for the linear distribution system. Fortunately the effect is only 0.24° of RF phase per centigrade and per cryomodule and is therefore uncritical.

The maximum power of 5 MW is symmetrically devided by a three dB power splitter and feeds the two cryomodules, see Fig. 3.2.22 and 3.2.23. The individual three stub wave guide tuners for impedance- and phase matching of each cavity provide the possibility of $\pm 30°$ phase adjustment and to correct for VSWR up to 2:1.

Circulators are indispensable. They have to protect the klystrons against reflected power and, in conjunction with load resistors and the power input coupler, they define the loaded cavity impedance as seen by the beam. One possibility consists of placing the circulator between the klystron and the 3 dB splitter. Since, due to cavity filling, there is almost total reflection of the RF power at the beginning of the pulse, the standing wave RF voltage which occurs in the circulator and in some parts of the wave guide system may double. In other words, with respect to sparking protection, the equivalent

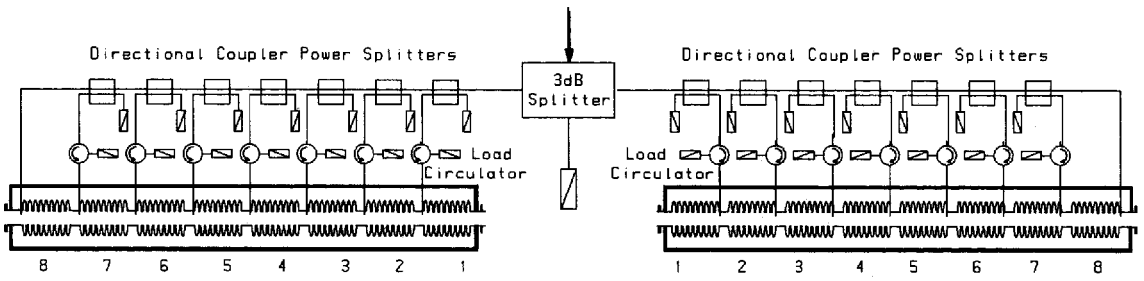

Figure 3.2.22: *Layout of the RF distribution scheme. One 5 MW arm from the 10 MW Multibeam-klystron feeds two cryounits. There are eight 9-cell cavities in each unit. The coupler hybrids branch off equal amounts of power into the individual cavities. There is an individual circulator for each cavity.*

power to be considered is 4 times the real power entering into the circulator, i.e. almost 20 MW. Assuming a breakdown field of 30 kV/cm, the recommended power rating for WR 650 wave guide is 14.8 MW for straight wave guide under ideal conditions, which means dry and clean.

Of course, the wave guide lengths can be arranged so that the reflected powers from each cryomodule will add up constructively in the load associated with the 3 dB power splitter rather than propagating to the circulator. This can work perfectly only if both power signals arrive with equal amplitude and proper phase at the 3 dB splitter. Clearly it is unrealistic to hope that this will always be the case.

Therefore the wave guide section between the klystron and the 3 dB splitter must be filled with a protective gas. In the TTF SF_6 of normal pressure, which can increase the power handling capability by up to 8 times, was used. The disadvantage of SF_6 is that, if sparking occurs, aggressive radicals are formed, and one has to change the gas in order to avoid wave guide corrosion. For TESLA SF_6 seems impractical because small amounts of radiation may also result in decomposition of the gas. Other gases would require an overpressure of several bars to get the same relative power capability as SF_6 at normal pressure.

Other problems stem from the fact that the development of a low insertion loss (0.1 dB) circulator which is capable of handling the 5 MW peak power under total reflection conditions is problematic. So far no circulator which works reliably at 2.5 MW at total reflection has been realised. In addition, a wave guide RF window is needed to separate the SF_6 from the normal air in the rest of the system. Here we have succeeded in building three pill-box windows capable of handling total reflection at any phase angle of RF pulses of some 3 MW peak power and 2 ms length. It does not seem possible to go up to 5 MW with this design. Other designs might become much more complex.

Therefore the alternative solution of using individual circulators for each cavity,

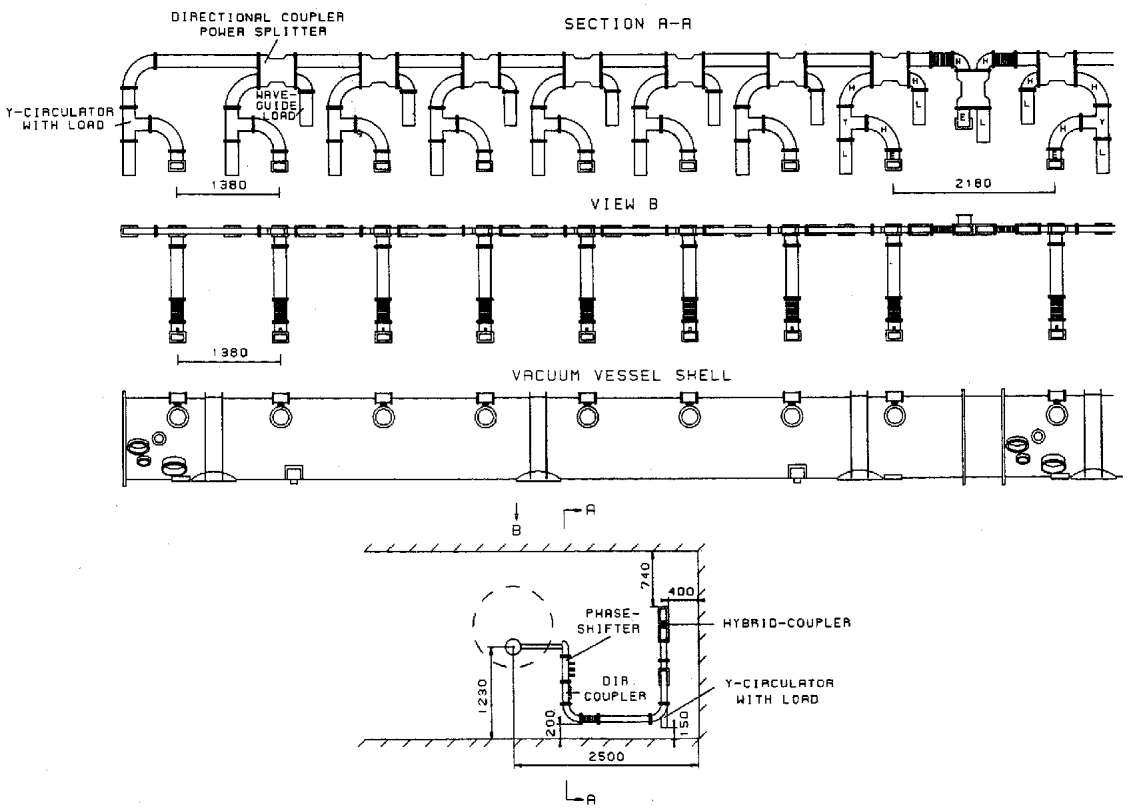

Figure 3.2.23: *Detailed layout of RF distribution scheme.*

which has been successfully tested in the TTF seems increasingly attractive. All the above mentioned technical problems disappear in this case. No protective gas and hence no window would be necessary in any part of the wave guide. These small circulators exist and have excellent characteristics. The insertion loss is 0.1 dB, the VSWR at total reflection better than 1.2 depending on phase angle. It has been measured that the total VSWR seen by the klystron windows can be kept below 1.2 with the RF distribution scheme shown in Fig. 3.2.22. With the help of an additional three post wave guide impedance matcher identical to the ones close to each cavity power input coupler this VSWR can still be minimised.

A further improvement due to the individual circulator solution is the increased decoupling of the cavities. Since there are RF pick-up antennas in the forward- and reflected power ports of the circulators, no extra directional couplers are needed in the wave guide arms which results in a cost reduction. Another cost reduction comes from the fact that the circulator loads need to be dimensioned only up to the average power per cavity and the loads connected to the directional coupler hybrids see only less than 100 W of average power and can be very simple. If there were no individual circulators some of these loads could see almost 4 times the average power sent to an individual cavity.

Our experience from the TTF with the investment cost for the small circulators

suggests that the overall cost of this solution will not be more expensive but much more reliable than the one of high peak power circulators.

Frequency:	1300 MHz ± 10 MHz
Power:	5 MW peak during 2 ms, 20 kW average
Isolation:	30 dB typ., 26 dB min.
VSWR:	1.1:1 max. for all ports
Flange:	CPR 650 F
Waveguide:	WR 650, normal wall thickness

All aluminum components shall be fabricated using 6061-T6 alloy.
Finish MIL C5541 class 1A.
We need seven different types of power splitters with coupling ratio:

1	.	9.03 dB ± .1 dB
2	.	8.45 dB ± .1 dB
3	.	7.78 dB ± .1 dB
4	.	6.98 dB ± .1 dB
5	.	6.02 dB ± .1 dB
6	.	4.77 dB ± .1 dB
7	.	3.00 dB ± .1 dB

Table 3.2.15: *Specification of WR 650 directional coupler power splitters*

Power:	.5 MW peak during 2 ms, 2 kW average.
VSWR:	1.05 : 1 by full power
RF leakage:	-95 dB
Physical length:	< 500 mm
Flange:	CPR 650 F

Table 3.2.16: *Specification of WR 650 wave guide load for circulators.*

Frequency:	1300 MHz $\pm$ 5 MHz
Peak power:	0.5 MW. Due to total reflection of the RF signal during an important fraction of the pulse duration the maximum standing wave voltage will correspond to 2 MW
Average power:	2 kW
Insertion loss:	.1 dB
VSWR:	better than 1.2:1 for total reflection.
Isolation:	30 dB, min. 26 dB
RF pulse length:	2 ms
Repetition rate:	10 Hz

Table 3.2.17: *Specification of circulator*

3.2.4.8 Low Level RF Control

The cavities in the TESLA linacs are operated in pulsed mode at an average gradient of 25 MV/m with each klystron driving 32 cavities. The pulse repetition rate is 5 Hz and the RF pulse length is 1300 μs from which 500 μs are required to fill the cavity and 800 μs are needed for the acceleration of the beam. During the beam pulse the fluctuations of the accelerating field - defined as the vector-sum of the fields in 32 cavities - must be kept small to reduce the uncorrelated contributions to energy spread to less than $5 \cdot 10^{-3}$ for an ensemble of 32 cavities.

The major sources of field perturbations which have to be controlled by the low level RF system are caused by fluctuations of the resonance frequency of the cavity and by fluctuations of the beam current. Fluctuations of the resonance frequency are a result of deformations of the cavity walls induced by mechanical vibrations (microphonics) or the gradient dependent Lorentz force (also referred to as radiation pressure or ponderomotive force).

Mechanical vibrations caused by roughing pumps or the compressors of the cryogenic system are always present in an accelerator environment. These vibrations induce a modulation of the resonance frequency. The spectrum of the resulting phase and amplitude errors is a convolution of the spectrum of excitation and the mechanical resonances of the cavity. The microphonic noise is not predictable from pulse to pulse and is expected to be uncorrelated over the length of the linac.

The cavity detuning due to the Lorentz force acting on the walls of the cavity is proportional to the square of the cavity field. The TESLA cavities are stiffened to reduce the Lorentz force detuning constant to -1 Hz/(MV/m)^2. The error due to Lorentz force is predictable due to the repetitive excitation of the cavity and considered as correlated noise.

The bunched structure of the beam current induces a sawtooth like profile on the accelerating gradient. At the gradient of 25 MV/m a single bunch with a charge of $3.6 \cdot 10^{10}$ e$^-$ will induce a transient with a magnitude of 10^{-3}. Bunch-to-bunch charge fluctuations will modulate the amplitude of the transients thereby inducing bunch-to-bunch energy fluctuations.

A digital feedback system will provide control of the accelerating field. The accelerating field of each of the 32 cavities is measured, the vector-sum is calculated, and the amplified error signal drives the vector-modulator of the incident wave which is common to all cavities since they are driven by the same klystron. The digital approach allows for maximum flexibility in the choice of the control algorithms, automated calibration of the vector-sum, and extensive diagnostics and exception handling capabilities. The main features of the digital feedback are a sampling rate of 1 MHz for the individual cavity probe signals, digital in-phase and quadrature detection of cavity field and amplitude of incident wave and reflected wave, calculation of the vector-sum which includes gradient calibration and the correction of phase offsets for each cavity, and the feedback algorithm. The feedback algorithm includes time-optimal control and a Kalman filter to correct for loop delays on the order of several μs and provides an optimal state estimate in presence of detector noise. Adaptive feed forward is added

to minimize the control effort by compensation of repetitive errors.

RF Control Requirements Usually the requirements for an RF control system are stated in terms of achieved amplitude and phase stability. In addition, the extra power needed for control as a result of the Lorentz force and microphonics must be minimized. It is, however, also important to address issues such as reliability, operability, robustness and maintainability in the design. The low level controls must support procedures for the turn on of the RF system (commissioning and routine operation), calibration of gradient and phase for the vector-sum, and control of the frequency tuner.

Amplitude and Phase Stability The requirements for amplitude and phase stability of the vector-sum of 32 cavities are dictated by the maximum tolerable energy spread at the interaction point. The goal is an rms energy spread of $\sigma_E/E = 2 \cdot 10^{-3}$. Gradient and phase fluctuations will result in bunch-to-bunch energy spread while finite bunch length combined with the sinusoidal time dependency of the RF wave and induced bunch wake potential will result in intra-bunch energy spread. The intra-bunch energy spread can be minimized by proper phasing of the cavities i.e. the beam is accelerated a few degrees off-crest[27]. It is desirable to keep the bunch-to-bunch energy spread below the intra-bunch energy spread of $5 \cdot 10^{-4}$ in order to assure that the bunch-to-bunch chromatic effects will not be a dominating factor. Considering that correlated field fluctuations can be suppressed to better than $3 \cdot 10^{-4}$ the requirements for uncorrelated gradient and phase have been set to $\sqrt{N} \cdot 3 \cdot 10^{-4} = 5 \cdot 10^{-3}$ and 0.5^o respectively. This is due to the fact that the effect of uncorrelated errors on the final energy spread is reduced by $\sqrt{N}$, where $N = 302$ is the number of klystrons in each linac, and that a phase control to 0.5^o results in an energy spread contribution of the order of $3 \cdot 10^{-4}$ when operating 4^o off crest.

Operational Requirements The turn on procedure for the RF system is fairly complex due to the large number of cavities driven by the same klystron. It is therefore important to have fully or semi-automate procedures for the calibration of the vector-sum, phasing of cavities, and operation of the frequency tuner. Also gradient and phase changes should be controlled by a single knob as well as the RF system be turned on and off with a single button. In case of operational problems the control system must provide the operator guidance for trouble shooting and allow RF experts for completely manual operation.

RF Control Issues The amplitude and phase errors to be controlled are of the magnitude of 5 % and 20 degrees respectively as a result of Lorentz force detuning and microphonics. These errors must be suppressed by a factor of at least 10 which implies that the loop gain must be adequate to meet this goal. Fortunately, the dominant source of errors is repetitive (Lorentz force) and can be reduced significantly by use of feed forward.

Lorentz Force The Lorentz force yields a steady state change of the resonance frequency of $-625\,\mathrm{Hz}$ when increasing the gradient from zero to $25\,\mathrm{MV/m}$. Due to the dynamics of the cavity which has a mechanical time constant of about 1 ms which is comparable to the RF pulse length, the actual frequency change during a 1.3 ms RF pulse is only 400 Hz. The dynamics of the mechanical system are described by:

$$\dot{\Delta\omega} = -\frac{1}{\tau_m} \cdot \Delta\omega + \frac{2\pi}{\tau_m} \cdot K \cdot E_{acc}^2$$

with the Lorentz force detuning constant $K = -1\,(\mathrm{Hz}/(\mathrm{MV/m})^2)$. If the tuning at the beginning of the RF pulse is choosen such that resonance frequency and operating frequency agree in the middle of the beam pulse ($\Delta\omega = 0$), the peak detuning will not exceed the bandwidth of the cavity of 215 Hz (HWHM). This choice of optimum pre-detuning of approximately -230 Hz also minimizes the RF peak power needed for control. The time dependency of the resonance frequency is shown in Fig. 3.2.24.

Microphonics The resulting phase errors can be as large as several ten degrees due the to the high loaded Q of the cavities of $Q_L = 3 \cdot 10^6$ corresponding to a bandwidth (HWHM) of 215 Hz. The sensitivity for the TESLA cavities is about 0.5 Hz per nanometer change in cavity length. Measurements in the TTF have shown typical microphonic noise levels of ± 30 Hz with a dominant modulation frequency of 27 Hz. The microphonics modulate the pre-detuning of the cavity and therefore the RF peak power requirement during the RF/beam pulse. A study of RF peak power requirements versus the amplitude of microphonics has shown that an amplitude of 100 Hz is acceptable.

Beam Loading The beam induced cavity voltage is $25\,\mathrm{MV/m}$ for the nominal average beam current of 8.3 mA while the generator induced voltage on resonance is $50\,\mathrm{MV/m}$ for an incident power of $213\,\mathrm{kW/m}$. These conditions result in the nominal steady state accelerating voltage of $25\,\mathrm{MV/m}$. Bunch-to-bunch charge fluctuations of 10 % rms will result in rms energy gain fluctuation of $1.4 \cdot 10^{-4}$ which can not be controlled by feedback due to gain bandwidth and power limitations. A gain bandwidth product of the feedback loop of 20 kHz allows, however, for a gain of greater than 10 at 1 kHz hence errors at this frequency can be suppressed by an order of magnitude.

Low Level RF Design The main components of the low level RF are the detectors for the cavity field, the controller for feedback, and actuators which control the incident wave to the cavity. For feedback one can choose the traditional amplitude and phase control system, one can apply feedback to in-phase (I) and quadrature (Q) component of the cavity field, or use direct RF feedback where the cavity probe signal is compared to an RF reference. The cavity can be operated in a self-excited loop configuration or it can be driven by a fixed frequency generator. All systems have in common an electrical signal which represents the cavity field that is compared to a reference signal. The resulting error signal is amplified and drives a modulator for the incident wave

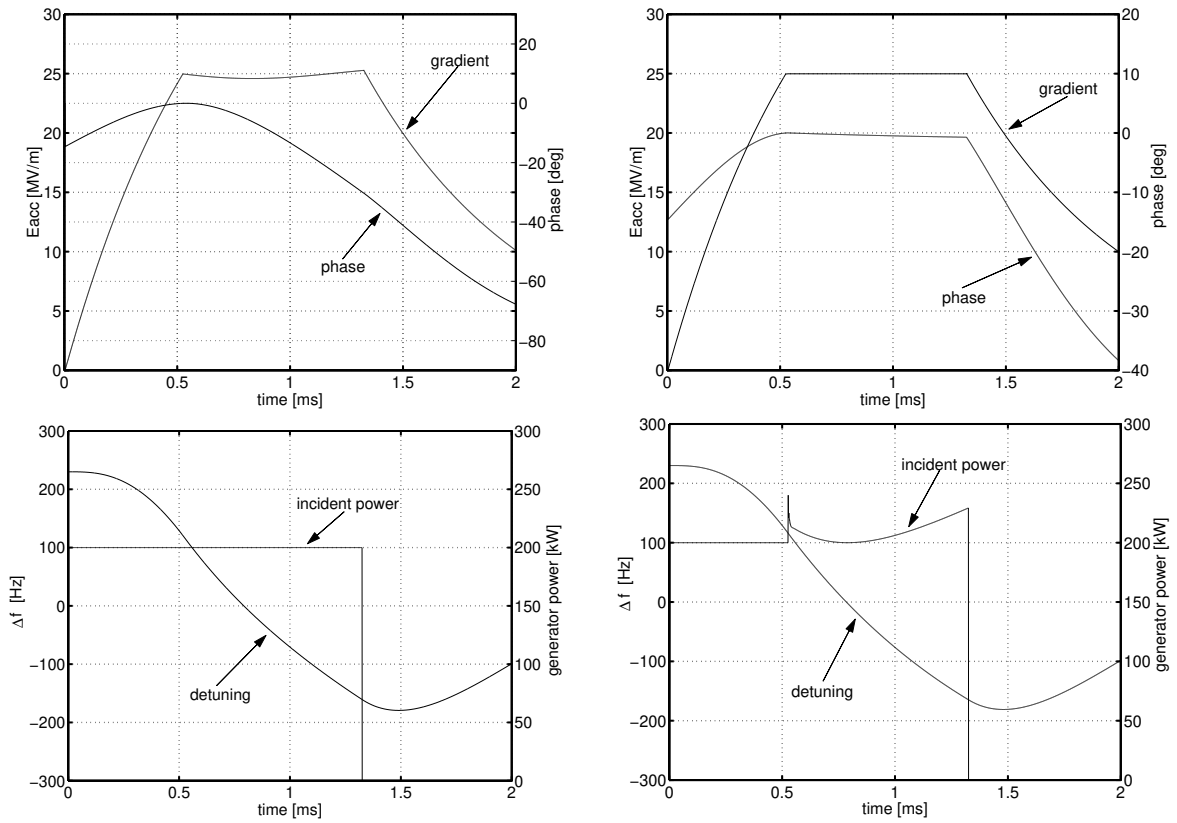

a) open loop b) closed loop

Figure 3.2.24: *Simulation of cavity response in a) open and b) closed loop including beam. The cavity parameters are the Lorentz force constant* $K = -1\,Hz/(MV/m)^2$ *and the mechanical time constant* $\tau_m = 1\,ms$*. The simulated beam is injected after* $500\,\mu s$*. In open loop the best flat top response is achieved with a pre-detuning of 230 Hz. The sum of generator and beam current during beam acceleration will induce a steady state gradient of* $25\,MV/m$ *when the cavity is operated on resonance. The closed loop response shows the additional power needed to control the time varying detuning caused by the Lorentz force.*

to the cavity. These can be amplitude and phase controllers, I/Q controllers, or other means to control the vector of the incident wave.

For the TESLA RF system a digital RF control scheme has been adopted. The concept of digital control provides enormous flexibility in the control algorithms, diagnostics, and exception handling.

Digital RF Control Design For the TESLA RF system the following signals are measured to determine the state of each RF station consisting of 32 cavities driven by one klystron:

- field vector of each of the 32 cavities
- vector of the incident wave to each of the 32 cavities

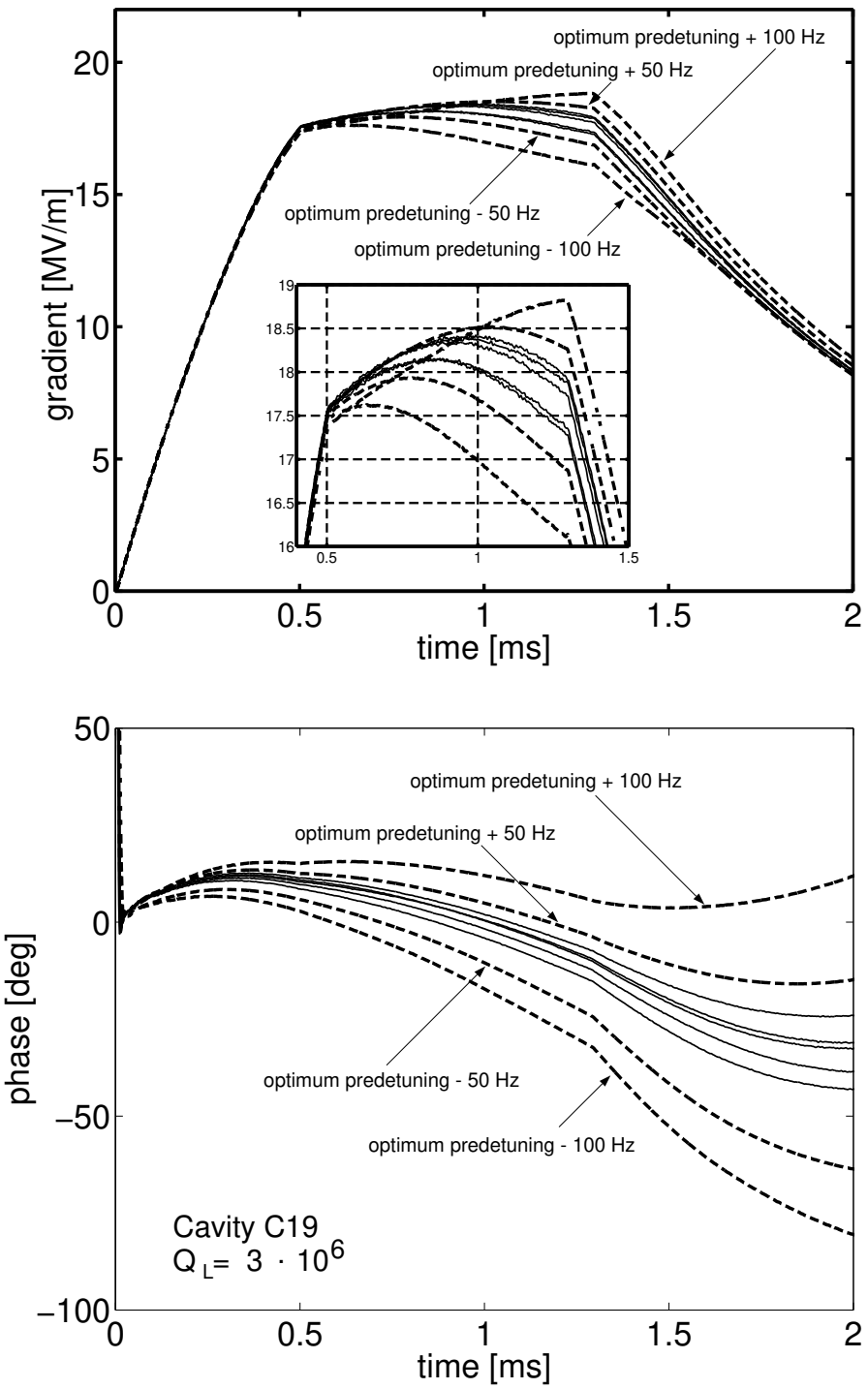

Figure 3.2.25: *Microphonics measured in the horizontal cryostat Chechia. The cavity is pulsed in open loop with simulated beam. The gradient and phase are modulated by the microphonics. The dashed lines show simulation results for 50 Hz and 100 Hz deviation from the optimum pre-detuning.*

- vector of the reflected wave from each of the 32 cavities
- vector of total incident and reflected wave measured at the klystron output

The actuators used for field control are:

- vector-modulator to control the incident wave common to 32 cavities
- cavity frequency control (motor activated tuner) for each of the 32 cavities
- manual adjustment for loaded Q and phase of incident wave for each of the 32 cavities using a three stub wave guide tuner and possibly a variable input coupler.

Fast control of the accelerating field can only be accomplished by modulation of the incident wave which is common to 32 cavities. Therefore fast control of an individual cavity field is not possible. The modulator for the incident wave is designed as an I/Q modulator to control the in-phase (I) and quadrature (Q) component of the cavity field instead of the traditional amplitude and phase modulators. The coupling between the loops is therefore minimized and control in all four quadrants is guaranteed.

The detectors for cavity field, and incident and reflected waves are implemented as digital I/Q detectors. The RF signals are converted to an IF frequency of 250 kHz and sampled at a rate of 1 MHz, i.e., two subsequent data points describe I and Q of the cavity field. The I and Q component which describe the cavity field vector are multiplied by 2x2 rotation matrices to correct the phase offsets and to calibrate the gradients of the individual cavity probe signals. The vector-sum is calculated and a Kalman filter is applied. The Kalman filter provides an optimal state (cavity field) estimate by correcting for delay in the feedback loop and by taking stochastic sensor and process noise into account. Finally the set point is subtracted and a time optimal gain matrix is applied to calculate the new actuator setting (I and Q control inputs to a vector modulator). Feed forward is added from a table in order to minimize the control effort. The feed forward tables are adaptively updated to reflect slowly changing parameters such as average de-tuning angle, microphonic noise level, and phase shift in the feed forward path.

Hardware The hardware of the digital feedback consists of 14-bit, 2 MHz ADCs (AD929 from Datel), the interface circuit to the input of the digital signal processors (DSP), the 6 DSPs (TMS320C40 from Texas Instruments), and two 16-bit, 10 MHz DACs which drive the vector modulator. Eight DSPs are used to acquire the probe signals of the 32 cavities and perform the matrix multiplication while one DSP is calculating the vector-sum and performing the feedback algorithm. The clock frequency of the DSPs is 50 MHz which allows for 25 instructions per microsecond. An additional DSP can be added to perform a more complex algorithm. The overall data processing time will be on the order of 2-3 μs. A cable delay of 600 ns, ADC conversion of 500 ns, and DAC conversion of 200 ns increase the total delay to 3-4 μs thereby adding less than 30 degrees phase shift at the unity gain crossing of 20 kHz. This leaves a phase margin of more than 60 degrees.

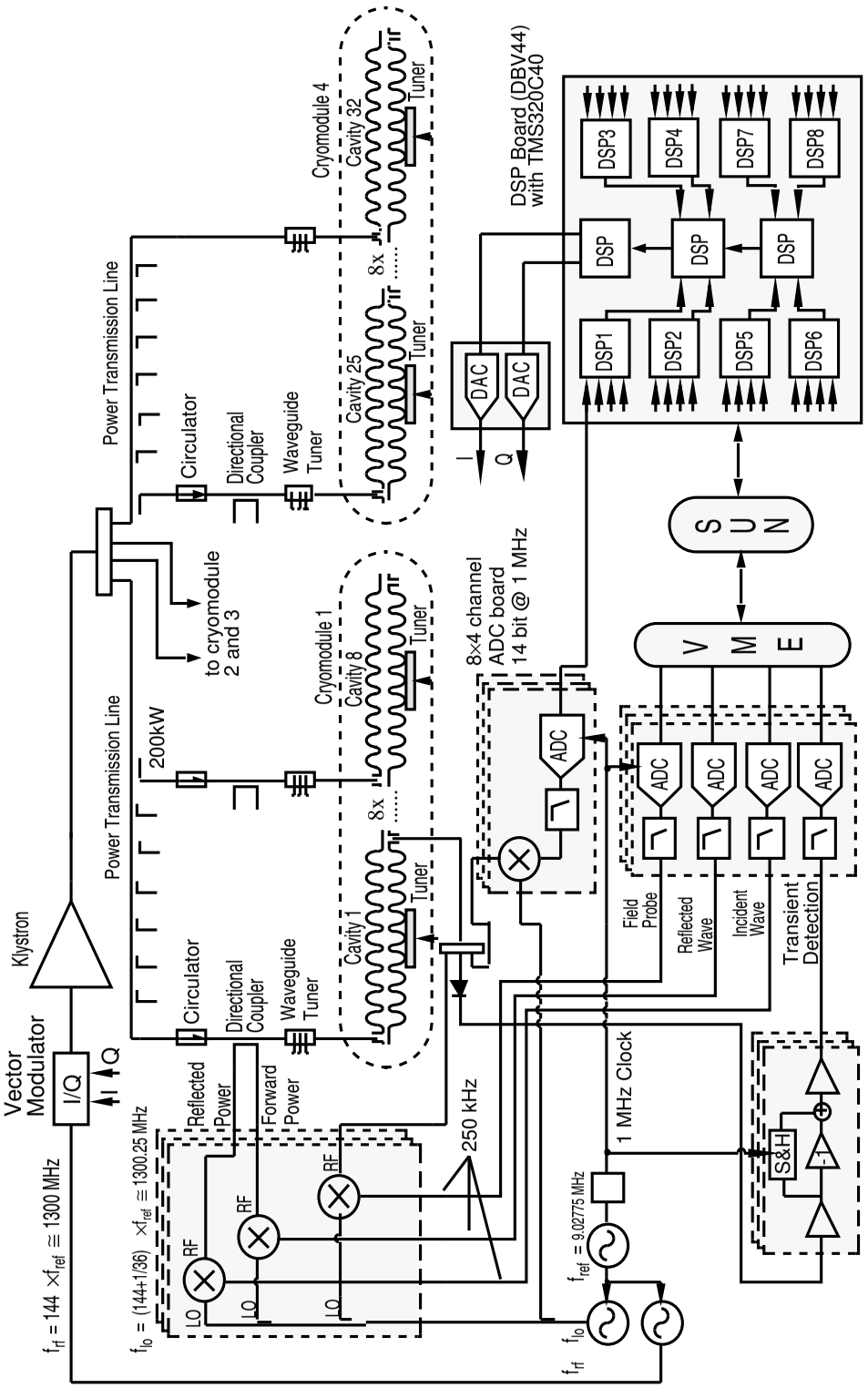

Figure 3.2.26: *Schematic of the Digital RF System for the TESLA Test Facility*

With the addition of the digital I/Q detectors for incident and reflected wave which are read by the control computers - these signals are not used in the feedback algorithm - the complete information about each cavity is available. Graphs of the individual signals are displayed for monitoring, optimization, and trouble shooting purposes. The tuner control is derived from the time dependence of the gradient signal. The calibration of the vector-sum and the phasing of the cavities is based on beam loading. The beam induced transients are observed at zero crossing and phase offsets are determined by nulling of the average transients. Dedicated hardware for transient detections allow for precise calibration of the vector-sum.

Feedback Algorithm The non-linear dynamics of a single cavity are described by a system of first order differential equations presented in state space form. The equations describe the envelope of the accelerating field as function of the driving terms which are composed of generator current and beam current. The last equation describes the coupling between accelerating gradient and the resonance frequency of the cavity.

$$\begin{pmatrix} \dot{\nu}_r \\ \dot{\nu}_i \\ \dot{\Delta\omega} \end{pmatrix} = \begin{pmatrix} -\omega_{1/2} & -(\Delta\omega+\Delta\omega_T) & 0 \\ \Delta\omega+\Delta\omega_T & -\omega_{1/2} & 0 \\ -\frac{2\pi\cdot K}{\tau_m}\nu_r & -\frac{2\pi\cdot K}{\tau_m}\nu_i & -\frac{1}{\tau_m} \end{pmatrix} \cdot \begin{pmatrix} \nu_r \\ \nu_i \\ \Delta\omega \end{pmatrix} + \frac{R\omega_{RF}}{2Q} \cdot \begin{pmatrix} 1 & 0 \\ 0 & 1 \\ 0 & 0 \end{pmatrix} \cdot \begin{pmatrix} I_r \\ I_i \end{pmatrix}$$

where ν_r, ν_i : real and imaginary component of the cavity voltage,
I_r, I_i : real and imaginary component of the total current (generator + beam)
$\Delta\omega + \Delta\omega_T = \omega_0 - \omega_{RF}$,
$\omega_0 = \omega_0(t)$: resonance frequency of the cavity,
ω_{RF} : operating frequency, $\omega_{1/2} = \frac{\omega_{RF}}{2Q}$: half width of resonance,
$\Delta\omega_T$: detuning by frequency tuner, τ_m : mechanical time constant,
K : Lorentz force detuning constant.

Linear and time invariant systems of the form $\dot{x}(t) = A \cdot x(t) + B \cdot u(t)$ are well understood in modern control theory and solutions for an optimum controller can be found in textbooks. For the above non-linear system which describes the cavity dynamics one can also find various solutions for a controller. It is, however, critical to keep the computational delay as small as possible to allow for sufficient gain bandwidth product and avoid instabilities due to delay. Since the data processing time (a few μs) will be short compared to the time constant of the cavity (700 μs), it is possible to correct for these delays and reach significantly higher feedback loop gains than in analog systems with the same delay.

The computational delay is minimized by treating the ensemble of 32 cavities like one cavity and applying the feedback algorithm only to the vector-sum. Simulations with realistic spreads in system parameters such as loaded Q_L, mechanical time constant τ_m, Lorentz force detuning constant K, power and phase of incident wave, calibration errors of the vector-sum, and initial detuning angle modulated by microphonics,

have demonstrated that the ensemble of 32 cavities is well described by the dynamics of a single cavity.

The present feedback algorithm applies a proportional gain to the error signal and uses a digital low-pass filter to reduce the sensor noise. More sophisticated algorithms such as time varying Kalman filter and time-optimal control are planned to be used in the near future.

The design of a feed forward algorithm is as important as the feedback algorithm. The Lorentz force induced gradient and phase fluctuations result in a repetitive error signal which can be compensated by feed forward which adds a fixed and negligible amount of CPU time. The feed forward tables are optimized by measurement of the average correction signal from the feedback loop and adjustment of the feed forward tables such that the average feedback signals are close to zero.

Measured Performance of the LLRF for the TTF

The digital feedback system has been extensively tested in the TTF with simulated beam to ensure that the open loop conditions are similar to the operating conditions under nominal beam loading. For simplicity the drive frequency has been varied to adjust the pre-detuning instead of the mechanical frequency tuner which must be used in routine linac operation.

Measured cavity parameters The cavity parameters for cavity D2 have been determined from open loop measurements. The cavity is pulsed and the transients for amplitude and phase are measured for different pre-detunings. The measured data is compared to simulation results in which the Lorentz force detuning constant and the mechanical time constant of the cavity are varied to achieve good agreement with the measurement.

Single cavity performance of the digital feedback system The performance of the digital I/Q controller for a single cavity operated at 20 MV/m is shown in Fig. 3.2.28. With feedback loop gains of 40 dB, the measured amplitude and phase fluctuations of the accelerating field are less than 0.5% rms and 0.5^o rms respectively thereby exceeding the uncorrelated noise requirements. The measured signal is dominated by 250 kHz noise as a result of systematic errors on the local oscillator signal caused by the gain imbalance and orthogonality errors in the vector modulator. This noise will be reduced significantly in the future with a new driver board which allows for individual adjustment of the four reference phases to guarantee precise 90^o steps.

The overshoot on the gradient signal at the time of (simulated) beam injection is due to inadequate adjustment of the feed forward tables at the time of the measurement. In the future, adaptive algorithms will be used to adjust the feed forward tables automatically to minimize the control effort of the feedback loops. The fast fluctuations on the gradient and phase signal on a time scale of a few ten microseconds are

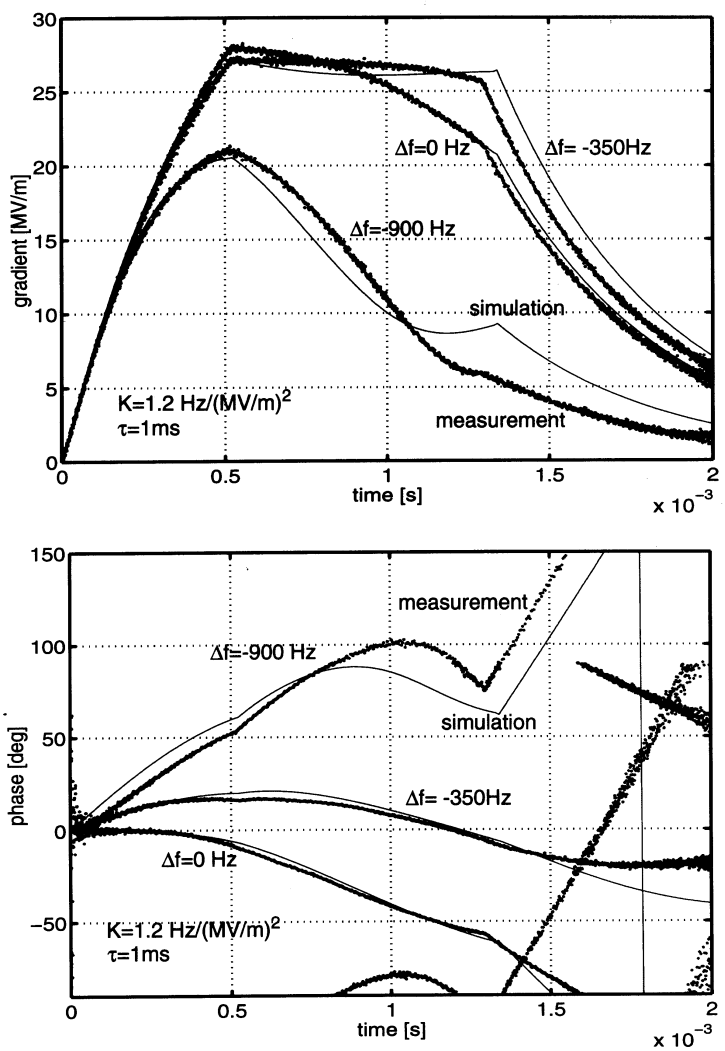

Figure 3.2.27: *Comparison of measurement and simulation results for cavity D2 in pulsed mode. The pre-detuning is varied. The Lorentz force detuning constant and the mechanical time constant of the cavity have been adjusted for good agreement.*

probably a result of phase noise on the reference line but further investigations are necessary to confirm and eliminate this noise.

It has been demonstrated that the digital RF system for the TTF provides the field regulation required for the TESLA linacs when controlling a single cavity. Simulations with measured cavity and other RF system parameters have shown that the regulation of the vector-sum of 32 cavities will not be a problem since the transfer function of an ensemble of many cavities is similar to that of a single cavity. It is however critical that the vector-sum is calibrated to better than 10 % in gradient and better than 1^o in phase, and that the klystron operated in its linear regime at all times.

Assuming realistic parameter spreads in loaded Q, the cavity parameters K and τ_m, errors in the calibration of the vector-sum, and microphonic noise levels of ± 50 Hz,

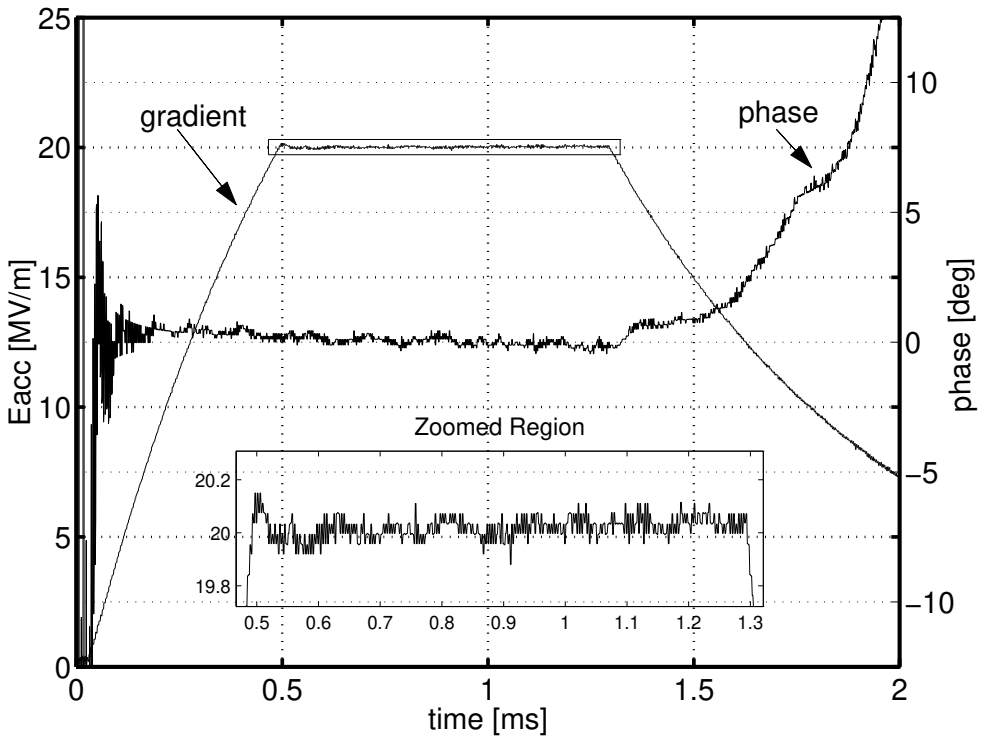

Figure 3.2.28: *Performance of the digital feedback system. Amplitude and phase stability exceed the requirements.*

the achievable average gradient will be approximately 2 MV/m lower than the average operable gradient. For an average energy gain of 25 MeV/m, the average operable gradient must be therefore of the order of 27 MV/m. The discrepancy is explained by the fact, that the combination of microphonics and parameter variations lead to modulated deviations from the ideal flat-top characteristics in the individual cavities thereby reducing the available energy gain.

3.2.5 Cryogenics

The present TESLA design requires the cooling of about 20,000 superconducting cavities down to $\leq 2\,\mathrm{K}$ by saturated superfluid helium in a bath. Grouped in numbers of 8 into 2448 cryomodules of about 12 m length the cavities are assembled along the 32 km length of the linear collider. Sections (units) of about 2.5 km length are supplied from a single refrigerator which has to provide also 4.5 K one-phase cooling for superconducting magnet packages (quadrupoles and correction dipoles) and for a radiation shield as well as 40 K to 80 K cooling for a second radiation shield and HOM absorbers. Generally two neighbouring refrigerators are housed in a common refrigerator hall above ground. Because of doubling the dynamic heat load due to the use for a Free Electron Laser (FEL), a special situation occurs in the first part of the linear accelerator near the DESY site.

Each refrigerator has a size roughly comparable to the ones used for HERA. Heat loads have been calculated for the static (without RF and current) and for the dynamic (full RF for 5 Hz beam bunch repetition rate respectively 10 Hz in the first two cryogenic units and 100 A current for magnet packages) cases. Dynamic nominal heat loads at 2 K dominate, reaching a nominal value of about 2 kW for units 3 to 12 and about 4 kW for units 1 and 2. A complete overview of the cryogenic loads at different temperature levels is given below.

Cooling schemes have been developed allowing stable steady state operation and cool down of smaller sections (half strings) partly in sequence. Refrigeration at below 2 K requires the use of cold compressors in the cold box. System and cold box designs have been studied by industry [28], [29] (2 firms), the results of which have been incorporated here as far as possible.

Within a year the cooling will have to run continuously over a period of about 10 months including cool down and warm up times (about 10 days each). Two months are foreseen for maintenance. An important aspect is the availability which is aimed at close to 100 % for the whole refrigeration system. Studies and proposals from industry have been used here too.

The whole cryogenic system will be generally operated from a central control room using workstations with X-Windows for visualisation which are connected to front end systems via high speed communication links for process control and data collection.

The total space required for the refrigeration system above ground in each refrigeration hall is about $2500\,\mathrm{m}^2$.

3.2.5.1 Layout

The two linacs consist of 19584 superconducting 9-cell cavities, each contained in a vessel made from titanium, in which it is cooled to a temperature of $\leq 2\,\mathrm{K}$. For ease of installation and cost minimisation 8 cavities are grouped and assembled into a common cryostat (module). A high order mode (HOM) absorber is housed in the beam tube at each module interconnection. A magnet package containing a superconducting quadrupole of varying length for beam focusing, a vertical and a horizontal correction dipole for beam steering and a "pill box" type beam position monitor is housed in every

second module from 3 GeV to 50 GeV, in every third module from 50 GeV to 150 GeV and in every fourth module above 150 GeV (see Chapter 3.2.2). Thus the length of a module varies from 11.37 to 13.12 m.

For cooling purposes 12 modules are grouped in a "string" of 141.69 to 142.552 m length (see Fig 3.2.30).

Finally, 17 strings with string interconnection boxes (SCBs) between neighboured ones and with feed and end boxes form a unit of about 2500 m length containing 204 modules cooled from a single refrigerator (see Fig. 3.2.29). The maximum number of magnet packages in a unit is 102.

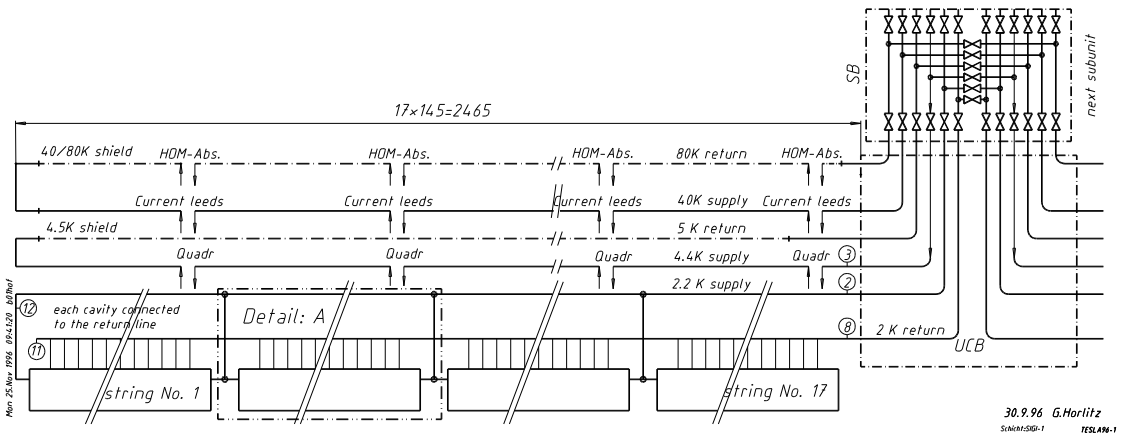

Figure 3.2.29: *Cryogenic supply of a unit*

The whole linear collider consists of 12 units placed in an underground tunnel. All modules are mounted horizontally (along an equipotential line with respect to gravity) with the exception of the modules of the first 2 units at the DESY site end which follow a line with a slope of –5 mrad (Fig. 3.2.31).

3.2.5.2 Overview of Cryogenic Load

Static and dynamic cryogenic heat loads of a module without magnet package and of the magnet package of maximum length have been estimated and are listed in Tables 3.2.3 and 3.2.8. Static load in this case means the load without any RF and beam in the cavities and without current in the superconducting magnets. Dynamic loads are shown for maximum accelerating fields (25 MV/m), quality factor $Q_0 = 5 \cdot 10^9$, 5 Hz beam repetition rate and 100 A current in the magnets. The dynamic heat load dominates (about a factor 10 higher than the static load) at 2 K, is relatively small at 4 K and is considerable at 70 K. While most of the accelerator will be operated at 5 Hz beam bunch repetition rate the cavities in the first two units will run at 10 Hz because this part will be used for coherent γ ray production in a Free Electron Laser (FEL) in addition.

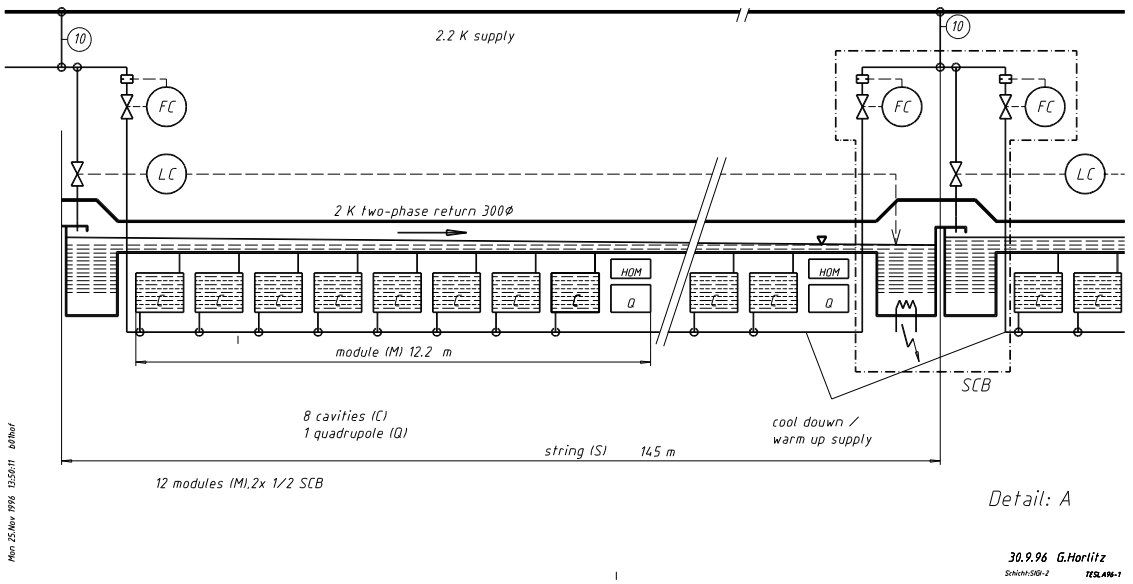

Figure 3.2.30: *Cryogenic supply of a string (detail A of Fig.3.2.29)*

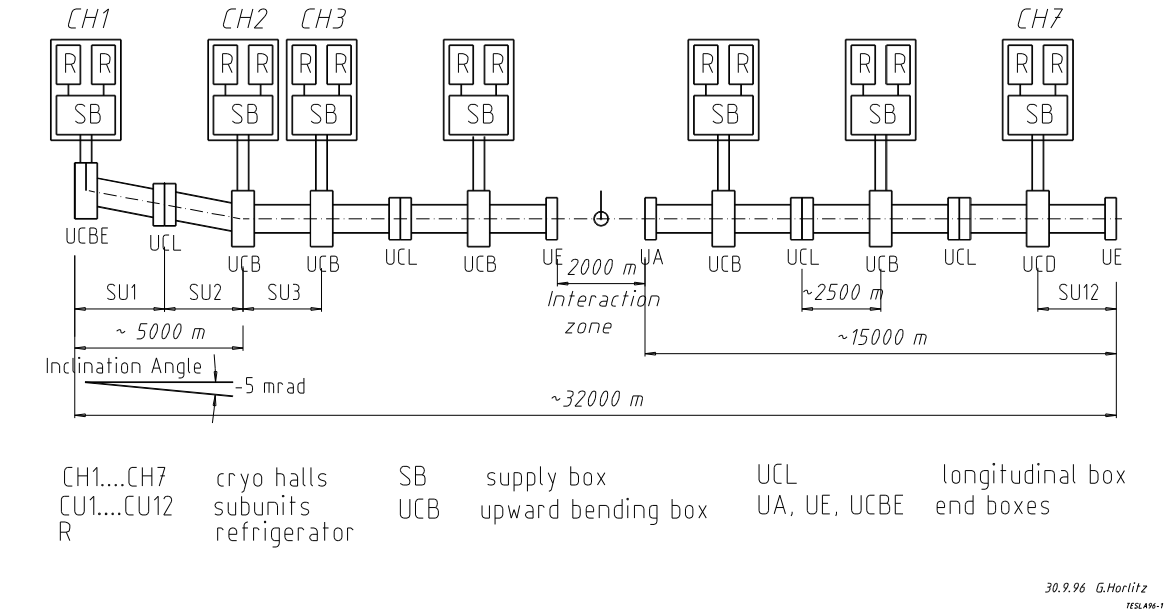

Figure 3.2.31: *Cryogenic supply of the collider*

Heat loads have been estimated also for the string interconnection, feed and end boxes as well as for the transfer lines up to the valve box at the refrigerator above ground (Table 3.2.18). Nominal heat loads for the standard units 3 to 12 and the special ones 1 and 2 are contained in Table 3.2.19. There are small differences (due to different lengths of magnet packages) among the standard units and between unit 1 and 2, but these have been neglected here. The total loads in the first two units

are higher by a factor of 1.9 at 2 K, a factor of 1.2 at 4 K and a factor of 1.4 at 70 K. Table 3.2.19 shows also the design heat loads for the layout of the cryogenic plants which contain a safety factor of 1.5.

From the heat loads the total electrical power needed has been calculated and listed in Table 3.2.20. The conversion factors used are 800 W_{el}/W at 2 K, 250 W_{el}/W at 4 K and 25 W_{el}/W at 70 K.

Additional heat loads, units 1-2, 10 Hz (W)						
	2 K	**2 K**	**4 K**	**4 K**	**70 K**	**70 K**
	static	**static + dynamic**	**static**	**static + dynamic**	**static**	**static + dynamic**
16 interconn. boxes	19	27	83	83	736	736
end box A	1	1	4	4	40	40
end box B	1	1	4	4	40	40
distribution box	16	16	67	67	844	844
transferline	13	13	10	10	105	105
vacuum barrier	5	5	20	20	200	200
sum	**55**	**63**	**188**	**188**	**1965**	**1965**
Additional heat loads, units 3-12, 5 Hz (W)						
	2 K	**2 K**	**4 K**	**4 K**	**70 K**	**70 K**
	static	**static + dynamic**	**static**	**static + dynamic**	**static**	**static + dynamic**
16 interconn. boxes	19	23	83	83	736	736
end box A	1	1	4	4	40	40
end box B	1	1	4	4	40	40
distribution box	16	16	67	67	844	844
transferline	13	13	10	10	105	105
vacuum barrier	5	5	20	20	200	200
sum	**55**	**59**	**188**	**188**	**1965**	**1965**

Table 3.2.18: *Additional nominal heat loads for cryogenic supply of a unit*

3.2.5.3 Cooling

The cavities have to be cooled to $\leq$ 2 K in order to assure the required acceleration voltage (25 MV/m) and quality factor $Q_0(> 5{\cdot}10^9)$. For this purpose the helium vessels of the cavities are filled with superfluid helium (Helium II) at a pressure of $<$ 31 mbar.

One-phase helium of 2.2 K and about 1.2 bar is flowing from the refrigerator through

Units 3 –12 (5 Hz) (W)						
	2 K	**2 K**	**4 K**	**4 K**	**70 K**	**70 K**
	static	**static + dynamic**	**static**	**static + dynamic**	**static**	**static + dynamic**
204 cryomod.	216	2205	2095	2613	10294	16151
quads	11	20	44	55	1679	3516
add. heat	55	59	188	188	1965	1965
sum (nomimal)	**282**	**2284**	**2327**	**2856**	**13938**	**21632**
plant design	**423**	**3426**	**3491**	**4284**	**20907**	**32448**
Units 1 – 2 (10 Hz) (W)						
	2 K	**2 K**	**4 K**	**4 K**	**70 K**	**70 K**
	static	**static + dynamic**	**static**	**static + dynamic**	**static**	**static + dynamic**
204 cryomod.	216	4194	2095	3131	10294	22008
quads	11	29	44	66	1679	5353
add. heat	55	63	188	188	1965	1965
sum (nominal)	**282**	**4286**	**2327**	**3385**	**13938**	**29326**
plant design	**423**	**6429**	**3491**	**5078**	**20907**	**43989**

Table 3.2.19: *Nominal heat loads of the units (incl. additional heat loads of Table 3.2.18) and values assumed for the cryo plant design (incl. a 50 % safety margin).*

AC-power (MW)	**static**	**stat. & dynam.**
units 3-12		
nominal	1.156	3.083
plant design	1.734	4.624
units 1-2		
nominal	1.156	5.009
plant design	1.734	7.514
total (units 1-12)		
nominal	**13.874**	**40.844**
plant design	**20.811**	**61.266**

Table 3.2.20: *Nominal operating AC-power requirement for the cryogenic system and requirement for full capacity (incl. 50 % safety margin).*

all cryomodules of a unit (see Fig.3.2.29). At the end of each cryogenic string a fraction of this helium is expanded in a JT valve into a liquid/gas separator inside the string connection box or inside the end box of the unit (see Fig. 3.2.30). Liquid as well as gas is flowing back to the refrigerator through the 300 mm (350 mm in case of units 1 and 2) diameter 2 K helium two-phase pipe. At the position of each cavity liquid helium is flowing into the helium vessel. Heat generated at the cavity is transported through the liquid to the surface where liquid is evaporated. Excess liquid – if any – at the end of each string is collected in a helium bath and evaporated there with the aid of an electric heater while the helium gas is passing forward through all strings back to the refrigerator. Proper control of the JT valve will assure that there is nearly no excess liquid helium entering the bath.

As in the first unit supplied from a refrigerator on the DESY site the beam has a slope of –5 mrad, the JT valves for expansion of the one-phase 2.2 K helium sit in the string interconnection boxes at the string entrances (seen from the refrigerator). The liquid Helium II thus flows off from the refrigerator while the gas returns in opposite direction. It is believed that this counter flow of gas and liquid in the 350 mm diameter helium two-phase pipe is possible in this flow regime (306 g/s at maximum) without creating slugs and mist in the liquid. However, detailed measurements in a test set-up need to be performed.

Pressures, temperatures and liquid levels in the 300 mm (350 mm) diameter 2 K two-phase helium tube are governed by the pressure drop of the flowing gas and liquid, by the evaporation of the liquid and by the hydrostatic pressures for the different cases: horizontal and inclined beam tube. Extensive calculations have been done by G. Horlitz [30]. The pressure (temperature) in the tube decreases from 31 mbar (2.0 K) at the far end of the unit down to 28 mbar (1.97 K) respectively 21 mbar (1.88 K) at the near end (seen from the refrigerator) of the unit for the standard respectively the first two units. The liquid level in the 300 mm (350 mm) diameter tube has its maximum (about 2 cm high) at the liquid entrance just behind the phase separator and decreases down to zero towards the end of a string.

One-phase helium of 4.5 K and 5 bar is flowing from the refrigerator through all quadrupoles of the unit in series, warming up to about 4.7 K towards the far end of the unit. On its way back it is cooling the 4.5 K radiation shields, returning to the cold box at a pressure of ≤ 2.3 bar.

Helium gas of 40 K and 19 bar is flowing from the refrigerator through heat exchangers at the HTS current leads of the superconducting magnet packages of the unit and returns to the refrigerator cooling the 70 K radiation shields and the HOM absorbers at the module interconnections. As the cavities used for TESLA have been heat treated and thus freed from dissolved hydrogen, fast cool down will not be necessary which eases the operation of the cryo-plant. However, in case fast cool down becomes necessary, it can be provided.

3.2.5.4 Cryogenic Plant

There will be seven refrigeration halls each containing two refrigerators (see Fig. 3.2.31). Generally each refrigerator is cooling one unit. Only the first two units because of their enhanced heat load at 10 Hz operation will be cooled from two refrigerators each. This concept allows to standardise plant design (for instance by using identical heat exchangers, cold boxes and piping) and thus standardise operation and maintenance routines as well as spare part inventory. Differences between the refrigerators for the first two and the remaining units are only in the turbines, the cold compressor sizes [28] and the numbers of warm compressors [29].

Each refrigerator has its own compressor system consisting of seven compressor skids (2 low pressure, 3 medium pressure, 2 high pressure ones) and three oil removal skids [28] (see Fig. 3.2.32). There is a complete redundant compressor system in each refrigeration hall. The low pressure (LP) skid operates with a suction pressure of 1.05 bar and compresses gas returning from the 4.4 K bath, from the 5 K shield and from the exhaust of the cold compressor line. The medium pressure (MP) skid operates at variable suction pressure and compresses gas returning from the turbine exhaust keeping constant the pressure ratio across the turbines. The high pressure (HP) skid compresses gas from the LP and MP skids to a pressure of 19 bar. In this scheme the efficiencies of both compressors and turbines are very high.

During steady state operation after entering the cold box the gas is running through a simple guard adsorber which removes small impurities (see Fig. 3.2.33 for cold box layout). It can be bypassed for regeneration [28]. Further down in the refrigerator the gas passes through several heat exchangers and is expanded in turbines. There are four expansion stages [28]. The first consists of 2 turbines in series and cools and expands the gas from 80 K, 17 bar of the shield cooling return, to about 40 K and medium pressure. If the expansion ratio of the turbine is high enough only one turbine is sufficient here [29]. The second stage also consisting of 2 turbines in series expands from high pressure at 21 K to medium pressure at 11 K. The third stage expands from high pressure at 10 K to medium pressure at about 5.5 K. The fourth stage expands from high pressure at about 5.9 K to about 5 bar at 5.4 K. This gas flow is then used for cooling the 102 (at maximum) quadrupoles and the 4.5 K shield and will later on flow through the cavities [28]. Before entering into the quadrupoles this gas is subcooled in a coil type heat exchanger inside a helium bath. The bath is filled by liquid obtained after JT expansion of the gas returning from the 4.5 K shield. The liquid level is controlled by an electric heater. At the far end (seen from the refrigerator) of a unit the temperature of the quadrupole cooling gas will be ≤ 4.8 K. Returning to the cold box this gas cools the 4.5 K shield.

For cavity cooling 4.5 K liquid at 1.2 bar is taken out of this bath, subcooled to 2.2 K in a heat exchanger by the returning gas stream and expanded at each cavity string to a pressure of about 26 mbar [28]. The low pressure is obtained by running the returning gas through 5 cold compressors. Between the first two and the last three cold compressors the gas flow is recooled to 5.6 K for ease of cold compressor control. The fifth cold compressor is needed only in the RF-off mode in order to achieve the required

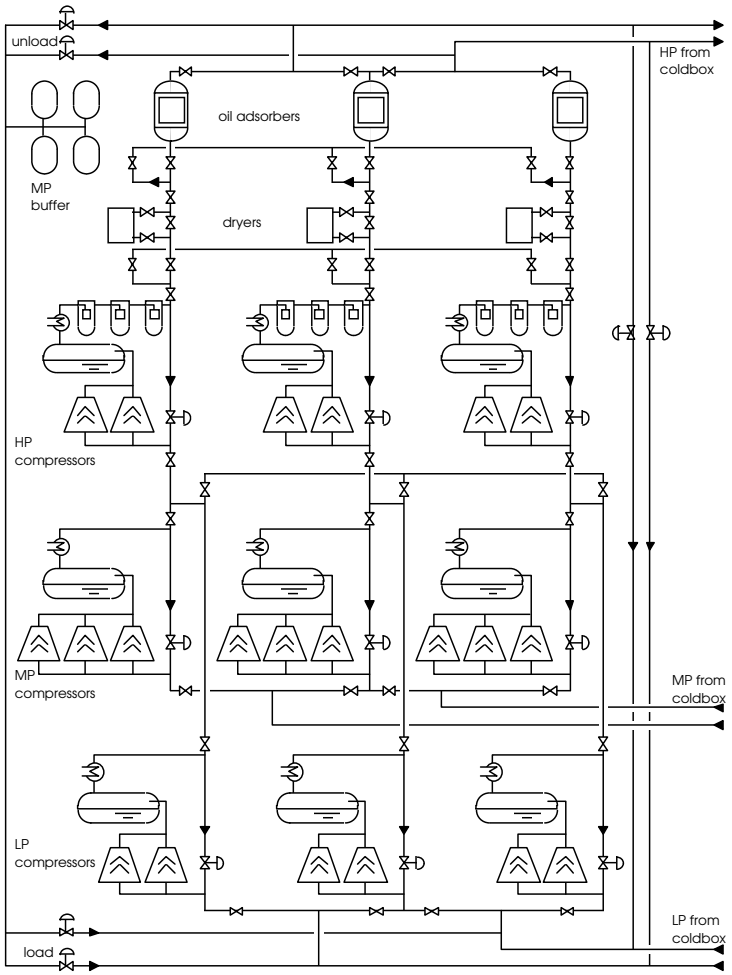

Figure 3.2.32: *Warm compressor system of a refrigeration hall [28].*

outlet pressure of 1.2 bar. When the RF is in full operation this cold compressor is bypassed [28].

During cool down liquid nitrogen is used for precooling. The purified helium gas can be fed into the refrigerator cold box either at room temperature (during the first cool down phase) or at 80 K [28]. For purification during the cool down phase there is a full flow switchable adsorber unit outside the refrigeration cold box.

3.2.5.5 Components and Subsystems

Warm compressors are oil lubricated screws with casing and rotors made of cast iron utilising radial sleeve bearings. To prevent leakage of process gas double mechanical shaft seals are provided. Each compressor has a hydraulically operated slide valve for stepless capacity control of the compressor flow between 10 % and 100 % [28].

The dehydration skid consists of switchable dual bed adsorbers filled with a molecular sieve [28]. Regeneration is accomplished by closed loop gas circulation at elevated

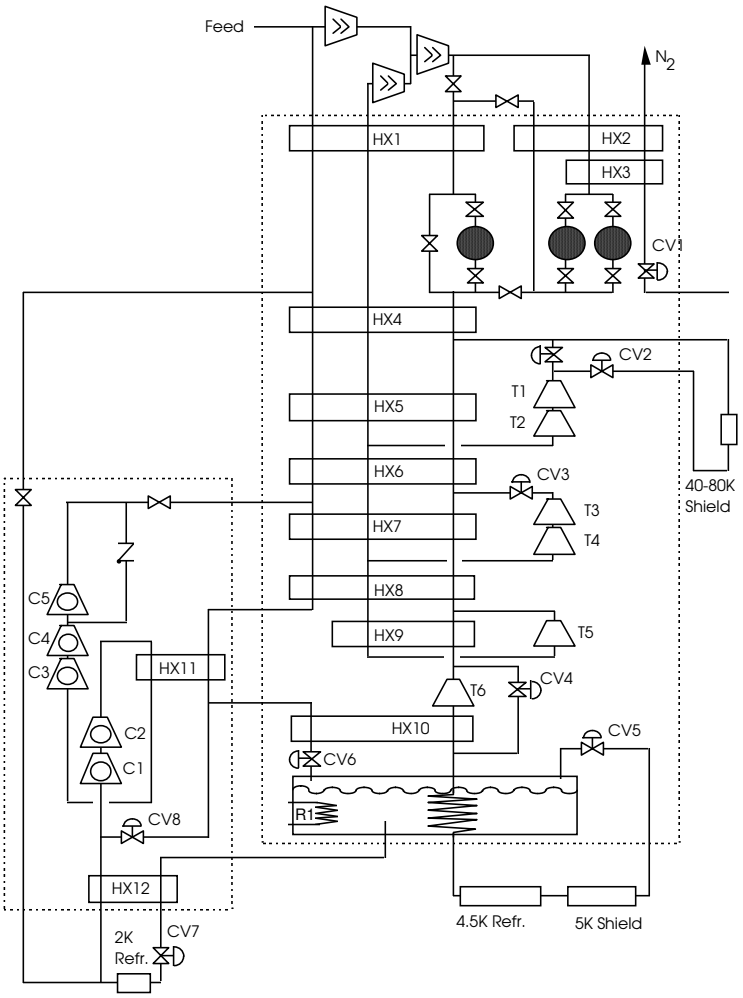

Figure 3.2.33: *Cold box layout [28].*

temperature, subsequent evacuation and cool down.

The oil removal system is skid mounted and consists of a three stage coalescing filter system, a charcoal adsorber and a dust filter [28]. The adsorber will remove both, vapour phase and liquid impurities to less than 10 ppb per weight. At present horizontal installed cylindrical tanks with a total volume of 1000 m^3 for every two cold boxes are foreseen for storing warm medium pressure (20 bar) helium gas. They may be installed outdoors.

Helium is stored as a liquid in a dewar of 120 m^3 volume serving two cold boxes each. During shut down periods the evaporating gas is compressed into the warm buffer by one compressor unit. The total storage capacity has a margin of 26 %.

The outer shells of cold boxes, cold compressor boxes and valve boxes are designed as vertical vacuum tanks made from carbon steel [28]. For easy access the vacuum jacket can be disconnected and lowered from the top.

Heat exchangers are very compact aluminum brazed counter flow plate fin types of

up to five different gas streams in the same core [28].

Different types of turbines may be used. The Linde turboexpander is a small, single stage centripetal turbine which is braked with a directly coupled, single stage centrifugal brake compressor [28]. It is equipped with dynamic gasbearings which function at ambient temperature. For start up auxiliary magnetic bearings are used. The speeds range from 75000 rpm to 282000 rpm. The gas cooler at the warm compressor side is cooled with water. The turbine housing is fastened to the top plate of the cold box and projects vertically into its vacuum space. The bearing cartridge forms an integral part of the turbine and can easily be removed from outside without breaking the vacuum of the cold box. The main features of the L'Air Liquide turbines are static gas bearings operating at room temperature, relatively large clearances not very sensitive to impurities, high expansion ratios and easy way of speed control [29]. Several turbine sizes exist with speed between 50000 rpm and 600000 rpm.

There are also different types of cold compressors under consideration. The Linde cold compressor is a new design which has been tested at CERN successfully. It is a single stage radial flow turbo-compressor [28]. This concept offers high reliability, high efficiency and a compact design. The standardised cartridge design allows easy access to the machine without interfering with the cold box vacuum. Lubricated ceramic bearings are used to carry the vertical shaft. The electric motor is surrounded by process atmosphere. The maximum operating speed would be about 1000 rpm. The L'Air Liquide cold compressor successfully used for Tore Supra and CEBAF has active magnetic axial and radial bearings and roll bearings for emergency [29]. A new development for CERN is using fully pneumatic bearings [29].

There are several filters within the cold box to protect the turboexpanders from being damaged by mechanical impurities. Cryogenic adsorbers are installed inside the cold box at 80 K and 20 K level [28]. They protect the colder equipment from impurities. They consist of an activated charcoal bed fixed between rigid upper and lower filter packages. Replacement of the bed is possible. Regeneration is performed by the circulation of warm gas.

The string interconnection boxes (SCBs) contain a JT valve expanding the 2.2 K forward flow into a phase separator, a barrier for flow of liquid between neighboured strings, a liquid collecting box with electric heater, valves and instrumentation [28].

Feed and end boxes of each unit contain in addition cold/warm transitions and pneumatic valves for the beam tube.

Transferlines will contain sleeves for thermal and vacuum separation.

The vacuum of each cold box will be pumped continuously by a system consisting of a two stage primary pump, an oil diffusion pump with water cooled baffle and all necessary valves and instrumentation.

3.2.5.6 Control System

The whole system consisting of 7 refrigerator halls (14 refrigerators), and valves and instrumentation in the collider tunnel generally will be operated and controlled from one central control room. Workstations with X-Window are used for visualisation.

These workstations are connected to the front-end systems through a high speed communication link. The front-end systems collect all I/O data and include all the process control functionality based on standardized program blocks. Every major subsystem like cold box, or compressor unit will have its own I/O rack in order to collect all data from the plant and the string of cryomodules. Intelligent sensors are connected directly to field buses. All temperatures have to be monitored precisely. Temperatures of the cavities are measured accurately using pressure gauges for the 2 K two phase flow.

Local control terminals (operator interfaces) will allow access to the plant control, especially during commissioning, for service and maintenance at every single unit.

3.2.5.7 Availability of Cryogenics

Availability of the cryogenic system for high energy experiments is a very important issue. It is anticipated that the availability of the whole cryogenic system of TESLA will be close to 100 %. This is achieved by several methods. Full redundancy will be installed for all process steps except for the refrigeration cold box. In each refrigerator hall containing two refrigerators there will be a redundant third warm compressor line as well as a redundant third cold compressor line. Utilities like instrument air and cooling water supply will be installed as parallel independent systems with redundancy. Electrical power will be buffered with uninterruptable power supply units (UPS) wherever possible.

Cold boxes will have individual availability of $> 99\,\%$. Important components like turbines, cold compressors, adsorbers and filters will have their own vacuum boxes and will be accessible from outside the cold box without breaking the cold box insulation vacuum [28].

In case that a refrigerator fails completely the concept of having two refrigerators in each refrigeration hall allows to cool two units from one refrigerator. Both units can be kept cold without running the RF until the defective plant has been repaired. If the heat loads stay within the calculated limits one could even run the collider at reduced bunch repetition rate (for instance 3 Hz) if the remaining plant in that refrigeration hall is running at full capacity, which can be further increased by using liquid nitrogen and liquid helium from the storage dewar for pre-cooling.

3.2.5.8 Utilities

The expected power consumption per cryogenic hall (two refrigerators) is listed in Table 3.2.21 [28].

3.2.5.9 Space Requirements

The space required at each refrigeration hall for the compressor system including oil and water cooler is about 40 m $\times$ 45 m. For cold boxes, cold compressor boxes, oil adsorbers and a liquid helium dewar the required space is about 25 m $\times$ 25 m.

Electrical power	3300 V	10750 kW
	380 V	87 kW
	220 V	3 kW
	24 V	3 kW
Cooling water		
cold box (for turbine and baffle cooling):		
	max. temp.	20 °C
	Δ T	10 °C
	consumption	15 m^3/h
compressors:		
	max. Temp.	30 °C
	Δ T	10 °C
	consumption	1050 m^3/h
Air for instrumentation		
	minimum pressure	7 bar
	consumption	150 Nm^3/h

Table 3.2.21: *Utility requirements per cryogenic hall.*

3.2.6 Failure Handling

As has been mentioned in Section 3.1, the long macropulses and also long bunch to bunch distance in the TESLA Superconducting Linear Collider have extremely positive consequences with respect to failure handling: a safety system can be employed which can "turn off" the beam even within one macropulse in case an emergency is indicated by enhanced loss rates. And even more, superconducting accelerating structures as well as the used superconducting quadrupole magnets have typical quenching times much longer than the single macropulse. Therefore the operation of the TESLA Linear Collider would be extremely safe.

In this section main emphasis is put on the discussion of possible beam transport failures during the passage through the main linac with its 15 km length. A beam hitting the beam tube wall, i.e. in most cases the iris of a superconducting accelerating cavity, can easily destroy the cavity if it is well focused. Similar to a beam dump window problem the beam macro pulse power will not only heat the hit spot. It will cause an "explosion" or cracking of the material. The system would be "vented" with more or less clean Helium from the surrounding He vessel. A shutdown including a warm up and cool down cycle would be necessary. This has to be avoided.

Since the bunch train is 240 km long, only 6.2 % of the bunch train is in the 15 km long linac during the macropulse. Producing a beam inhibit signal at any of the subcomponents should not take longer than approximately 10 μs. The maximum signal travelling time is determined by the linac length. At a typical speed of 5 ns/m (standard coaxial cable) the length of 14.57 km corresponds to roughly 75 μs, thus the triggering of a beam injection inhibit can start after 85 μs.

In a superconducting linac changes of the magnetic fields or of the accelerating fields happen on a time scale long compared to this delay time until injection inhibit. Quenching of superconducting magnets might start within a macropulse but the only consequence could be a slight drop in the field strength. The magnets need typically much more than 800 μs for a total quench. Nevertheless, the consequence of a switched off quadrupole is shown later (see below). Similar to this a quench of a group of accelerating cavities (e.g. 32 cavities) needs time. Here it is more important to study the consequences of a jump in the reference phase or the consequence of a klystron failure. This has been done, and the results are described in section 3.2.6.2.

3.2.6.1 Philosophy for beam injection

The general philosophy for beam injection should be as follows. An exception handler will check the "o.k."-state of all subcomponents along the linac. For the magnets it would be a check of the stationary operation, i.e. basically a check if a magnet has quenched. The case of having a short circuit in one of the coils is not as dangerous as for a warm magnet. The current would still take the superconducting path (i.e. the winding), and if not (e.g. during ramping) the magnet would start quenching because of heat production in the short circuit. This would be detected.

For the superconducting accelerating cavities the exception handler can do much more. The filling time before beam injection is about 500 μs, thus there is plenty of

time to check the actual amplitude and phase after e.g. 300 to 400 μs.

During the macropulse the beam transmission can be measured as well as the beam position along the linac. The results can be evaluated between macropulses (200 ms $\hat{=}$ 5 Hz repetition rate are enough for a very complete analysis) and can be used to detect slow changes.

As a summary it can be stated that a system check can be performed about 100 to 150 μs before beam injection. And the achieved "o.k." is valid until the end of the following macropulse. Nothing severe can happen as long as the beam injection parameters are fixed by a collimator, and as long as the linac operator does not overwrite safe limits for the settings of magnets.

3.2.6.2 Magnet and Cavity Failure's Consequence on Beam Optics

The consequences of switched off qaudrupoles and switched off groups of cavities have been studied. For the beam optics in the linac a scheme essentially identical to the one described in section 3.3 has been used.

Figure 3.2.34 shows the envelopes along the linac. The matching between the different FODO sections is possible by using five quadrupoles each, three of them at the end of the preceding section, and two of them at the beginning of the following section.

Figure 3.2.35 shows the consequence of switched off quadrupoles. The maximum beam size increases by a factor of three to five, depending on the position along the linac. The picture shows only two selected quadrupoles but switching off any of the other quadrupoles gives similar results although the combination of several switched off quadrupoles can clearly yield bigger beam sizes. This is shown in Fig. 3.2.36. Thus it will be necessary to monitor all quadrupoles before beam injection, e.g. together with the accelerating cavity's status during cavity filling. This is possible. The only consequence is that a magnet failure has to be repaired or compensated by using preceding quadrupoles before injection of any further macro pulses.

A klystron failure has only a minor influence on the beam optics. Figure 3.2.37 reflects the insensitivity to a variation of the injection energy. Similar to this, a switched off klystron (32 cavities) can be hardly seen in the enveloppes. Figure 3.2.38 gives the comparison between normal operation (solid lines) and irregular conditions (dashed lines) simulated by switching off the klystron output 50 μs after the end of cavity filling, i.e. at t = (0.5 ms + 50 μs) instead of t = (0.5 ms + 800 μs). After switching off the klystron the cavity field starts decaying but finally increases because of beam induced voltage. Taking the amplitude $E_{acc}(t)$ and the phase into account, one can easily calculate the energy gain per cavity over the beam pulse. The subsequent bunches get a time dependent energy gain. If one would not interrupt beam injection, the difference between the first and last bunch would be about 32 MeV per cavity or about 1 GeV per 32 cavities, i.e. per klystron. The consequent use of the above mentioned exception handler reduces this "energy spread" to about 0.15 GeV which is only 6×10^{-4} of the final beam energy.

A jump in the linac reference phase during the beam pulse can be treated in the

same way. The klystron power would reach its maximum and the exception handler would switch off the klystron after about 50 μs. The energy spread over the bunchtrain in this case reaches a peak value of 19 %, still small enough for safely transporting the beam to the end of the linac. The beam then hits the energy collimators and the enhanced loss rates trigger the safety dump system.

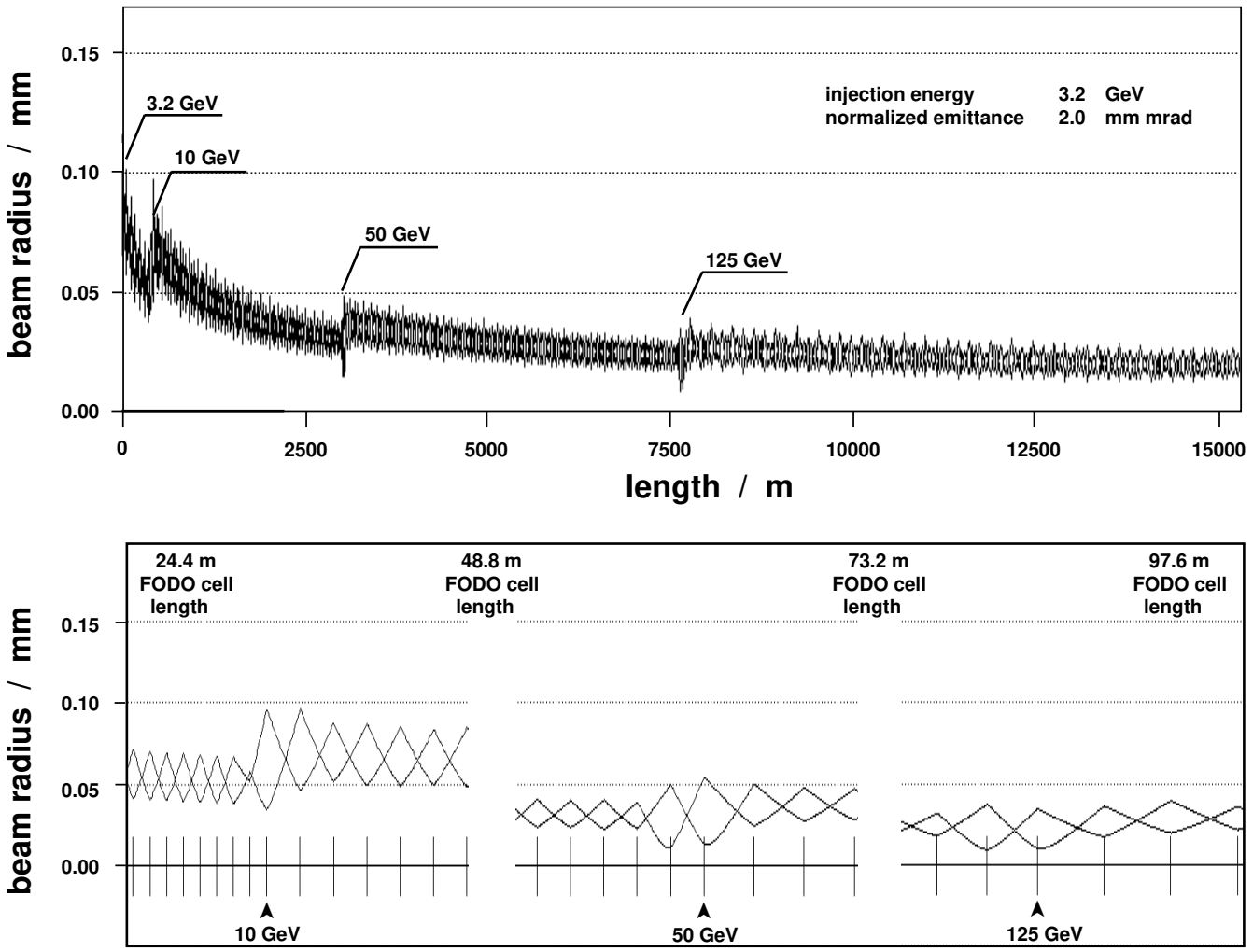

Figure 3.2.34: *Beam enveloppes along the linac. The matching between the FODO sections is done by five quadrupoles each.*

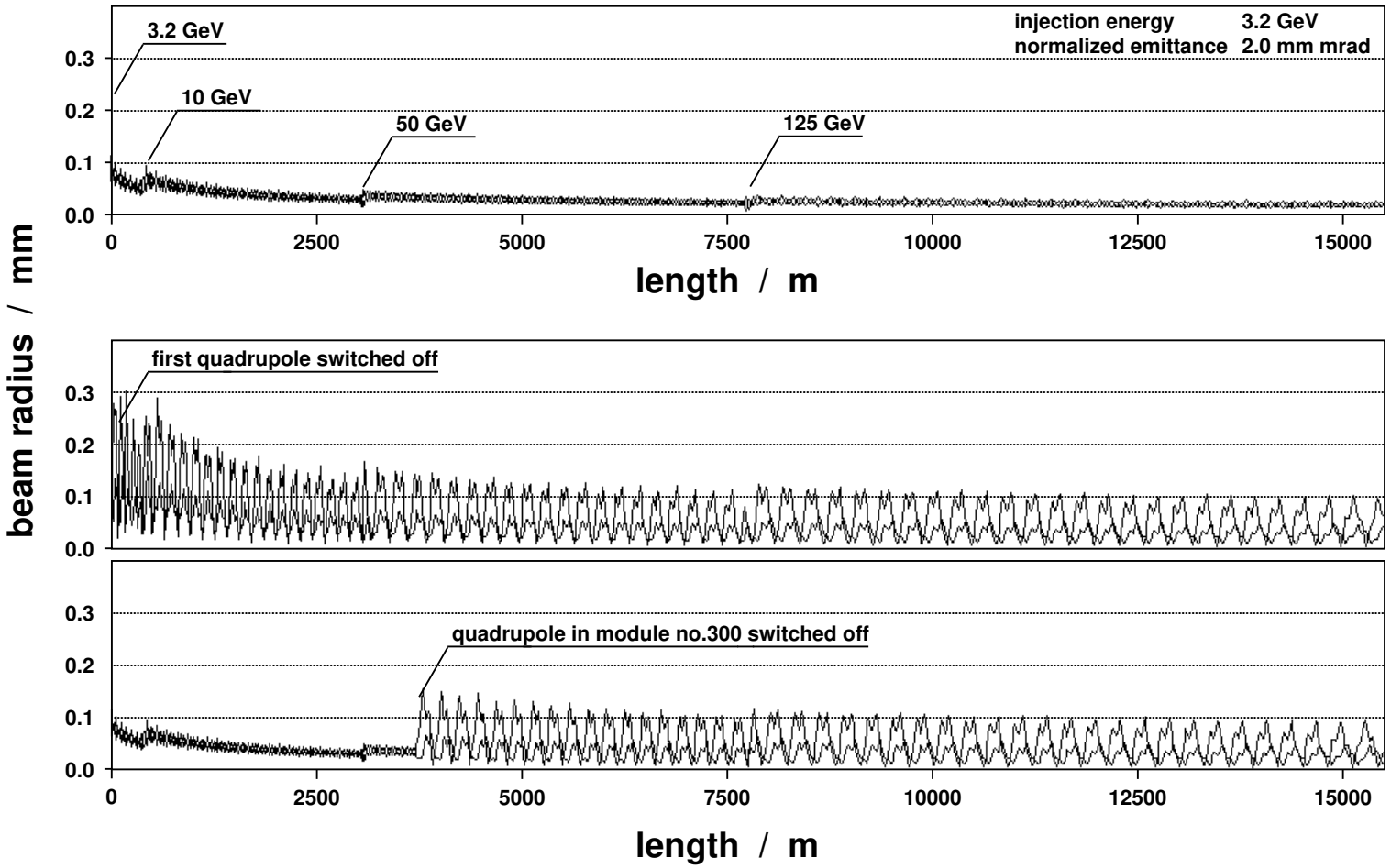

Figure 3.2.35: *The consequence of switched off quadrupoles. The maximum beam size increases by a factor of three to five, depending on the position of the quadrupoles.*

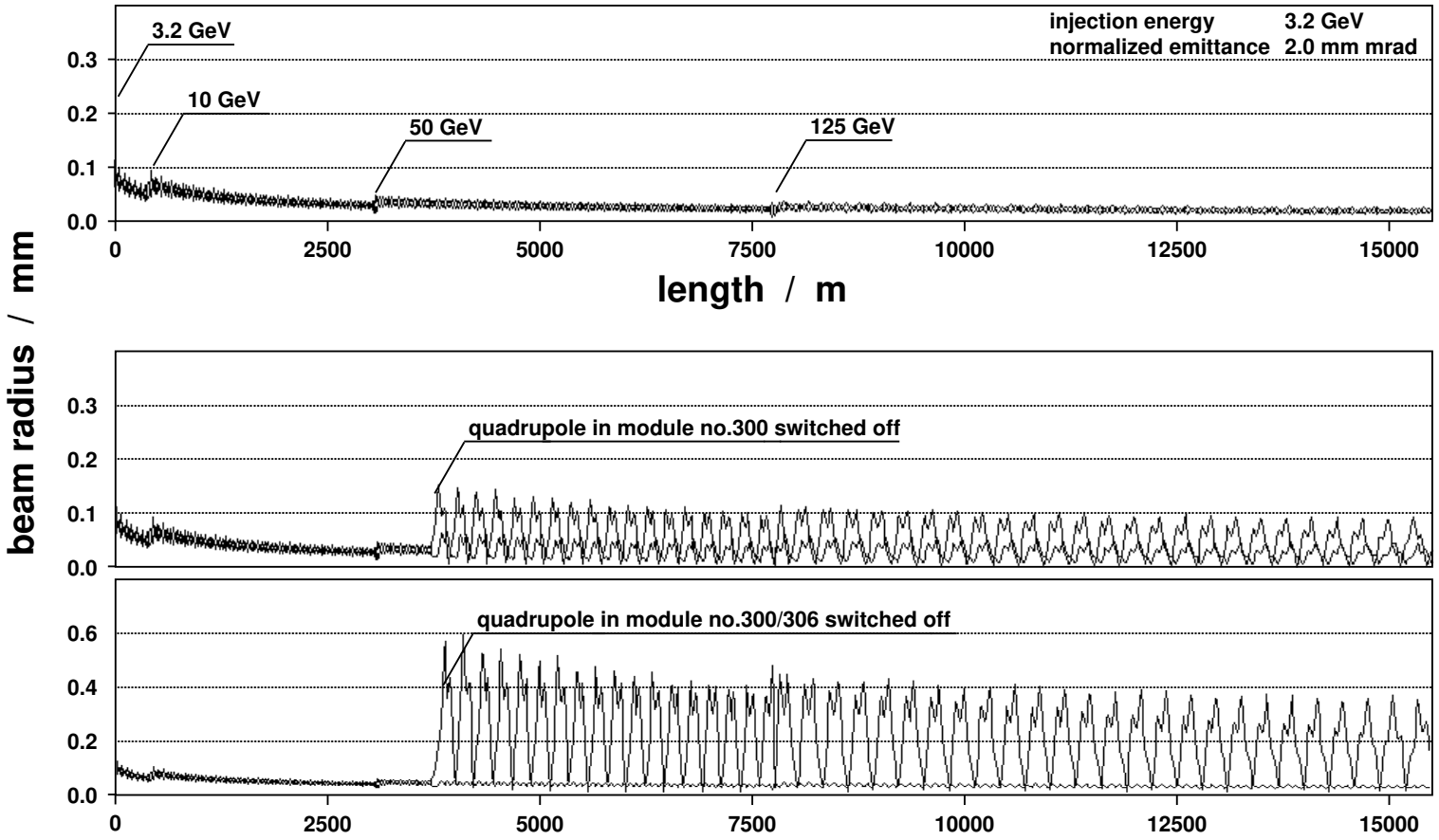

Figure 3.2.36: *An unfortunate combination of switched off quadrupoles yields larger beam sizes. The available aperture still corresponds to more than 50 standard deviations.*

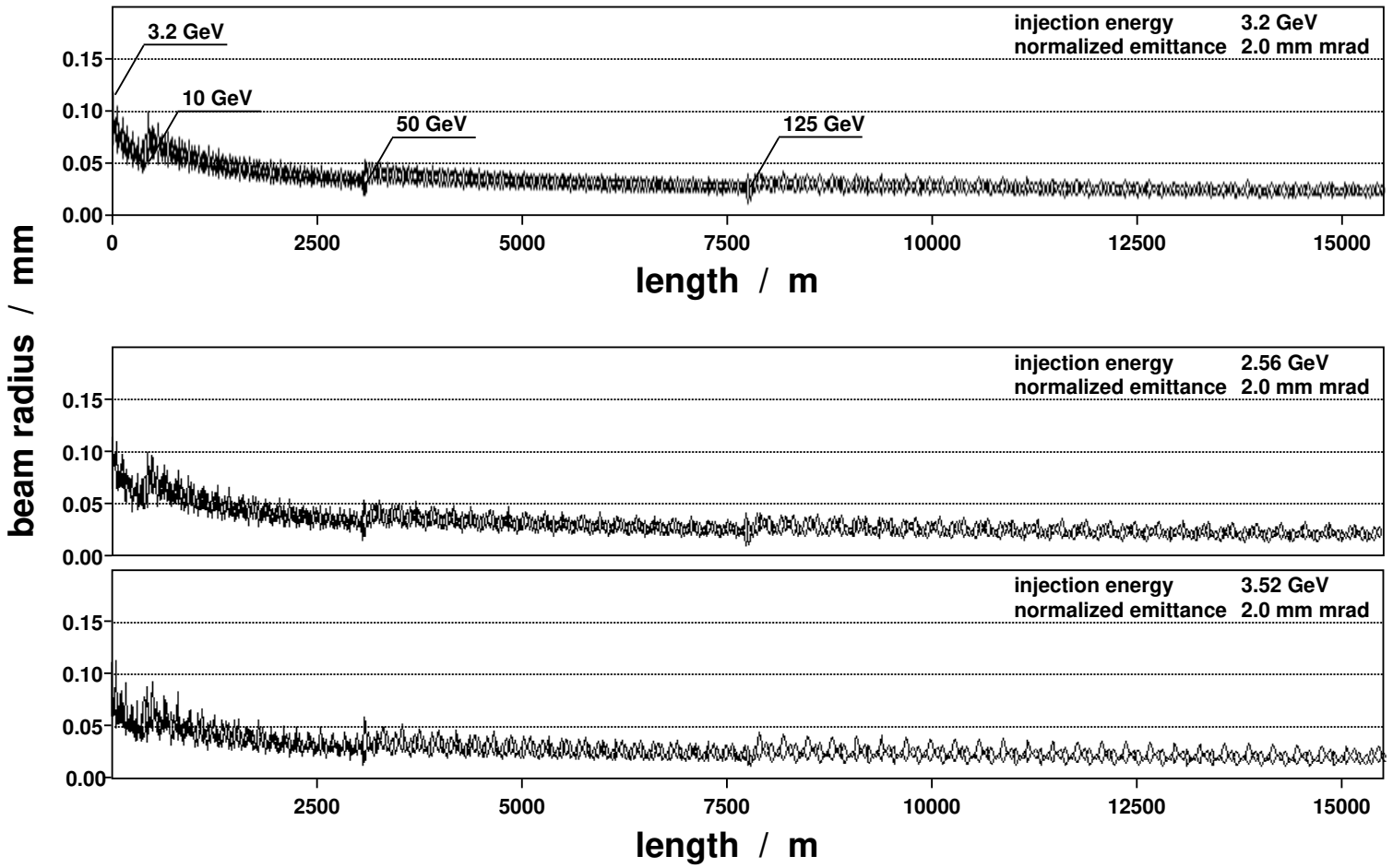

Figure 3.2.37: *The impact of different injection energies.*

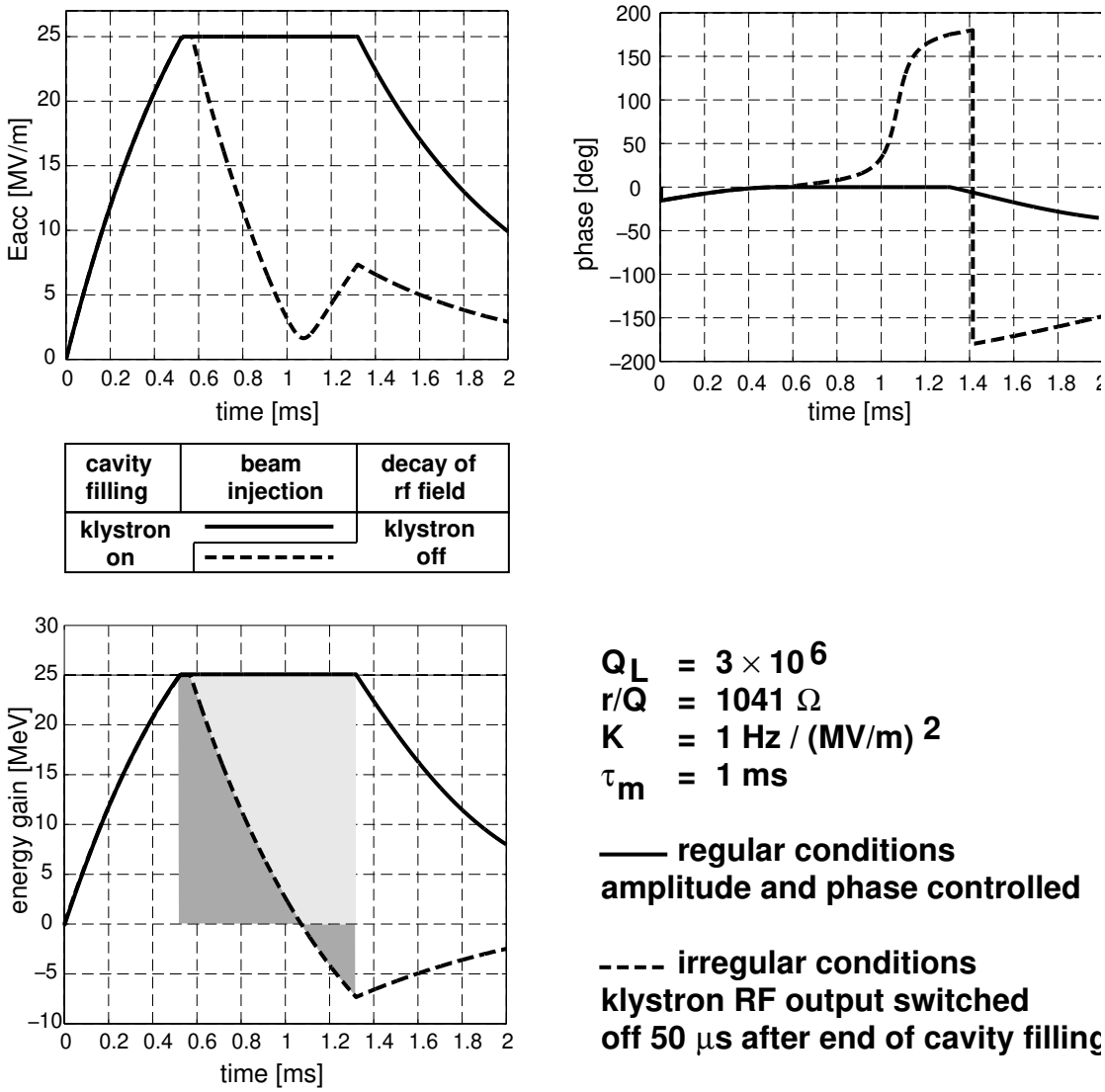

Figure 3.2.38: *Comparison between normal operation (solid lines) of a single accelerating cavity and irregular conditions (dashed lines) in which the klystron output is switched off 50 μs after the end of cavity filling. After switching off the klystron the cavity field starts decaying but finally increases because of beam induced voltage. The subsequent bunches get a time dependent energy gain.*

Bibliography

[1] C. Reece et al., Part. Acc. Conf. Dallas (1995)

[2] P. Kneisel, B. Lewis, Part. Acc., 53 (1996), 97,

[3] Ph. Bernard et al., Proc. Eur. Part. Acc. Conf. Berlin 1992

[4] B. Bonin, DESY-CERN School "Superconductivity in Particle Accelerators", Hamburg 1995

[5] W. Weingarten, DESY-CERN School "Superconductivity in Particle Accelerators", Hamburg 1995

[6] Th. Schilcher, TESLA-Report 95-12 (1995)

[7] B. Bonin, Supercond. Sci. Technology 9 (1996), pp 453 - 460

[8] H. Padamsee, Proc. 5th Workshop on RF Superconductivity, Hamburg 1991, p. 904

[9] H. Padamsee et al., Proc. 4th Workshop on RF Superconductivity 1990, KEK, Ed. Y. Kojima

[10] E. Kako et al., Proc. 7th Workshop on RF Superconductivity, 1995, Saclay, Ed. B. Bonin

[11] J. Graber et al., Nucl. Instr. Meth.A350 **(1994)** 572

[12] G. Müller, Proc. 3rd Workshop on RF Superconductivity, 1988, Argonne, Ed. K. Shepard

[13] J. Sekutowicz, TESLA-Report 97-02 (1997)

[14] W. Albach, G.A. Voss, Zeitschr. Angew. Phys. **9** (1957) 111

[15] F. Alessandria et al., *Design, Manufacture and Test of the TTF Cavity Cryostat*, Adv. Cryogenic Engineering 41A, p. 855, 1996.

[16] *High Voltage Breakdown in the Electron Gun of Linear Microwave tubes*, A.M. Schroff, and A.J. Durand in "High Voltage Vacuum Insulation" by R.V. Latham (Ed), Academic Presss, March 1995, ISBN 0124371752

[17] J.C. Terrien, G. Faillon, and P. Guidee, *RF Sources for Recent Linear Accelerator Projects*, 16th International Linac Conference, August 1992, Ottawa, Ontario

[18] Oleg A. Nezhevenko, *The Magnicon: A New RF Power Source for Accelerators*, IEEE Particle Accelerator Conference Vol. 5, May 6-9, 1991, San Francisco, CA, USA.

[19] Oleg A. Nezhevenko, private communication

[20] H. Pfeffer, C. Jensen, S. Hays, L.Bartelson, *The TESLA Modulator*, TESLA Report 93-30

[21] K.P. Juengst and H.Salbert, *Fast SMES for Generation of High Power Pulses*, 14th International Conference on Magnet Technology, 1995 Tampere Finland.

[22] W. Bothe, *Pulse Generation for TESLA, Considerations on SMES-Variants*, TESLA-Collaboration Report, April 1996.

[23] H. Salbert, *Theoretisches und experimentelles Modell einer gepulsten Hochleistungspulsversorgung mit supraleitendem magnetischem Energiespeicher*, Dissertation, Universitt Karlsruhe, 1996.

[24] W. Bothe, *Pulse Generation for TESLA, a Comparison of Various Methods*, TESLA Report 94-21

[25] W. Bothe, private communication.

[26] *The TESLA TEST FACILITY LINAC-Design Report*, Ed. D.A. Edwards, Tesla Report 95-01

[27] A. Mosnier and O. Napoly. *Energy Spread Induced in the TESLA Linac,* TESLA Report 93-07.

[28] Linde Kryotechnik AG, *Study for the Cryogenic System TESLA*, October 1996.

[29] L'Air Liquide, private communication, October 1996.

[30] G. Horlitz, *A Study of Pressures, Temperatures and Liquid Levels in the 2 K Kelvin Refrigerator Circuit of a 1830 m TESLA Unit under Different Conditions and System Configurations*, TESLA 94-17, December 1995 and G. Horlitz, *The Cryogenic System for the Superconducting e^+e^- Linear Collider TESLA*, Proceedings of the NIFS-Symposium on Cryogenic Systems for Large Scale Superconducting Applications, National Institute for Fusion Science, Toki, Nagoya, Japan, May 1996, to be published.